5-24-2018

THE FABRICATION OF HIGH-ASPECT RATIO GRATINGS FOR TALBOT INTERFEROMETER WITH MEDICAL IMAGING APPLICATION.

Vikaram Singh
Louisiana State University and Agricultural and Mechanical College, vsing15@lsu.edu

THE FABRICATION OF HIGH-ASPECT RATIO GRATINGS FOR TALBOT INTERFEROMETER WITH MEDICAL IMAGING APPLICATION.

A Thesis

Submitted to the Graduate Faculty of the
Louisiana State University and
Agricultural and Mechanical College in
partial fulfillment of the
requirements for the degree of
Master of Science in Electrical Engineering

in

The Department of Electrical and Computer Engineering

by
Vikaram Singh
B.Tech, Ideal Institute of Technology, Uttar Pradesh, India, 2010
August 2018

Acknowledgements

Foremost, I would like to express my profound gratitude towards the committee members Dr. Kidong Park, Dr. Georgios Veronis, Dr. Manas Gartia, Dr. Mehdi Farasat and Dr. Varshni Singh: their encouragement and remarks were inspirational in shaping up this thesis. I am extremely obliged for their able guidance during this study.

My sincere thanks and gratitude to Dr. Kidong Park for his guidance and kind support. My foremost thanks and gratitude to Dr. Varshni Singh at Center for Advanced Microstructures for introducing me to the topic; his engagement and insights were key to this thesis. I am also thankful to Mr. Quoc Nguyen for training me on the equipment and techniques required for my study.

Furthermore; I would like to thanks the members of Center for Advanced Microstructures and Devices for providing the facilities, support, and cooperation. It was a pleasant and enthusiastic environment to work around.

Last but not the least; I am thankful to my friends Vamshi Vasireddy, Kiran Makineedi, Harnath Manikonda, and Manoj Gaddipati for extending their help and kind support during the course of this Masters. I would like to especially thank my family Rachna Singh, Kushal Pal Singh, and Yasasvi Singh for all their love and encouragement throughout my academic career.

Table of Contents

List of Tables

List of Figures

Abstract

X-ray Phase contrast-based Talbot interferometer creates high contrast between weak and strong absorbing materials, which makes it effective in imaging soft tissues. However, its performance is bounded by the aspect-ratio, features and symmetry of its gratings. For 40 KeV energy X-rays, the analyzer grating thickness should be 100 μm or more to achieve > 90% absorption in order to obtain high contrast images. Moreover, the smaller period in grating is desired for higher resolution. Therefore, researchers are exploring various fabrication techniques to achieve greater aspect-ratio gratings. Utilizing modern LIGA techniques, the aspect-ratio of gratings can be improved with a simplified and precise fabrication process. This thesis focuses on the fabrication of gratings with aspect ratio of 25; 100 μm tall and 8 μm period with 50 % duty cycle. X-ray lithography, electroplating and micro-machining were used during the fabrication of these gratings. Also, a silicon nitride based membrane X-ray mask with grating patterns was fabricated to perform X-ray exposure. Multiple approaches were implemented to optimize the processing conditions and parameters for gratings fabrication. The thesis experimentally compared the adhesion of PMMA resist acting as a mold, in which metal gratings were electroplated, to Copper oxide and titanium oxide. For each of two oxides, wafers were prepared separately, starting with depositing copper (Cu) and titanium (Ti) as seed layers and later oxidizing them. Later, both the wafers were bonded with 2.5 mm thick PMMA resist wafer. They are further flycut down to 100 μm and later is exposed at and XRLM-1 beamline at CAMD/LSU. The resist development results are compared and adhesion was analyzed for both copper oxide and titanium oxide.

The adhesion in PMMA resist was better to copper oxide layer in comparison to the titanium oxide. However, titanium oxide is preferable because PMMA molds are damaged during copper oxide etching. Copper oxide, unlike titanium oxide is not conductive which prevents electroplating of gratings; therefore, etching of copper oxide is required. Finally, the wafers were electroplated to nickel and later the resist is stripped. We have achieved gratings with aspect ratio of ~21 with 4.64 μm period and 100 μm height.

Chapter 1
Introduction

Medical imaging has been revolutionized by Talbot Interferometer, which utilizes phase contrast and absorption base imaging to generate high quality images for bones as well as soft tissues and low absorbing materials [1]. Talbot Interferometer is capable of generating high contrast and high-resolution images. Its performance depends on the aspect ratio of analyzer grating. For any structure the ratio of its thickness to its width is known as its aspect ratio. The dimensions of a grating effect the quality as well as resolution of the X-ray images, the taller grating absorbs more photons, thus increases the contrast. Whereas, smaller periods between the gratings increases the resolution and sensitivity. The smaller periods between gratings also reduces the interferometer size [1][2], thereby making it compact. Therefore, in order to enhance the performance, it is essential to achieve greater high-aspect ratio (HAR) for gratings [2]. Figure 1.1, shows the beneficial of HAR gratings over the image. It can be seen that HAR gratings in figure 1.1(b), provide higher resolution and contrast image in comparison to the image in figure 1.1(a). However, the fabrication of high aspect ratio analyzer gratings it has been a challenge. To the best of my knowledge, only 60um tall good quality gratings with aspect ratio of 22 has been reported [48]. However, height of the grating was 60μm, which gives good absorption for low KeV X-rays. For 40 KeV X-rays, to generate high contrast (>90% absorption), the grating should be at least 100 μm tall. This study uses X-ray lithography for fabrication of HAR gratings followed by metal electroplating and some modification in substrate surface. However, fabrication of such tall HAR gratings has several challenges, for example, structural deviation, collapsing structures, cracks, swelling of resist, residues, etc. This

study compares two different type of surfaces to optimize the process parameters to fabricate HAR gratings mold using X-ray lithography followed by metal electroplating. The X-ray lithography is performed at CAMD, the synchrotron source at LSU. X-rays propagating through grating undergoes diffraction which is utilize for contrast imaging.

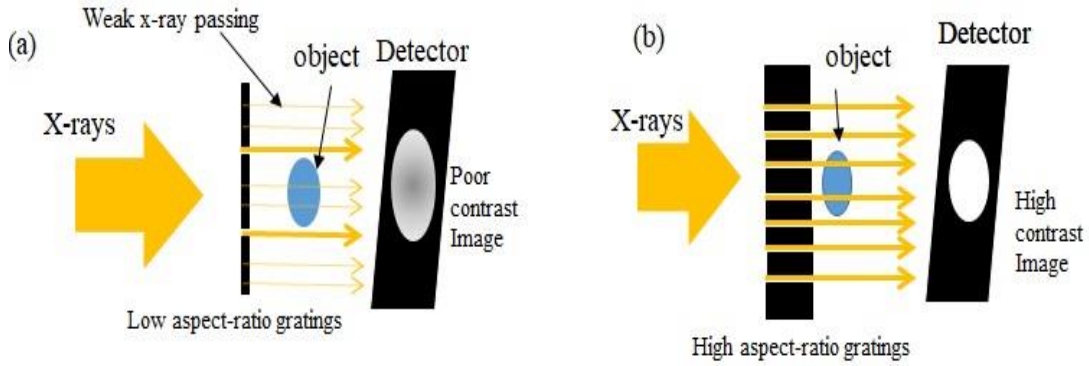

Figure 1.1: High resolution interferometer: (a) Interferometer with low resolution unable to scan a small size sample and (b) Interferometer with high resolution successfully covering a small size sample.

HAR grating were fabricated using LIGA (lithographie, Galvanoformung and Abformung) principle [34]. The fabrication of HAR structures requires; X-ray lithography, hard resist such as PMMA and some modification in substrate surface. [5][9] The fabrication also includes electroplating, micro milling. Debonding and collapsing structures are the major concern during fabrication, they occur because of internal stress between polymer and the metallic substrate, stress between structures due to improper design, overdeveloping of resist or human errors. Several techniques were applied to overcome the fabrication challenges. For example, to reduce internal stress of resist and wafer or stress in between them, the wafer and resist are thermally treated before processing. To reduces stress between the structures, supporting structures were introduced in gratings. Lastly, each LIGA step is processed with great caution to minimize any human

error. The substrate is selected based on its adhesive and conductive properties. Since PMMA is known for poor adhesion to smooth surface a rough seed layer of Copper oxide or titanium oxide is introduced in between substrate and resist to improve the adhesion in between them [50] [56].

The prime focus of the thesis is to fabricate 100 μm tall gratings with the aspect ratio equal to or greater to 25, that can be used in Talbot interferometer.

Chapter 2, presents a literature review on the prior researches in the field of X-ray lithography and fabrication of high-aspect-ratio gratings. The progress in fabrication of grating by silicon etching and X-ray LIGA are mentioned in this chapter.

Chapter 3 is a brief introduction to Talbot interferometer, and the LIGA technology. It describes the working principle of Talbot interferometer and Talbot effect. Also, discusses the X-ray propagation to matter based on that grating dimensions are calculated.

Chapter 4 is a in detail explanation of the fabrication process for X-ray mask and gratings. It illustrates the procedure followed to fabricate the X-ray mask with 1.5 μm thick membranes, surface modification and HAR grating fabrication. In addition, it also provides details of XLRM beamline and X-ray exposure.

Finally, chapter 5 discusses the results obtained from the fabrication of X-ray mask and HAR gratings.

Chapter 2
Literature Survey and Background

The HAR gratings have been fabricated in past using different techniques, this chapter discusses these previous works. Chapter includes three approaches for fabricating HAR gratings, namely; (1) Combination of photolithography and wet Silicon etching, (2) Photolithography followed by plasma dry Silicon etching, and (3) Fabrication by combining UV and X-ray lithography. Over the years, all three of these methods have evolved, resulting in improvement in quality and aspect ratio of the grating. In the end, chapter concludes by summarizing the literature reviews along with brief mention of favorable points and key challenges associated with the fabrication technique for HAR gratings favored in this thesis.

2.1 Grating Fabrication Based on Combination of Photolithography and Silicon Etching.

In last few decades, deep silicon etching in combination with photolithography is being widely utilized to create HAR structures, as discussed by Wu et al. in their review paper. They categorized silicon etching into anisotropic wet etching and anisotropic plasma dry etching [6]. Deep and narrow hole with the aspect ratio of 15-18 were etched into the wafer using wet chemical etching and the dry etching by DRIE [11] [12].

2.1.1 Anisotropic Wet Silicon etching

Utilizing Photolithography and wet chemical etching, Hung et al. created deep silicon trenches with 50 μm depth with 20 μm period on <100> silicon substrate using aqueous $HFAgNO_3$ and HF/H_2O_2 [20]. David et al. [21], fabricated analyzer gratings utilizing E-beam lithography and wet etching, with a period of 2 μm and the aspect ratio

of around 9. Initially, a silicon mold with a 2 μm period and 11 μm depth were created, it was followed by the deposition of gold resulting in 10 μm thick gratings. Figure 2.1, presents the fabricated gold grating, which are used as analyzer gratings in interferometers, giving 75-90 % X-ray absorption at 17.9 KeV [21]. Following previous work, David et al. [51] fabricated two types of gratings; 50% duty cycle and another 25% duty cycle with two different Au deposition methods. Applying first method, the aspect ratio of 12 was achieved and grating structures of 2 μm period and 12 μm height were fabricated with 50 % duty cycle and are shown in figure 2.2.

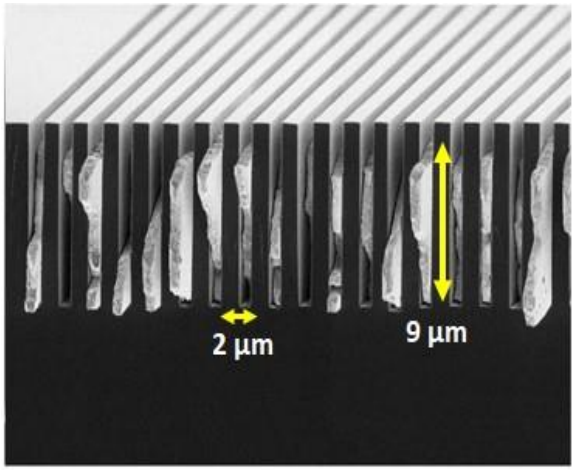

Figure 2.1: Analyzer grating fabricated by David et al. by depositing gold in between groves in silicon mold. These grating are 10 μm tall with 2 μm periods [21].

During fabrication, 1 μm trenches are created by wet silicon etching. Later, aluminum is deposited at 450 as a sacrificial layer by help of evaporation. Further, gold is deposited over the Aluminum by evaporation followed by its etching. Finally, Au is electroplated in between trenches and Au gratings are achieved. Whereas, by second method, gratings of higher aspect ratio of 24 with 2 μm period and 24 μm height were achieved [51]. In this method, trenches with 25 % are created by silicon etching followed by deposition of gold.

Finally, the gold is electroplated over the silicon grating, which figure 2.2 (b) represents. However, the grating fabricated by second method has higher aspect-ratio, the duty cycle is not 50 %, which is critical for interferometer grating [54].

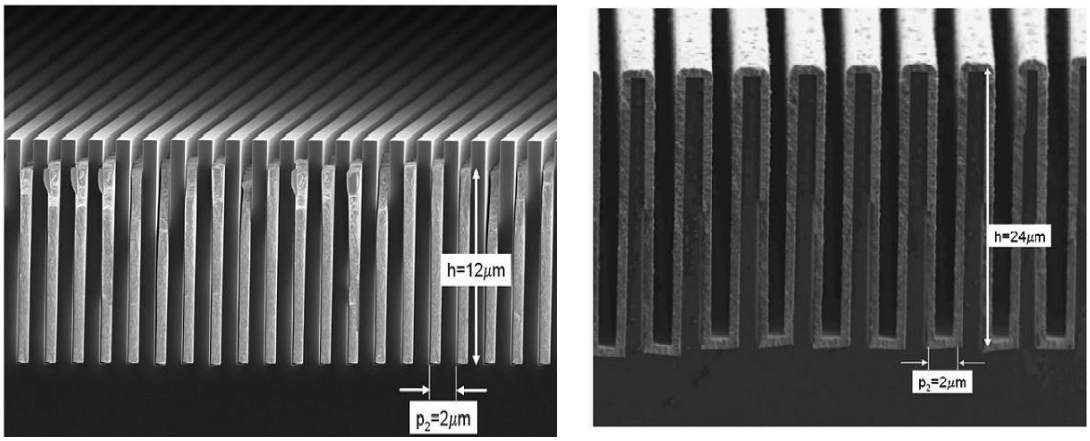

Figure 2.2: The cross section of David's gratings (a) The grating structures 2 μm period and 12 μm high created by wet etching of silicon (b) The grating structures with 2 μm period and 24 μm fabricated by dry etching of silicon [51].

2.1.2 Dry silicon etching

Dry silicon etching or plasma etching is another method which is favored in fabrication HAR gratings. Silicon dry etching provides better definitions to edges and produces in fine and deep rectangular microstructures [15] [16]. Noda, fabricated the high-aspect grating using silicon etching based on reactive ion etching using inductively coupled plasma. However, Noda used two different techniques for the sidewall protection. Initially, the gratings were fabricated by protecting the sidewalls by polymer layers using Bosch process. As a result, the gratings with 20 aspect-ratio with the height 40 μm and period 5.3 μm were fabricated [51]. Second technique uses silicon dioxide by thermal oxidation as a new sidewall protection layer. The grating with height of 60 μm and period of 5.3 μm resulting in aspect ratio of 20 [36]. Keshu et. Al [48], proposed an economical method to

fabricate HAR grating. Instead of using silicon wafer, multiple foils of 20 μm thick TA and 10 μm Al were stacked together, alternatively. These stacked foils are later pressed

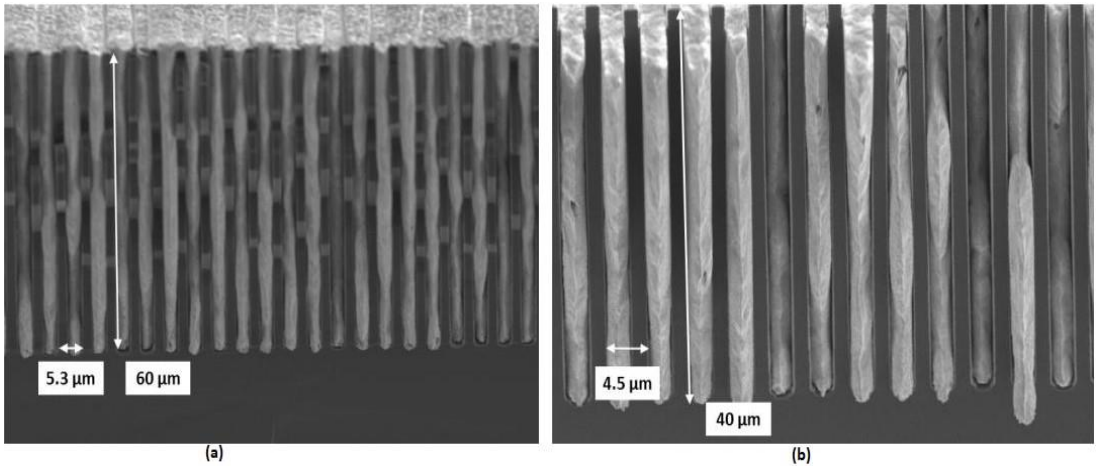

Figure 2.3: The cross section of Nodas gratings (a) The grating structures 5.3 μm period and 60 μm high [51] and (b) The grating structures with 4.5 μm period and 40 μm high absorber structures [36].

between two copper plates at 200 % while being covered under lead-tin solder. Further, the grating patterns are patterned in resist by photolithography. Finally, the silicon is dry etched and the gratings of 600μm and 10μm width are achieved with 60 aspect ratio. However, these gratings were later used as source grating in Talbot interferometer [48]. Further, using similar concept, Tukaji and et all, fabricated a 100 μm thick gratings by stacking two silicon wafers coated with cr/au coating. Au surface of the wafers was intramolecularly bonded face to face by using diffusion bonding.

Afterward, the Silicon on one side of the wafer is polished down to 100 μm and a photoresist is patterned over silicon layer by the help of UV lithography. Later, utilizing the Bosch process, the silicon is etched by plasma etching and trenches in silicon substrates are created.

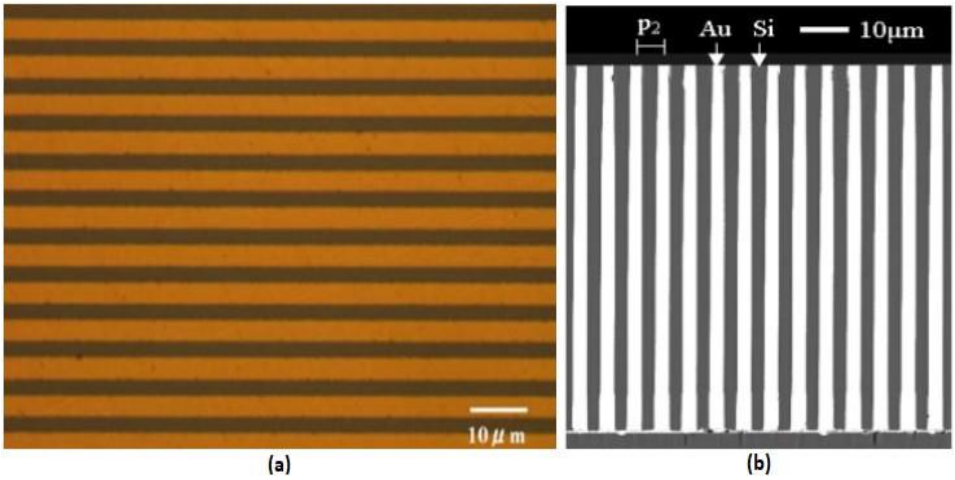

Figure 2.4: The Nodas gratings (a) The top view of the grating structures with 5.8 μm period, and (b) the cross-section view of gratings showing Au and Si structures with 5.8 μm period and 100 μm height. [48]

The etching is continued till the gold surface at the bottom of trenches is visible. Finally, gold is electroplated inside the trenches, resulting in gold grating structures stacked between silicon gratings. Figure 2.4, present a correction view of the fabricated grating of 5.8 μm period and 100 μm height [23].

Silicon etching provides tall gratings with small width. However, deep silicon etching, especially dry etching gives rough sidewalls. Even tough, wet silicon etching has smoother structures profile but the etching rate is slow. Smoother surface can be achieved by adding oxygen during dry etching but it may affect the selectivity [6].

2.2 Fabrication of grating using UV lithography and X-ray lithography.

The process comprises of UV lithography, X-ray Lithography and electroplating. The resist is coated over the substrate, which is processed by photolithography, and electroplating metal in between resist structures.

2.2.1 X-ray Lithography

H. Smith and Spears at MIT first proposed X-ray lithography in 1973 through patent publication [38]. In 1975, X-ray lithography with electrodeposition was introduced by International Business Machines (IBM), where Romanwkiw and others deposited gold in resist trenches, resulting in the metal structures 20 aspect ratio. Later, H. Smith and Spears at MIT achieved seven minutes exposure time for PMMA resist with 3 μm thick mask membrane. It proved that the exposure can be conducted with thinner mask membrane and gold can be used as the absorbent material. In addition, their article showed that X-ray lithography could be used on the silicon devices as well. However, in early stages, many were concerned about the use of X-rays and its progress. Later in 1982, Siemens AG and the Fraunhofer Institute for Solid State Technology conducted a study targeting to produce a small separation nozzle for Uranium enrichment [40]. A plastic mold was fabricated through X-ray lithography using PMMA resist. The mold comprises of identical separation nozzles in a big number, which were later replicated in its corresponding sectional view structures through electrodeposition. The 100 μm thick PMMA sheet was exposed to X-rays using an X-ray mask of 0.25 μm beryllium window and 18 μm gold and copper absorbing structures.

Additional researches conducted by the same collaboration resulted in fabrication of microstructures and sensors. Rigid and high aspect ratio structures were fabricated by introducing titanium as a sacrificial layer. The article published by Becker, E., Ehrfeld includes survey of a part of activities conducted at KNRC [39]. In early stages, X-ray lithography was performed at low radiation synchrotron which led to several hours of exposure time. Thus, restricting the photoresist thickness and structure height. With

increased synchrotron radiation intensity, microstructures with greater structural height are fabricated without much swelling and stress on the photoresist. X-ray lithography provides smooth and well-defined structures wall with aspect-ratio of 1:100 [43]. To achieve extreme structural heights, PMMA resist is bonded over the wafer [19]. Once, this PMMA is exposed to radiation, its long polymer chains start breaking resulting in the decrease of average molecular weight of the PMMA. J. Mohr analyzed the poly-(methyl methacrylate) (PMMA) been used as the resist for X-ray lithography [8]. Center for Advanced Microstructure and Devices (CAMD), LSU initiated a research to fabricate complex high-aspect ratio structures. In 2012, Jinka, studied the micromaching process and fabricated a multi-leveled mold insert with complex, high aspect ratio microstructures [25].

2.2.2. Development of PMMA resist

X-ray exposure breaks the macromolecular chains of the PMMA resist and brings it to solvated state [7]. Later, this solvated area is removed by developing it in a developer. The developer should be a non-swelling and low-stress to minimize debonding of structures [49] [26]. The PMMA dissolution in different developing solution is analyzed and GG developer is best developers for thick PMMA [52]. The fabrication of high aspect-ratio with X-ray lithography on plane and nonplanar surfaces is studied by Marques. It proposes some modification in the LIGA process followed for fabricating high aspect-ratio structures [22]. Similar procedure is applied in this thesis for the fabrication of gratings. Later, the metallic structures were created by electroplating Gold and Nickel in between the PMMA wall.

2.2.3. Fabrication of gratings

Using X-ray Lithography with X-ray mask having titanium layer membrane, Matsumoto fabricated the gratings with 8μm period and 20 μm thickness, resulting in an aspect ratio of 5. The X-ray mask was prepared by using narrow-pitch optical mask and UV lithography followed by Au electroplating and resist striping. These gratings were used in interferometer for 17.7 KeV X-ray energies [29]. Further, in 2007, Noda et al. fabricated the grating structures by using SU-8 negative resist and X-ray mask with Ti windows. Initially a silicon wafer coated with 0.25 μm thick Ti layer is selected as substrate for X-ray mask. This wafer is spin coated with Su-8 negative resist, which later is processed through UV lithography followed by Au plating resulting in Au patterns. Ti membrane is created on X-ray mask by Ti etching and Si etching, respectively from the backside. The final Au patterns were of 8 μm width and 4μm thickness. Later, the gratings are fabricated by exposing the 30 μm thick spin coated SU-8 resist to X-rays, followed by resist developing and Au electroplating. Final Au structures were achieved with 29 μm height and 8 μm period. [36] Later, improving over the previous results, Noda, fabricated gratings with an aspect ratio of 12, having period of 5.3 μm and thickness of 33 μm using the same mask. The figure 2.5 (a), shows the resist molds fabricated by the figure 2.5 (b), represents the fabricated grating by Noda et. al, showing the height of 29.1 μm [32]. Later, Noda uses X-ray mask with carbon membrane as carbon has extremely small thermal expansion coefficient [33]. The X-ray mask was fabricated on 6-inch carbon wafer with gold grating patterns of 5.3 μm period and 4 μm height.

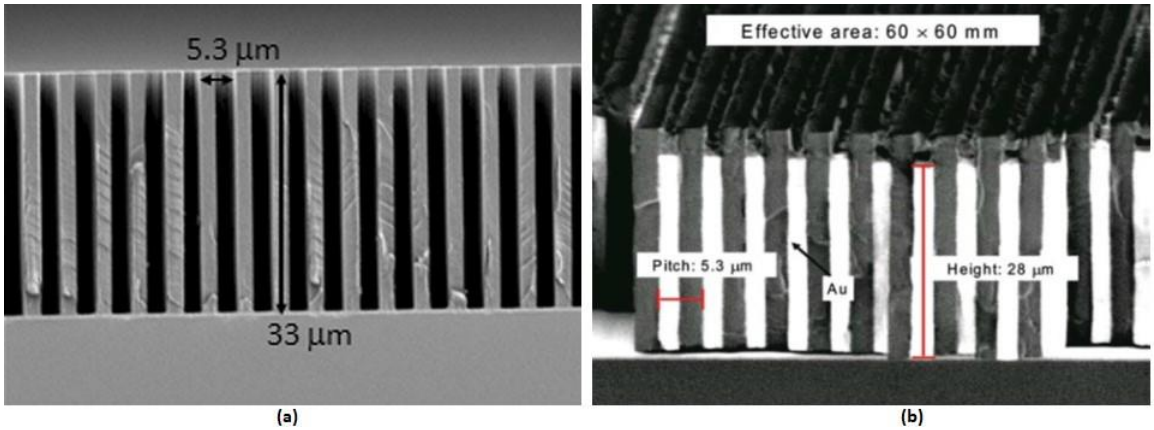

Figure 2.5: The cross section of Noda's gratings (a) The grating structures 5.3 μm period and 33 μm thickness and (b) Photograph of X-ray mask with 5.3μm period.

The wafer is coated with SU-8 resist for 40 μm thickness and was exposed to X-rays in presence of carbon membrane X-ray mask. Further, this X-ray exposure was followed by resist development and gold electroplating. As the result, grating with 40 μm height and 5.3 μm period with an aspect-ratio of 14 μm were achieved [34].

2.3. Summary

This literature review highlights the major advancement in the field of fabrication of HAR gratings. The review mentions the studies conducted for the fabrication High aspect-ratio gratings and the dimension of gratings achieved by these studies.

- Both anisotropic wet and dry etching, and X-ray lithography techniques used for grating fabrication have successfully resulted in HAR.
- The grating fabrication by the combination of photolithography and silicon etching achieves greater aspect ratio and taller gratings but deep silicon etching results in rough structures profile.
- Grating fabricated with UV lithography and X-ray lithography has have high aspect

ratio but 40 μm thickness is only good enough for X-rays 17.7 KeV energy. However, this study the gratings are fabricated for 40 KeV application. Thus, for 90 % X-ray absorption, 100 μm tall gratings are required.

This study adopts on the fabrication technique based on the combination of UV lithography and X-ray lithography and uses the synchrotron radiation facility at LSU,

Chapter 3
Introduction to Grating Interferometer and LIGA Techniques

3.1. Talbot Interferometer

3.1.1. Talbot Effect

In 1836, Henry Fox Talbot discovered Talbot effect [41]. According to him, when a plane periodic wavefront passes through an object, it reconstructs object's transfer function patterns, known as self-images, at regular intervals away from the object. The distance between the object and its self-image is known as Talbot distance. This phenomenon is called as Talbot effect.

The Talbot distance is given by $Z_t = m \times g^2/\lambda$ where, λ is the wavelength and 'g' is the period of the grating. It is near-field diffraction effect and it is quite similar to far field diffraction considering the fact that all the waves that are transmitted through different windows diffracts and interfere with one another, here 'z' is the distance from grating.

3.1.2. Working principle for Talbot Interferometer

Talbot interferometer working principle is based on Talbot effect. When X-rays from an incoherent or a coherent source hits a phase grating with a period *p*, they get diffracted by the order of ±1 and propagate with some deflection angle $\theta_s = \lambda/p$. These diffracted waves produce an 'interference pattern' on a certain distance, also known as 'self-images'. The interference pattern from phase grating is superimposed on an absorption grating G_2, which has a similar grating period as G_1. Then the opening of analyzer grating coincides with the minima of interference pattern's intensity. Thus, detector observes only the low intensity levels. As the wave is refracted through an object, its phase changes. Talbot interferometer is sensitive to these phase changes. To measure

the angle of refraction in wave, the phase displacement is calculated in interference pattern recorded at the detector. This phase displacement can be calculated either by phase stepping method or Moire method [44]. Figure 3.1, presents the schematic diagram of Grating based Talbot interferometer setup.

3.1.3. Gratings used in Talbot Interferometer

Talbot interferometer uses three different gratings; therefore, it is also known as grating interferometer. Depending on their working in Talbot interferometer, the gratings are categorized as follows.

3.1.3.1. Phase Grating

The phase grating is used to create phase shift of π or $\pi/2$. They are binary grating with 50% duty cycle and generates the maximum contrast at Fractional Talbot distance which is given as:

$$Z_{tn} = m \times \frac{Z_t}{16} \tag{3.1}$$

The fractional Talbot distance Z_{tn} changes to D_{tn} when 'm' is odd.

$$D_{tn} = \frac{{g_1}^2}{8\lambda} \tag{3.2}$$

where, g_1 is the period of phase grating G_1. To have most intense interference pattern, the incoming X-ray waves should be diffracted by the order $m = \pm 1$, which acts as a perfect beam splitter.

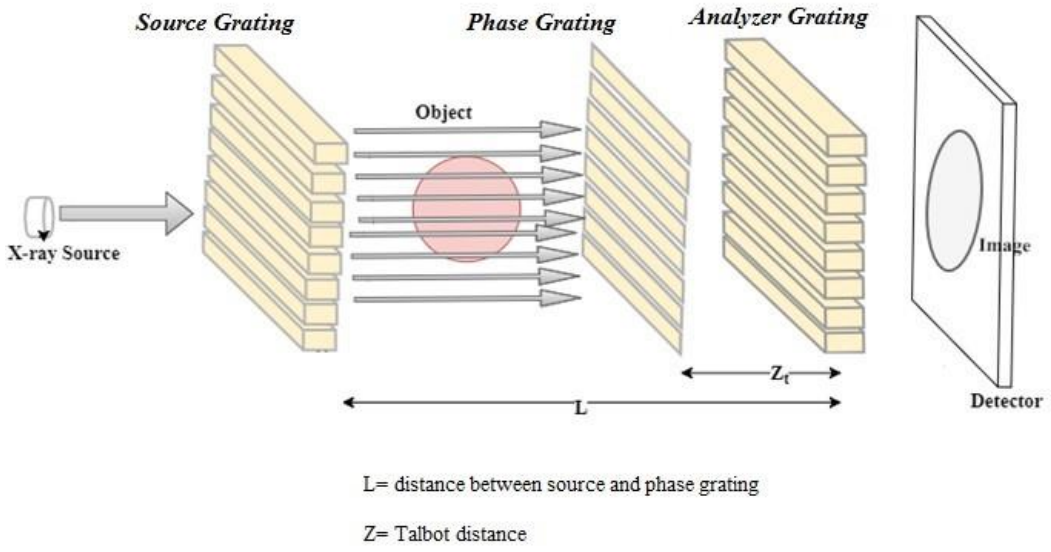

Figure 3.1: Grating based Interferometer

It can be achieved better by π phase grating. The grating designed to achieve π phase shift will produce interference pattern of $g_1/2$ period. Whereas, $\pi/2$ gratings will generate interference pattern with same period as phase grating.

These gratings are made of silicon since it is a low X-rays absorbing material. The height of Phase grating is calculated for phase change π. The phase shift is given as $\Delta\varphi = \delta\bar{k}\,\bar{r}$. Since $\bar{r}$ is the distance traveled by the wave, it can be replaced by $'h_1'$, the height of the grating. Thus, the phase sift equation is given as,

$$\Delta\varphi = \delta k \bar{h}_1 \tag{3.3}$$

further,

$$h_1 = \frac{\Delta\phi}{\delta k} \tag{3.4}$$

as $k = \frac{2\pi}{\lambda}$

$$h_1 = \frac{\Delta\phi}{\delta 2\pi\lambda} \tag{3.5}$$

Depending upon the required phase change, the value of $\Delta\varphi = \pi/2$ *or* π or $\delta = 2\pi\rho_a (Z+ f^0) r_0/k^2$ as mentioned in the previous chapter. To obtain good sensitivity and small setup, the period of G_1 should be in order of few micrometers. For the study, the period of $4\mu m$ is selected for phase grating. The trench width of grating is given as $t_1 = g_1 \times dutycycle$. The interference pattern formed behind phase grating G_1 is the function of the distance between phase grating G_1 and analyzer grating G_2, and changes periodically along z-axis [42].

3.1.3.2. Source Grating

The source grating is used to create multiple X-ray sources. They are kept in between X-ray source and the sample. The period of source grating is given by;

$$g_0 = g_2 \times \frac{L}{Z_t} \tag{3.6}$$

where, L is the distance in between source and the analyzer grating G_2. The source grating is also made of gold and the height of the grating is controlled by the absorption needed at the grating G_0.

3.1.3.3. Analyzer grating

To detect the interference fringes produced by the G_1 (phase grating), G_2 is placed. Behind the analyzer grating is a detector with large pixels compared to the grating period. Since the detectors have large pixels, they are incapable of differentiating interference fringes from G_1, thus G_2 is used. The pixel size of the detector also limits the period size of G_1 and G_2. The analyzer grating is an absorption grating, with period similar to the interference pattern $g_2 = g_1$, when the phase change is $\pi/2$ and $g_2 = g_1/2$, in case of π phase change. This study considers that G_1 grating is designed for $\pi/2$ phase change. Thus, the period of G_2 is similar to G_1 with 50% duty cycle. G_2 is made of gold as it is high X-ray

absorbing material and the height of the grating is limited by the absorption (it should be around > 90%). Greater absorption will produce better contrast in the images.

3.1.4. X-rays propagation in a Matter

Since X-rays are preferred for phase contrast imaging due to their better penetration and low absorption while passing through matter. To study the propagation of X-rays, let us consider the case of a monochromatic plane waves passing through a slab of matter. The wave equation propagating through a material is given by

$$\Psi(\bar{r}) = E_0 e^{ik.r^-} \tag{3.7}$$

n in above equation is the refractive index of the matter is given by

$$n = 1 - \delta + j\beta \tag{3.8}$$

The real part $(1 - \delta)$ in the above equation indicate the propagation of the wave in the medium. Whereas, the imaginary part $(j\beta)$ indicates the attenuation of wave in the medium. Both δ and β values depends on the material properties and the wavelength of the wave.

$$\delta = \frac{2\pi\rho_a Z r_0}{k^2} \tag{3.9}$$

where, ρ_0 is the atomic density of the material, r_0 is the classical electron radius and is given by $2.82X10^{-5}A^0$, Z is the atomic number and $k = |\bar{k}| = 2\pi/\lambda$ is the length of wave vector.

Near the absorption edges the index of refraction is changed by the dispersion correction f^0, and since the gratings are similar to edge, the equation is given by

$$\delta = 2\pi\rho_a(Z + f^0)r_0/k^2 \tag{3.10}$$

While,

$$\beta = \frac{\rho_a \sigma_a}{2k} \tag{3.11}$$

where ρ_a is the atomic density of a material while σ_a is the atomic number of a material used. When wave passing through a medium having a refractive index 'n', it will go through attenuation and phase shift [45]. The change in phase is given by

$$\Delta\varphi = \delta \bar{k}.\bar{r} \tag{3.12}$$

The intensity of the wave is given by;

$$I = |E_0 e^{-\beta k r}| = I_0 e^{-2\beta k r} = I_0 e^{\mu r} \tag{3.13}$$

where $\mu = 2k\beta$ is the linear absorption coefficient and 'r' is thickness of the material, transmission coefficient (T) is given as

$$T = 1 - I \tag{3.14}$$

Using above equations 3.13 and 3.14, the absorption and transmission through gold grating is calculated and presented in Table 3.1, the energy of X-rays is assumed to be 40 Kev.

Table 3.1: Absorption and transmission at gold gratings with different thickness exposed to X-ray energies of 40 KeV.

Height of Grating	50 μm	100 μm	150 μm	200 μm
Attenuation (%)	71	91.2	97.2	99.2
Transmission (%)	23	8.8	2.6	0.8

3.2 LIGA

LIGA is the German acronym to Lithographie, galvanoformung, and abformtechnik. It is the combination of lithography, electrodeposition and molding, and

was introduced in 1982 [5]. Depending upon the final product, lithography is followed by electrodeposition or molding. Electrodeposition results in metallic structures while molding gives plastic structures.

3.2.1 Selection and Preparation of Substrate

As figure 3.3 indicates, the process starts with the selection of primary substrate. This substrate can be a wafer made of a dielectric material such as silicon, titanium, graphite or a polished disc of beryllium. The substrate layer should be conductive. Thus, the wafer is coated with a thin layer of gold, Titanium, Cu, etc. In some cases, a metal adhesive layer is needed to deposit metal over silicon wafer. Therefore, a very thin layer of metal adhesive layer is coated through deposition.

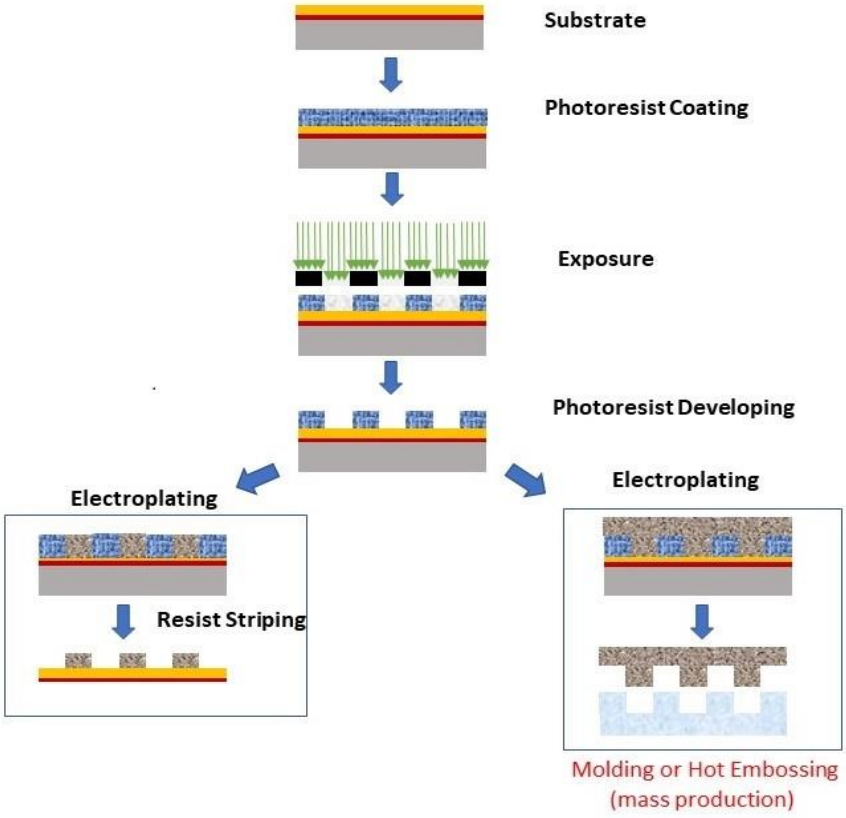

Figure 3.2: The LIGA process

3.2.2. Selection of photoresist

After preparing the substrate, photoresist is uniformly coated over the conductive side of the wafer. Depending on the resist type, coating can be done by resist spinning, bonding or lamination. Photoresists are made of photon sensitive polymer, which either gets polymerize or photosolubilize when exposed to the light. Other component of photo resist can be solvent, sensitizers, and other additives depending upon its application. Sensitizers in resist dictates the reaction in polymer resulting in either photosolubilization or crosslinking of the polymer. Photoresist, based on their tone can be categorized into two types: positive resist and negative resist. Figure 3.3, represents the behavior of both negative and positive photoresist when they are exposed to photons.

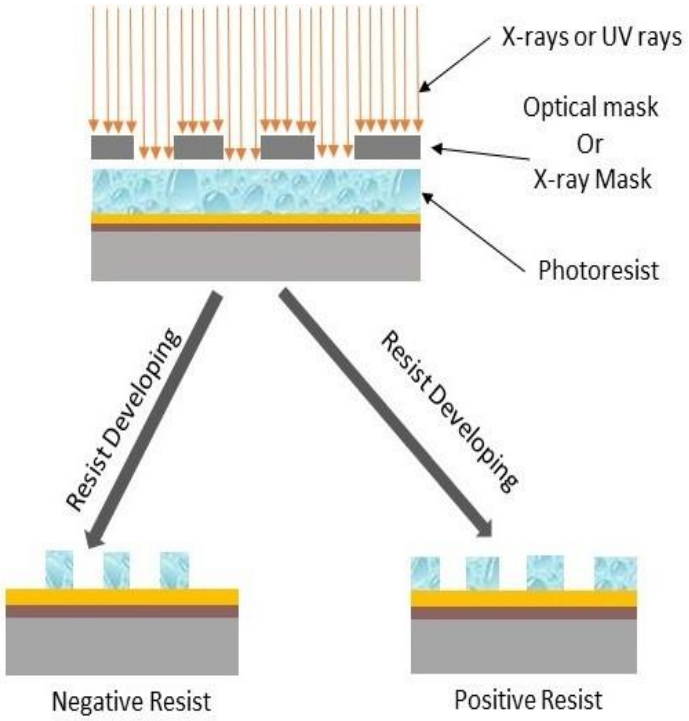

Figure 3.3: The behavior of negative and positive resist when exposed to UV rays.

The exposed area of negative resist gets polymerized and it will not dissolve in developer. Whereas, the unexposed area will dissolve in developer. As a result, only unexposed area will be removed in developer. Therefore, for negative resist, the mask contains photographic inverse of the pattern that is needed to be transferred on the wafer. In case of positive photoresist, the bonds will break in the exposed area and developer will remove the exposed area while the unexposed area will remain on the substrate after developing. Therefore, the mask patterns are transferred as they are on the wafer.

3.2.3 Baking of Photoresist

After spin coating the photoresist, it is heated at a specific temperature and for a specific duration, which is called soft baking. The resist has solvent contents which help them in spreading uniformly, however it creates issues in post processing. Therefore, these solvents are diffused by soft baking. Baking the resist helps in reducing built in stress. It also helps in improving the resist adhesion, eliminates the popping and bubbling in resist caused by nitrogen produced during photo exposure. Also, soft baking restricts dark erosion, thus helps in improving the resolutions. By diffusing solvent component, the risk of mask contamination is also avoided.

3.2.4. Photo exposure

Depending on the wavelength, the light source can be UV, X-ray and E-beam. During the exposure a mask is placed in between the light source and the photoresist. The mask has pattern made of low and high light absorbing materials. The part having low light absorbing material will expose the aligned area of photoresist. Whereas, the high absorbing material on mask will cover the photoresist aligning to respective area. This causes a pattern on the photoresist; this mask is made with specific patterns.

3.2.5 Development of photoresist post exposure

After exposure, the irradiated resist is developed under a developing solution. Depending on the tone, resist can be baked after the exposure. Photoresist requires base solution known as developer for the development. While developing, the variation in dissolution properties of the exposed photoresist is determined by the solubility rate of the photoresist. Depending on the type of photoresist, its reaction with developer changes. During development of negative photoresist, the unexposed resist is removed away, while the exposed area stays. It is vice-versa in case of positive resist. The time of resist development depends on the adhesion in between wafer surface and the resist [28] [34].

3.2.6 Electrodeposition of Metal

Post developing, a pattern is created in the photoresist, where deep trenches will expose the conductive surface of the wafer. Later, metal can be deposited in the exposed surface through deposition or electroplating. The resist structure provides support to the metallic walls. It is important that the selected resist should not be reactive to plating solution. The temperature of plating solution, pH, the current density at which metal is plated and the area to be plated are few key parameters needed to be set while plating.

3.2.7 Resist stripping

After the completion of plating process, the leftover resist can be stripped off by using chemical agents or photo exposure. The chemical agents are selected as per their etching rate to the material that has to be etched. The etching can be categorized as wet etching and dry etching. Whereas resist stripping is done to clean the resist from the wafer after structures are achieved. Each resist has a selective reaction to certain chemical known

as resist remover. Depending upon the required final product, the electroplating can be followed by hot embossing, as shown in figure 3.2.

Chapter 4
Development of Fabrication Process for Gratings

This chapter gives an insight to the procedure followed during fabrication of gratings. The aim of the study is to keep the width of gratings as low as possible which can be used to detect small pixel.

4.1 Desired dimension of the Grating

The aim of this study is to fabricate gratings of 100 μm height with the period of 8 μm and 4μm width. According to equation 4.1, the Lamberts law, a 100 μm thick gold structure will provide approximately 92 % absorption of X-ray at 40Kev. For high contrast images, the X-rays absorption should be greater than 90%, and a 100 μm thick grating structure fulfill this requirement. The study uses nickel at the grating material but similar results can be replicated by replacing it with gold. Figure 4.1, displays a schematic diagram for the target grating structure.

$$I = I_0(\exp -\mu\rho g) \tag{4.1}$$

Where g= is the thickness of the gold material, μ = mass absorption coefficient and ρ is the density of a material. therefore,

$$g = \frac{1}{-\mu\rho}(ln\frac{I}{I_0}) \tag{4.2}$$

4.2 Overview to Fabrication Process

The fabrication process followed in the study is displayed in figure 4.2 through a schematic diagram. The left side of the figure 4.2 is the procedures followed during fabrication of gratings. Whereas, the right side represents the fabrication process for X-ray mask.

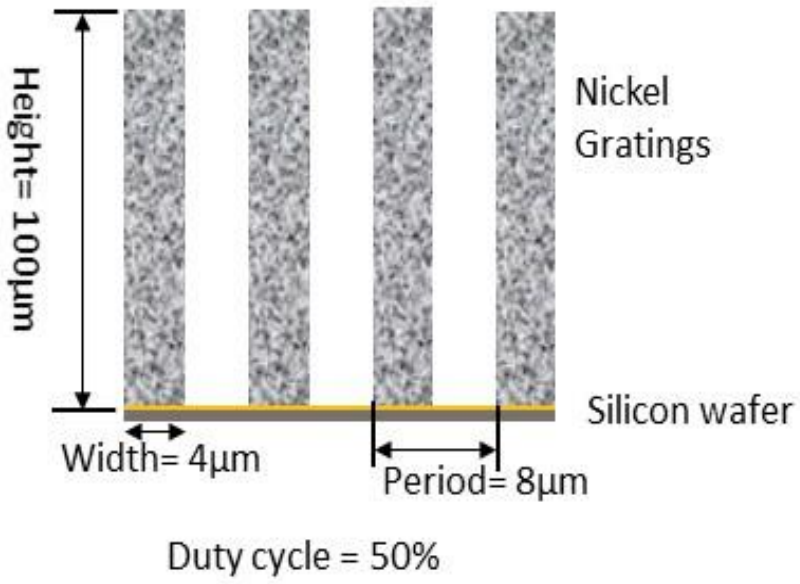

Figure 4.1: The schematic diagram of the grating desired as the end result of the study

In X-ray lithography, collimated x-rays are used as the exposure energies. X-rays provides higher lateral resolution and penetrating power; therefore, they are used for fabricating HAR structures. X-ray lithography is performed in a synchrotron facility at CAMD, LSU. The beamline holds an X-ray mask and a substrate on its rear end and operates at very high vacuum. In the beamline, X-rays passes through the X-ray mask and irradiate the PMMA resist on the substrate. Figure 4.3, demonstrates this process in a simple schematic diagram. Once, the PMMA resist is irritated, it is developed in the resist developer. Further, the metal is deposited into the resist mold created by resist development. The hard resist structure provide support to the metal structures, helping in achieving high-aspect ratio. In order to strip PMMA resist, the wafer is exposed to X-rays without the mask. Finally, the exposed resist was developed in developer and acetone, resulting in metal grating structures on the wafer.

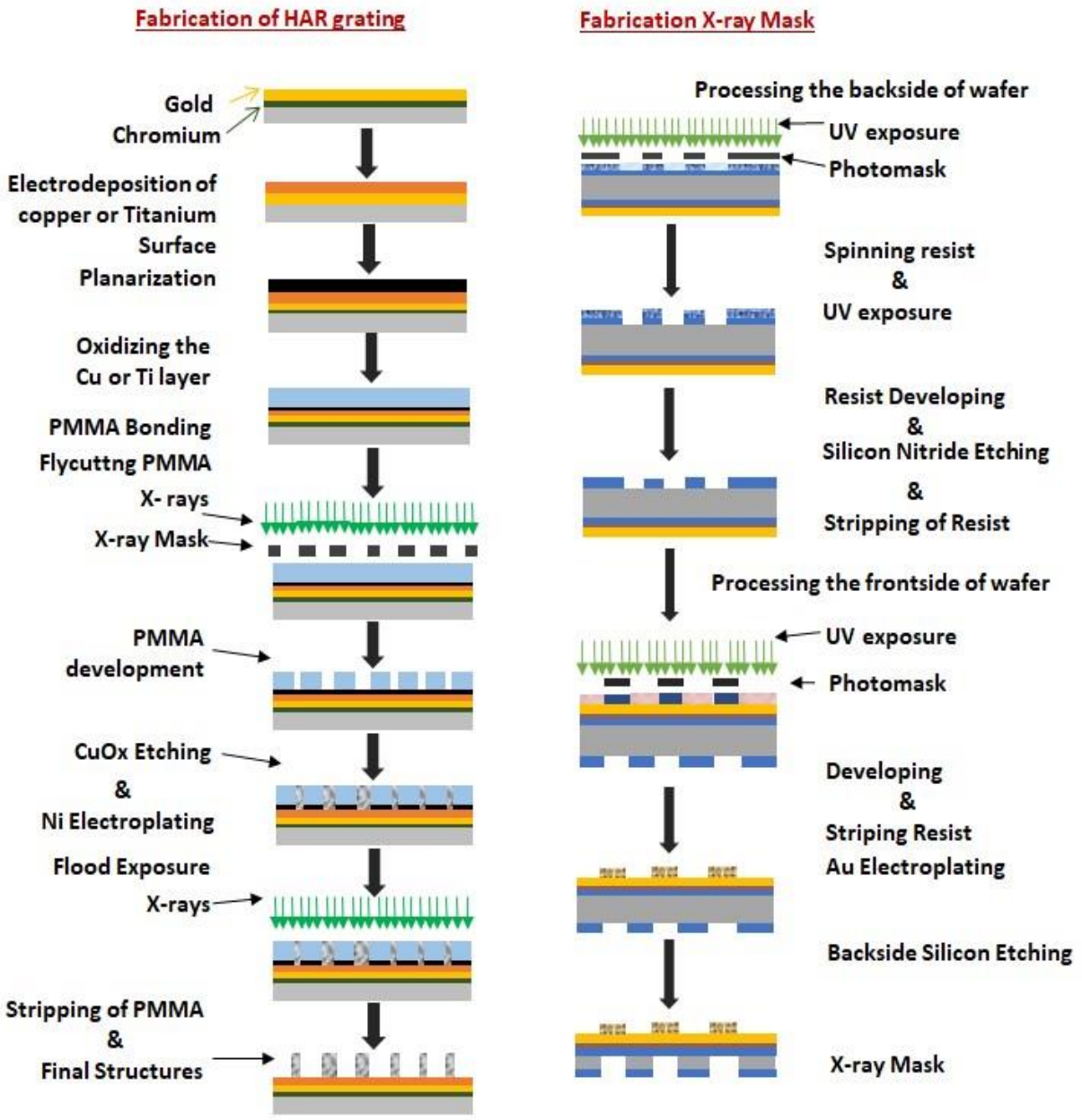

Figure 4.2: The schematic diagram presenting an overview of the procedure followed during fabrication of grating and X-ray mask.

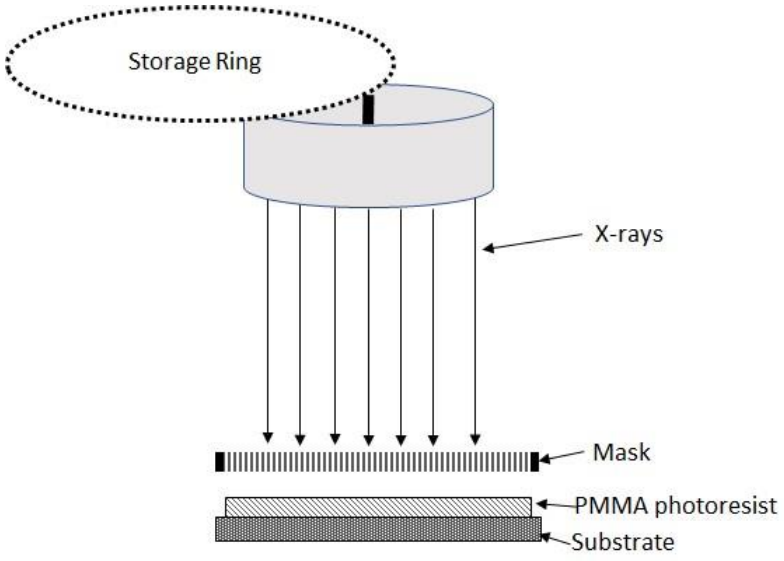

Figure 4.3: Schematic diagram of an X-ray lithography system

Design of HAR Gratings and X-ray mask: During X-ray lithography, X-ray beam is passed onto the resist through an X-ray mask. Thus, the patterns of X-ray mask are transferred to the resist. In case of positive resist, the grating patters are identical to the patterns on X-ray mask. Whereas, the pattern on negative resist are inverse to the patterns on X-ray mask. The patterns of X-ray mask depend on the patterns of photomask used during UV lithography. The photomask also known as optical mask is made of soda lime glass and patterned with chromium. The chromium blocks UV-rays, while soda lime glass acts transparent to them. The photomask used in this study has 9 square cells. Each cell is comprised of parallel lines with 4μm width having 4 μm gap in between them. This constitute of grating patterns with 8μm period with 50% duty cycle. Figure 4.4, represents the schematic diagram of photomask used for the fabrication of X-ray mask. The photomask has alignment marks marked at its corner top surface. These marks help in aligning the wafer with the mask during exposure.

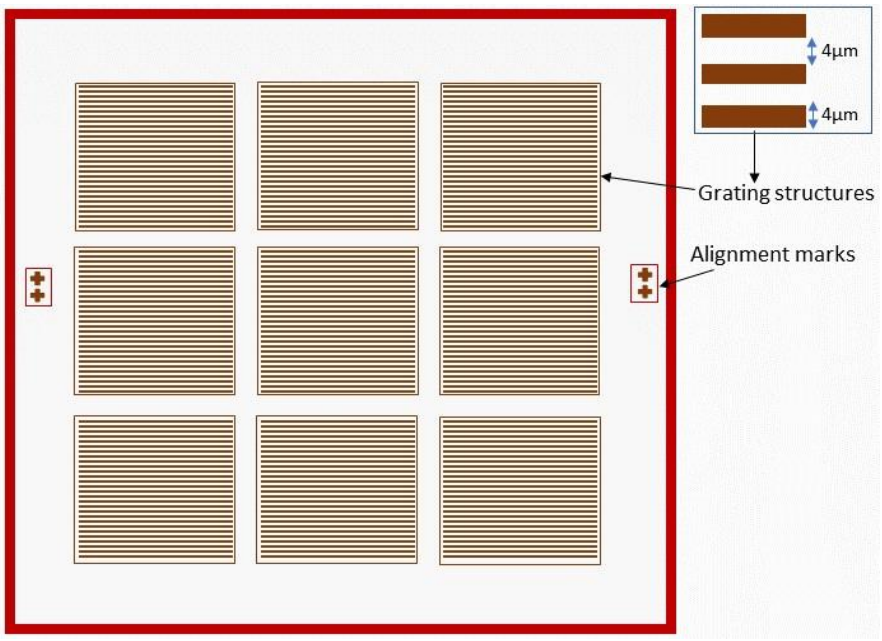

Figure 4.4: The photomask used during UV exposure to fabricate the X-ray mask

4.3 Fabrication of X-ray mask for X-ray lithography

In X-ray lithography is similar to shadow printing, where the patterns of an X-ray mask are transferred on the photoresist. The properties of X-ray mask differ from the normal photomask. It is patterned with a combination of low and high Z (atomic number) materials. The high Z materials are good absorbent of X-rays, thus block them from reaching the resist. Whereas, low absorbing materials acts transparent to X-rays. The mask and the substrate are kept in close proximity, allowing a good exposure. Fabrication of X-ray mask is a very complex procedure, it requires precise alignment of patterns on both backside and front side of the wafer, and it should be handled very carefully while etching because any turbulence can damage the silicon nitride window membrane. The schematic representation for X-ray mask fabrication is presented in figure 4.5. The following part of this section discusses the fabrication process of X-ray mask.

4.3.1 Preparation of substrate for X-ray mask fabrication

For the fabrication of X-ray mask, a 4-inch silicon wafer <100 > having silicon nitrite coating on its both sides are selected. Silicon nitrite is a low absorbent of X-rays; thus, its membrane is transparent to them. On the other side of the wafer, the layers of chromium and gold is coated by e-beam evaporation under vacuum. This side of the wafer is considered as its frontside. The thickness of wafer is 525 μm including chromium and gold layer. Gold provides conductivity to the wafer while chromium acts as adhesive between gold and silicon surface

4.3.2 Resist selection and its coating on the wafer

X-ray mask fabrication includes two different photoresists. The windows on the back side of the mask are patterned with the help of a positive resist S 1808. Whereas, the front side, grating structures are created by patterning NR 26 8000P negative resist.

Coating of Photoresist by resist spinner*:* The resists used in fabricating X-ray mask are viscus solutions. They are coated over the substrate by the help of a resist spinner. Initially, the resist is poured over the wafer, which is placed at a chuck attached in the center of the spinner as figure 4.6 indicates. The resist should be poured very carefully to avoid any turbulence since it can trap air in resist causing bubble in the coated layer. These bubbles are hard to remove and creates deformations in grating patterns. Later, the rotation speed and time is set for the spinner, and the wafer is rotated. Due to centrifugal force the resist will spread uniformly over the wafer. The thickness of the coated resist depends on its viscosity, molecular weight and the rotation speed of the wafer. High rotation speed reduces the thickness of coated resist.

.

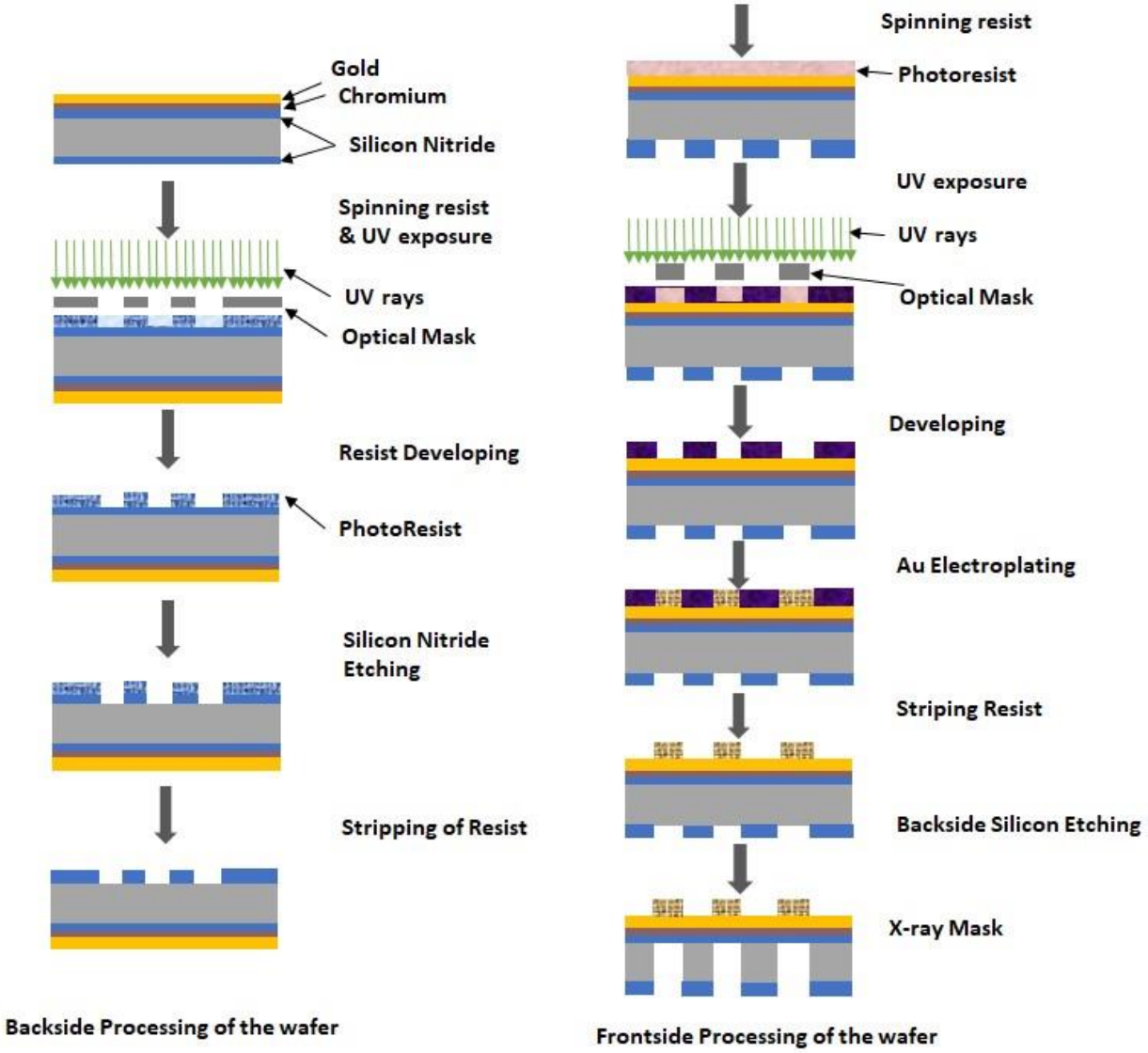

Figure 4.5: Schematic diagram of X-ray Mask fabrication

The equation 4.3, establishes the relation between resist thickness and other factors.

$$T = \frac{KC^{\beta}\eta^{\gamma}}{\omega^{\alpha}} \tag{4.3}$$

where, T is the thickness of the resist, K is the calibration constant, C is the polymer concentration, η is the intrinsic viscosity, ω is the spinner rotation speed (rpm) and α, β & γ are the exponential factors.

4.3.2.1 Soft baking of resist and UV exposure

Once the resist is spin coated, it is baked on hot plates, this process is known as soft baking. It reduces the solvent from the resist and improves the adhesion between resist and wafer. Post soft baking, the wafer is cooled down in a chamber and transferred to the exposure system, where it is exposed to UV radiation. The polymer in resist, reacts to the

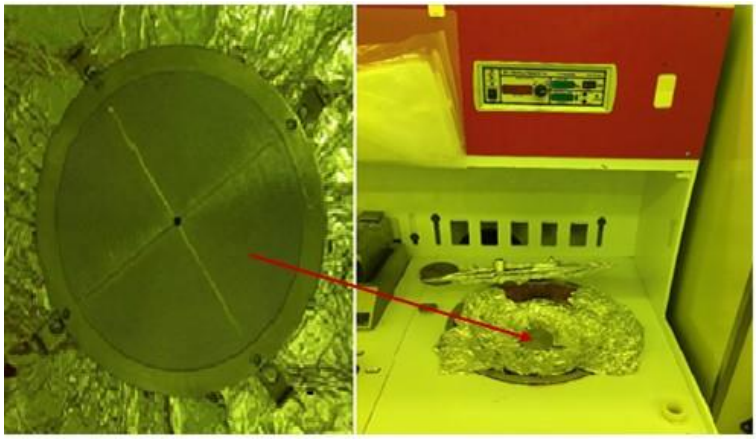

Figure 4.6: Headway Research PWM101 Light Duty Photoresist Spinner

UV radiation according to the tone of resist. The UV rays passes through photomask and irradiates the photoresist, imprinting the features of photomask onto the wafer.

Procedure for UV Exposure: Photoresist on the wafer is exposed to UV-rays at *Quintel UL 7000-OBS Aligner and DUV* Exposure Station acting as the UV source as image in figure 4.7 indicates. An optical mask (photo mask) placed on the platform and the vacuum is switched on to fix the mask. While placing the mask the metal side of mask should be facing towards the resist. After placing the mask, the wafer with resist is loaded on the spindle that goes under the mask. The contact switch is switched on it should turn red from green as soon as the wafer is placed under the mask. By switching on the contact, the wafer comes in close proximity of the mask. The UV-rays is passed through the optical mask and

hits the resist. An UV filter glass is placed on the top chamber. Before exposing, the exposure time is calculated based on the resist type, height of resist layer

Figure 4.7: Quintel UL7000-OBS Aligner and DUV Exposure Station

and the intensity of UV-rays. he UV-ray intensity is considered as an average of intensity meter reading at three different locations on the wafer.

$$\begin{aligned} exposure\ time &= \frac{height \times exposuredose}{Measuredintensity} \\ &= \frac{14 \times 70}{5.19} \\ &= 164seconds \end{aligned} \tag{4.4}$$

4.3.2.2 Developing the Resist

Photoresist requires base solution known as developer for its development. Exposing the photoresist brings variation to photoresist dissolution properties. While developing, this variation in dissolution properties defines the solubility rate of the photoresist. Depending on the type of photoresist, its reaction with developer changes. During development of negative resist, the unexposed resist is removed away. Whereas, the exposed area stays, and

vice-versa in case of positive resist. Over developing should be avoided as it may cause the structures to fall.

4.3.2.3. Etching and Resist Striping

Chemical agents are used to remove material layers. They are selected according to their etching rate to the material which has to be etched. The etching can be categorized in wet etching and dry etching. Whereas resist stripping is done to clean the resist from the wafer after structures are achieved. Each resist has a selective reaction to certain chemical known as resist remover.

4.3.2.4. Design of Experiment DOE

The DOE technique is the systematic approach to developed the experimental parameters based on the information collected through varying multiple inputs and observing their effect on the desired outcome. During fabrication of X-ray mask, the changes in resist patterning is studied by varying the processing parameters for silicon wafer and silicon wafer coated with Cr/ Gold.

The variations in resist spinning speed, soft baking time and temperature, exposure dose and duration, Post baking time and temperature and exposed resist development are closely monitored and final processing parameters are established, which are used for patterning the frontside and backside of the wafer. The table 4.1 and 4.2 are accounting the data excreted from the iterations of wafer processing for different variables.

Table 4.1: Establishing the processing parameters by DOE

Optimizing the softbaking parameters for NR 26 8000 resist.		
Test.	Soft baking Temp/Time	Comment
1	120^0C for 220 seconds	The final outcome indicates the photoresist is under baked.
2	135^0C for 200 seconds	Under baking of photoresist l
3	135^0C for 220 seconds	Under baking of resist
4	150^0C for 200 seconds	Photoresist is slightly overbaked.
5	150^0C for 180 seconds	Results were good.
Optimizing the UV exposure dose for NR 26 8000 resist.		
Tests	UV Exposure dose	Comment
1	150 mJ/cm^2	The trenches in between resist structures are widen, indicating that exposed photoresist is still soluble.
2	165 mJ/cm^2	The photoresist was properly developed with no resist residue.
3	190 mJ/cm^2	The photoresist residue at the bottom of developed area. Indicating slight polymerization of unexposed photoresist.
Optimizing the postbaking parameters for NR 26 8000 resist.		
Tests.	Postbaking Temp/ Time	Comment
1	70^0C for 360 seconds	The resist structures were under developed. The structures were thin.
2	80^0C for 360 seconds	In some area photoresist structures were undeveloped. Structures were thin.
3	90^0C for 360 seconds	The photoresist structures were not developed, wafer was over baked

Optimizing the postbaking parameters for NR 26 8000 resist.		
Tests.	Postbaking Temp/ Time	Comment
4	90^0C for 300 seconds	Photoresist is slightly overbaked.
5	90^0C for 300 seconds	Results were good.

Table 4.2: The developing parameters for NR 26 8000 resist.

Test	Time in 100% RD8	Time in 20% RD8	Comment
1	60 secs	4 mins	Photoresist was underdeveloped and wafer surface had resist residue.
2	60 secs	4 + 4 mins	Photoresist was underdeveloped and wafer surface had resist residue.
3	60 + 10 secs	4+ 2 mins	Photoresist was underdeveloped and wafer surface had resist residue. .
4	60 + 20 secs	4 + 3 mins	Photoresist was slightly underdeveloped.
5	60 + 20 + 20 secs	4 + 3 + 3 mins	Results were good.

4.3.3 Recipe for processing backside windows on the wafer

The fabrication of X-ray mask is done on < 100 > silicon wafer, which both sides are coated with 1 μm stress controlled LPCVD silicon nitride. The deposition process parameters are designed to minimize the stress in silicon nitride. Later, a positive resist S 1808 is spin coated over the selected wafer in a resist spinner. The wafer is spun at 4000 rpm for 30 seconds and then soft baked at the hot plate at 115^0 c for 60 seconds. After cooling down the wafer of 10 minutes it is exposed to UV-rays at Quintel UB7000 exposure system.

The UV-rays are passed through a photomask having 9 rectangular cells patterns, which are transferred on to the photoresist. The wafer is exposed to UV rays for the Exposure dose of 150 mJ/cm^2 for 26.5 seconds. The exposed resist on the wafer is developed for 75 seconds in MF 319 developer and later rinsed under DI water for 4 minutes. After resist development, silicon nitride underneath the exposed resist is exposed, which is further etched by using dry silicon nitride etching. The etched silicon nitride, will open up the silicon surface underneath, which is later etched at last to create silicon ntride membrane. However, the silicon etching is the last step of mask fabrication as these membranes are very fragile and may break structure patterning. Post silicon nitride etching, Cr and Au is deposited on the other side of wafer(frontside). Finally, the wafer is processed on the frontside to create grating patterns.

4.3.4. Recipe for processing the Frontside structures on the wafer

The grating patterns are imprinted on the frontside of the wafer. Although, the LIGA parameters such as spinning speed, exposure dose, baking temperature and resist developing rate are specified by the makers of the photoresist still due to complexity of structures or working conditions changes the processing parameters. Also, the molecular mass starts decreasing in the exposed area resulting in scission of polymer chains.

Initially, a negative resist NR26 8000p is uniformly coated over the wafer by resist spinner. Before baking, the resist is carefully scratched from the wafer edges to avoid any contact with the mask. After soft baking this wafer at 150^0C for 180 seconds the solvent from the resist are removed. Later, the wafer is cooled down and transferred to the Quintel where both front and back side of the wafer is aligned by help of alignment marks.

The aligned wafer is exposed to UV rays for 170 seconds. During exposure the resist falling quarts section of mask will get exposed to UV rays resulting in polymerization of resist. The wafer is then post baked at 90^0C for 300 seconds and again cooled down. Further, this wafer is developed by passing through RD8 developer and then diluted 20% RD8 solution, finally the wafer is rinsed under DI water and observed under microscope.

Table 4.3: The developing parameters for both silicon and gold wafers

Type of wafer	wgt. of wafer	Time in 100% RD8	Time in 20% RD8	Time in DI water
Silicon wafer	9.936 g	60 + 15 secs	3 + 3 min	4 + 4 min
Gold wafer	10.193 g	65 + 20 + 20 secs	4 + 3 + 3 min	4 + 4 + 4 min

4.3.4.1 Patterning the frontside of X-ray mask

To fabricate the x-ray mask, the wafer width silicon windows on the backside is processed for frontside patterning. The resist coating, soft baking, UV exposure, post baking and resist development are kept similar to that of gold wafer. Before exposing the photoresist, the alignment marks on the backside of wafer are aligned to the alignment marks on frontside of the wafer at Quintel UL7000-OBS Aligner and DUV Exposure Station. Once both the sides were aligned the wafer was exposed and then post baked for 90^0C on hot plates station for 3 minutes. The cooled down wafer is then developed by RD8 developer for three cycles as indicated in Table 4.3 for gold wafer. Later, the observation is made under optical microscope and the results are shared in next chapter.

4.3.4.2 Electroplating gold structures.

Once the resist is developed from the wafer is proceeded for gold electroplating. The gold plating tank is shown below in figure 4.8, the plating solution is made of NEUTRONEX@309 Replenisher A. The wafer was adjusted in the fixture which was then dipped in the solution. After adjusting the plating conditions, the Au plating is switched on. Once the plating is completed the wafer is taken back to the cleanroom and the photo resist is stripped from the wafer. Final product will result in a wafer having gold grating patterns on the frontside of the X-ray mask wafer.

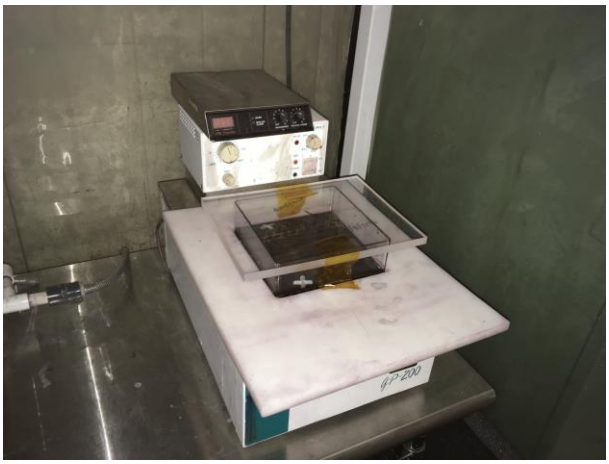

Figure 4.8: Gold Electroplating tank

4.3.4.3 Etching the silicon from the backside of window.

To create silicon nitride window membrane, the silicon is etched from these windows. The silicon is etched in a aqueous KOH^- or TMAH.

$$Si + 4OH^- \longrightarrow Si(OH)_4 + 4e^- \quad (4.5)$$

The etching rate of KOH depends on the crystalline orientation of silicon. The silicon etching of KOH is anisotropic, leaving V-etch pattern on sidewalls. Due to anisotropic etching reduces the

separation gap between cells. Therefore, the gap between cells in photomask is kept more than the required gap at the X-ray mask.

The patterned wafer is carefully transferred to a special fixture. This fixture is made of Teflon which is non-reactive to KOH. It covers the one side of the wafer and exposed the other side. The wafer is placed with the backside being open and frontside covered. Simultaneously, the 30% KOH solution is heated to 80^0 C while continuously stirring it by a magnetic stirrer, this increases its silicon etching rate. Later, the fixture is dipped in this prepared 30% KOH solution. Wafer is kept in the KOH solution for 5-6 hours. Since, the etching rate of KOH for silicon nitride is minimal, the etching stops at the silicon nitride layer. Post etching the fixture is transferred into a 70-80^0 C hot DI water, which left to gradually cools down to the room temperature. This reduces the strain of silicon nitride membrane caused by sudden change in temperature.

4.4 Fabrication of Gratings

The process for fabrication of grating can be categorized into three parts: Substrate preparation, X-ray exposure, and Resist development and processing

4.4.1. Substrate preparation and stacking of X-ray resist

For HAR structures, the selection of substrate material depends upon its adhesive strength to the X-ray resist. Commonly used silicon wafer with gold coating shows poor adhesion to sub-micron HAR structures. Therefore, surface modification is required to fabricate HAR structures. Previous studies have suggested that the copper oxide and titanium oxide have high adhesive strength to X-ray resist in comparison to gold. Therefore, CuOx and TiOx layers are utilized as seed layer to enhance the substrate adhesion. Initially, the copper layer is introduced on the wafer by electroplating while the titanium layer is deposited by e-beam deposition. Later, these copper surface and titanium

surface are oxidized in their respective oxidizing solution. Figure 4.9, represents a sketch overview of surface modification procedure followed during fabrication.

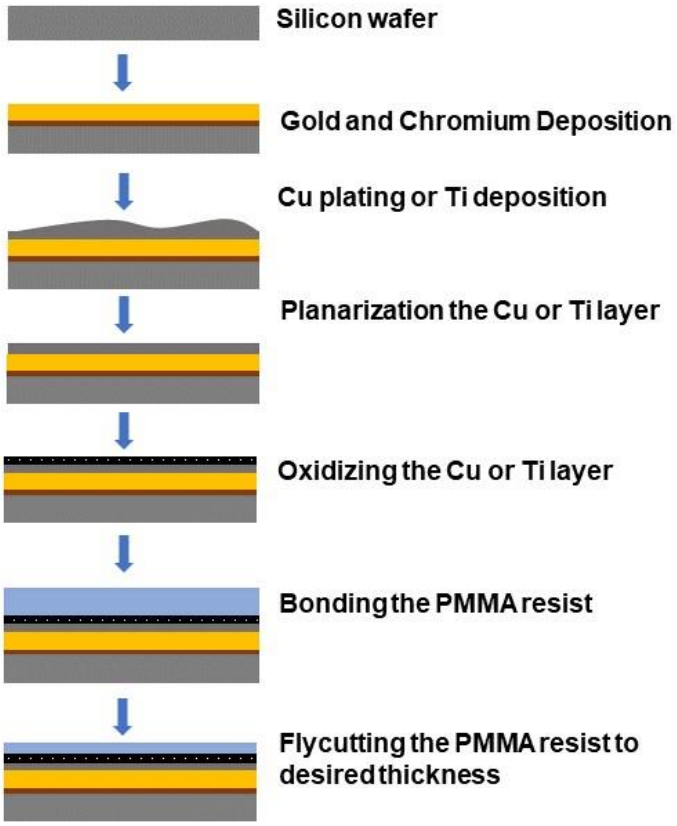

Figure 4.9: Steps for preparing the Substrate and resist coating for X-ray lithography.

4.4.1.1. Deposition of copper (Cu) or Titanium (Ti) on wafer to improve adhesion

The selected 4-inch silicon wafer with gold coating is further processed to achieve; 1) coating of 2 μm titanium layer or 2) coating of 10 μm cooper, both layers were deposited by electrodeposition. The titanium coated wafer can be ordered from the market where as Cu coating is done in CAMD.

Electroplating Copper*:* The layer of copper is electroplated over the conductive surface of wafer at a Cu electroplating tank. The wafer is attached to a plating Jig and dipped in the Cu platting solution. This plating solution is a mixture of copper sulfate, sulfuric acid and chloride ion in the composition, which table 4.4 highlights.

Table 4.4: Composition of Copper electroplating solution.

S. No.	Chemicals	Quantity
1	Copper sulfate	150-225 mg/l
2	Sulfuric acid	52-90 mg/l
3	Chloride Ion	25-80 ppm
4	DI water	-

Before placing the wafer in the plating solution, it important to make sure the wafer is clean, conductive and only the area in which CU layer is required should be exposed. Thus, a ring of green tape is applied on the edges of wafer. Wafer is attached to the plating fixture known as jig which has one sided opening. Once the fixture is dipped in the solution the electroplating starts at the current density of 10-15 mA/cm^2 for 1-8 hour. The opening of jig determines the CU plated area, which in this case is a circle of 86 mm diameter. Figure 4.10 displays the CU plating solution and Cu Plated wafer.

Planarization of Copper surface*:* Nonuniform surface may cause debonding of resist. Since, electroplating may be uneven, Cu layer is flycut with help of the Precitech Fly cutting machine to provide flat uniform surface. A Flycutting bit is attached under the spindle of Precitech, each time this bit runs over the Cu surface it scarps the surface. While, Flycutting the Cu surface, the initial cuts were ranged from 25-50 um and final cut of 5μm.

The spindle speed is adjusted to 2000-3000 rpm with forward and backward feed rate in range of 0.05-0.7 ipm. To avoid any irregularity in the height of Cu layer, it is measured under drop gauge at regular intervals. Once, the Cu surface is flycut, it is polished to get smoother surface for even oxidation.

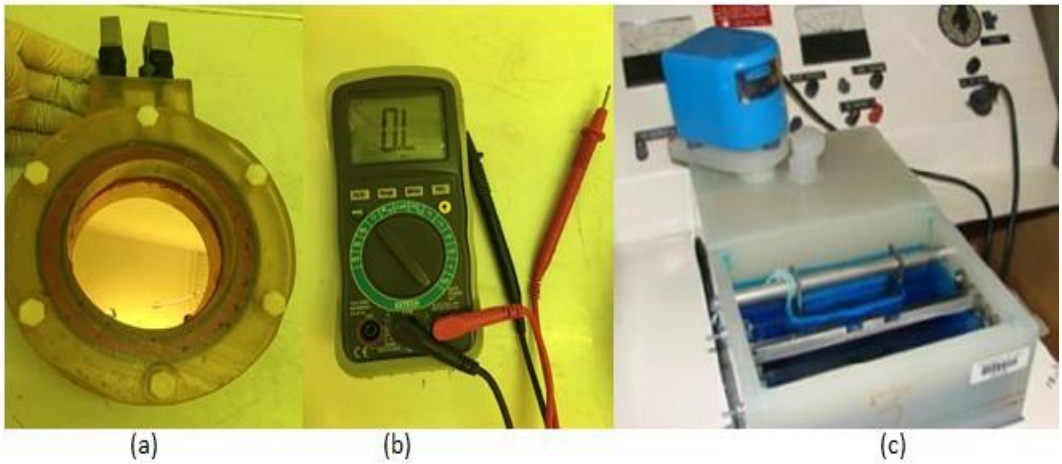

Figure 4.10: Electroplating of Copper: (a) The plating fixture and the substrate inside the fixture. (b)The multimeter to check the resistance on wafer. (c) The Copper electroplating bath.

Titanium deposition: A 2 μm thick layer of Titanium is deposited over the top gold surface of silicon wafer by electron beam evaporation, a physical vapor deposition process using E-Beam Deposition System. The deposition is very uniform thus the titanium coated surface did not require micro machining processing.

4.4.1.2 Copper Oxidation (CuOx) and Titanium Oxidation (TiOX) to improve adhesion

The X-ray resist, especially PMMA, exhibits great adhesion to rough surface After depositing the seed layer over gold surface, it is oxidized to improve the adhesion for PMMA resist. Both TiOx and CuOx layers will have tiny pours, which provides roughness to these layers. PMMA disc hold better on the rough surface resulting in thicker structures.

Copper Oxidation*:* After planarization of the cu surface of wafer, it is oxidized in oxidation solution. The copper oxide layer is rough and had good adhesion to PMMA resist. The oxidation solution is the mixture of Sodium chloride, Sodium Hydroxide, Sodium Carbonate and Sodium Chloride. Its composition is highlighted in the table 4.5. The chemicals are mixed in 2L bath, heated to 90^0C to 100^0 C, while magnetically stirring the solution. Once the solution is ready, the wafer is attached to the fixture as shown in figure and was dipped into the solution for 3 minutes until the copper surface turns black.

Table 4.5: Composition of Copper Oxidation solution.

S. No.	Chemicals	Quantity
1	Sodium Chlorite	58 g/l
2	Sodium Hydroxide	68g/l
3	Sodium Carbonate	11 g/l
4	Sodium Chloride	4g/l
5	DI water	1L

It should be stirred gently for uniform oxide layer coating. Once the copper surface turns black the wafer is washed under DI water to stop oxidation. It is important to prevent moisture around oxide layer to stop further oxidation so the wafer is kept inside oven and dried at 100^0 C for 2 hours. To find out the oxidation rate and prevent any irregularity while oxidation, a test run of oxidation process on performed on a copper disk.

Titanium Oxidation*:* The wet chemical process is used for oxidizing Titanium layer and compositions. The oxidizing solution is prepared by the composition of sodium

hydroxide, hydrogen peroxide and DI water. Solution is heated till 85^0C and continuously stirred with a help of magnetic stirrer. Once the oxidizing solution is ready, the wafers are completely immersed in it till the Ti surface turns black. Later, the wafer is transferred to DI water and then wafer is heated at 100^0 C in an oven. It is important to stir the wafer when it is in the solution to achieve uniform oxide coating.

4.4.1.3 Selection of X-ray resist (PMMA)

The X-ray resist should be sensitive to the X-rays radiation since it is used as a pattern recording layer. PMMA is chosen as the resist for this study. Since, it is highly sensitive to X-ray radiation, has high resolution and exhibit resistance to dry and wet etching. PMMA provides good adhesion with substrate layer and restricts any underplating. It has less stress and very minimal swelling post exposure. PMMA can be easily stripped without residue, and its solvent and catalysts are non-reactive to the seed layer. It is also very well suited to nickel and gold plating. Moreover, PMMA is a polymethylmethacrylate resist which are commercially available as a prefabricated plate or disk in different molecular weights. When radiate with X-rays, the chemical structure of exposed PMMA undergoes some changes. Also, the molecular mass starts decreasing in the exposed area resulting in scission of polymer chains.

4.4.1.4 Bonding the PMMA disk on the wafer

The PMMA disk is stacked over the wafer with the help of bonding under pneumatic pressure. At first, the PMMA sheet was cut into circular disc of 86 mm diameter and thickness of 27 mm. Further, these PMMA discs are cleaned by using in a soap solution and then rinse under DI water. After rinsing the discs are annealed at 100^0C in a conventional oven. The oven is programmed to maintain the temperature at 100^0C for two hours and then

letting it drop gradually in next 12 hours. In total, the PMMA discs were kept in oven for 14 hours during annealing. Once the PMMA discs are annealed, they are cleaned by using IPA and a special cloth. Annealing also reduces the stress in PMMA and increases its development rate [51] [52].

Preparing the Bonding glue*:* Bonding glue requires PMMA solution, which is prepared by taking 5 grams of 15% PMMA powder in a bottle. Then, 0.075 gram of 1% BPO is added which act as the hardener. Further, 50 μl of 1% MEMO is added with the help of a pipet and the mixture is mixed thoroughly for 6 minutes. Finally, 55 μl of 1% BPO is added and the mixture is kept in the vacuum oven for degassing to oxygen (bubble) removal. [55] Concurrently, both the wafers and PMMA discs prepared for bonding. To restrain the bonding solution in between the wafer and PMMA disc a green tape is applied at the edges of the wafer. Arrangement were made to fix the PMMA disc is in exact center of the wafer. Since, the bonding solution dries rapidly, it is prepared only when the PMMA disc and wafer are ready for bonding. Once the bonding solution is prepared, it is placed (1-2 ml) of in between wafer and PMMA disc by the help of a syringe. The bonding platform should be centered and flatten by the help of leveler and a scale. The bonding glue under PMMA discs was spread evenly and any bubble should be avoided while bonding solution is being transferred. Later, the PMMA disc is mounted on it as figure 4.22 indicted. The setup of wafer and PMMA with bonding glue is placed under pneumatic press at the pressure of 40-60 psi for 12-16 hours duration at room temperature [25].

Flycutting parameters for PMMA*:* Prior to flycutting PMMA the thickness of PMMA was measured under drop gauge. Initially, the PMMA thickness readings are taken at four different locations and the least one is considered as the final. Then the wafer PMMA

was flycutted down to 1000 μm. The feed rate for the forward and backward rate varied ranged from 1.50 - 1,80 ipm with the cut ranging from 75-100 μm cut. The spindle speed was setup at 8000 rpm. After reaching 1000 μm the PMMA surface was again measured in a similar manner as first time. Again. the wafer is again taken out and measured for thickness. Finally, the PMMA is cut down to desired thickness.

Figure 4.11: Pneumatic press at bonding station

For this study two type of wafer; CuOx wafer with PMMA resist and TiOx wafer with PMMA negative resist were used. Before exposing the actual wafer, the X-Ray is verified by exposing freestanding PMMA discs. It also helps in optimizing the exposing and developing parameters for grating fabrication.

4.4.1.5. Preparing the X-ray resist for Exposure

As the last step in figure 4.23, after bonding the PMMA resist over the wafer, the

PMMA is flycutted down to desired thickness of 40 μm and 100 μm with the help of Precitech Fly cutting machine. During flycutting, the spindle speed is rotating at 8000 rpm. A flycutting bit which has a diamond tip is connected to the spindle which is then moved in forward and reverse direction. The initial cut and final cut is fixed at 100 μm and10 μm respectively.

4.4.2 X-rays Exposure

Wafer bonded with PMMA resist is exposed to X-rays at the XLRM1 beamline with the help of an X-ray mask, figure 4.24 is the image exhibiting the setup of beamline working chamber where wafer is placed.

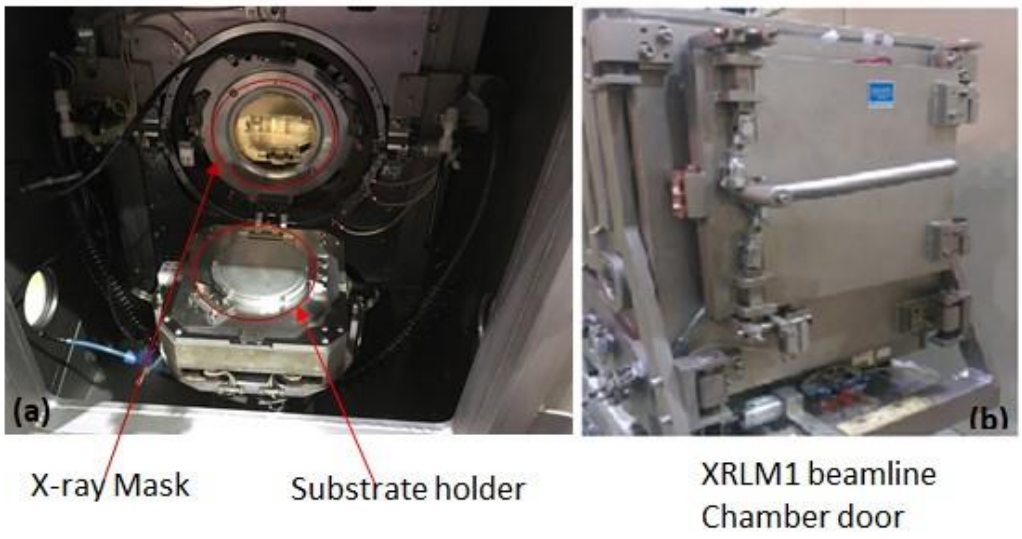

Figure 4.12: The XLRM1 beamline: (a) The X-ray mask and the wafer placed in side of the chamber (b) The working chamber door which is locked during exposure.

XRLM1 Beamline*:* The XLRM1 beamline operates in two mode (1) White Light and (2) Mirror light Mode. Our research uses the White light mode, it is without any optics. There are two beryllium windows in white mode having thickness of 100 μ m and 120um respectively. The transmitted bandpass spectrum ranges between 2.0 keV 7 keV (10 keV @

1.45 GeV. The source to exposure plane distance is 10.35 meter, while the horizontal acceptance at mask plane is 10 milliradians. The XLRM1 beamline is equipped with a DEX02 scanner from Jenoptik GmbH. The DEX02 scanner can vertically scan up to 100mm maximum with the maximum velocity of 50mm/sec.

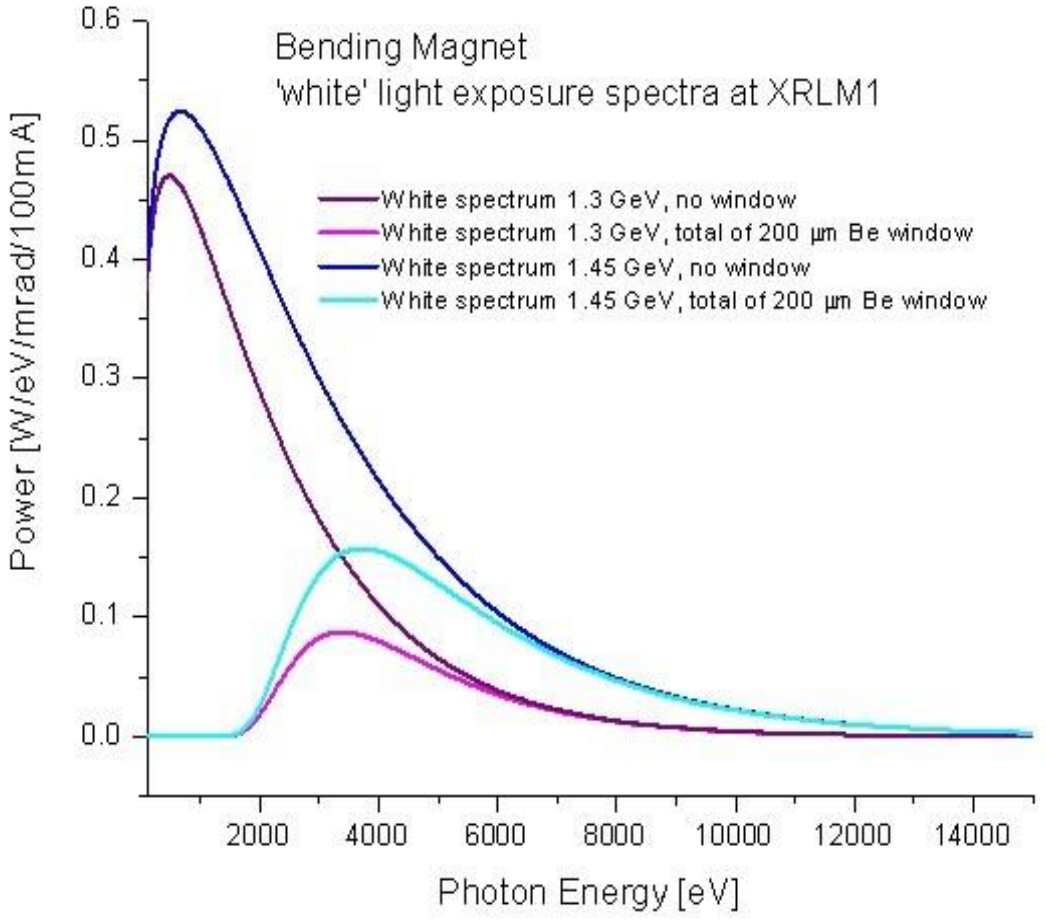

Figure 4.13: The Power Flux Spectrum for XRLM1 Beamline

The beamline also has some special feature such as tilting, rotating, dark chamber environment, aligned exposure option and mask/substrate cooling capabilities.

DoseSIM v3.2 and Dose calculation for X-ray exposure*:* The dose of for the exposure is calculated by using the software DoseSIM v3.2, developed by the Researchers at Institute of Micro Technology (IMT), Germany. It calculates the exposure dose based on the source radius of curvature of bending magnate, magnetic field of dipoles, X-ray electron energy, filter material and its thickness, material and thickness of the mask membrane, material and thickness of the front window, the gas in vacuum chamber, the pressure of the vacuum chamber, the type of resist and its thickness, tilt of substrate. The DoseSim V2 serves as a database of predefined parametric details which makes dose calculation very easy. DoseSim is also used to calculate the dose distribution or the dose deposited as a function of penetrated resistive depth. Figure 4.13, displays the power flux spectrum for the beamline. The exposure dose is calculated by dividing the bottom does by the dose rate at the surface of the resist. The exposure does controls the scanner of beamline. The dose calculation can be done by selecting the bottom dose or bottom dose can be calculated by assigning exposure dose.

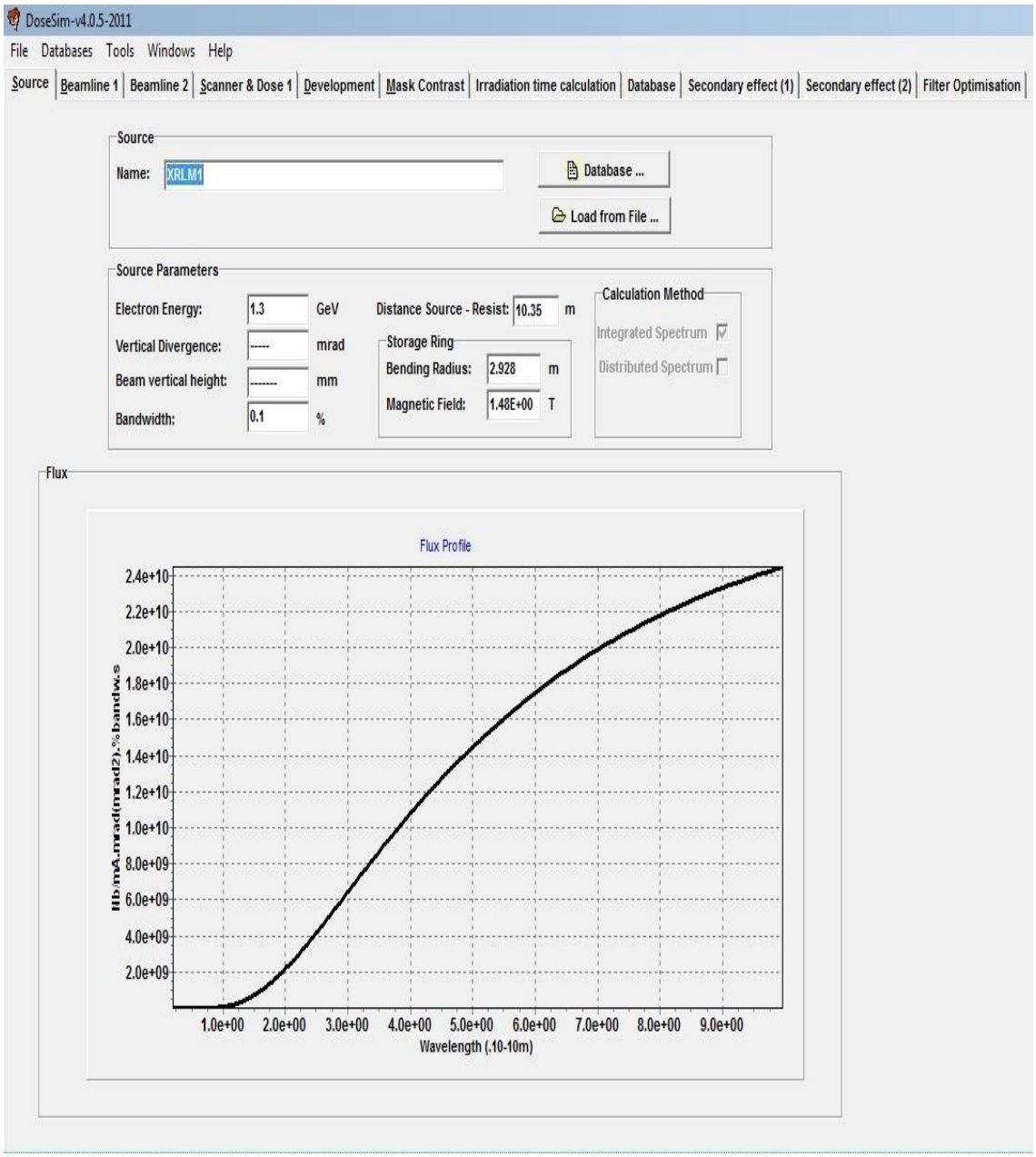

Figure 4.14: DoseSim V2 GUI asking for type of Beamline source.

Procedure for exposure dose calculation*:* Initially, the DoseSim V2 asked for the type of beamline source used for the exposure. As the wafer is exposed at the XRLM1 beamline, it is fed in TAB from the database. The database includes the critical data of the XLRM1 beamline. Figure 4.15 show the screenshot of the GUI of the software

requesting for the beamline source. The other parameters of the beamline XLRM1 such as Electron Energy, Distance between source and PMMA, bending radius, bandwidth, etc. are also fed in the software GUI. After feeding the beamline data, the second interface of the software request for the parameters related to front end windows, figure 4.16 displays this window. Depending on the number of mirror installed during the exposure, data is fed to the interface window. Initial tab requests for the material of front end window which is selected as Beryllium with the thickness of 100 μm. Next in line is the selection of number of window used, which is one for this exposure. The third interface window is to setup the scanner and the dose. As shown in figure 4.16, first tab requests for the vacuum condition in the beamline chamber. The beamline chamber is filled with Helium at 110 mbar pressure in a distance of 1 m. Second tab needs the material of the mask windows used. Since this study is using silicon nitride window X-ray mask; mask material is fed as silicon nitride with 1 μm thickness. Next tab asks for the material and thickness of filter mask, which is fed as gold and 0.032μm. Further the type of resist is selected as PMMA linear MW= 1.6M with thickness ranging from 40μ to 100 μm. This interface also asks for the tilt which is fed as 0^0 degrees.

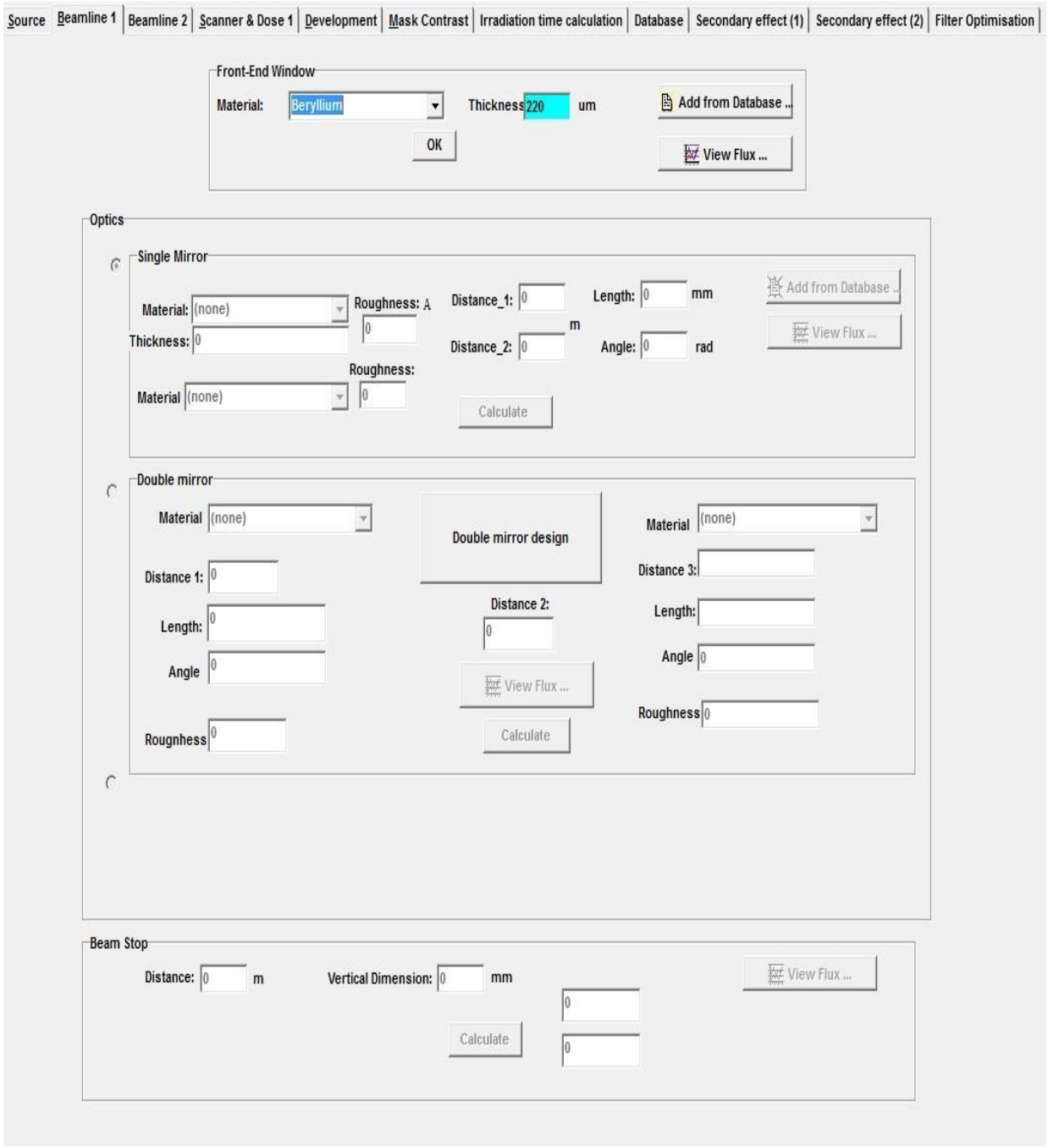

Figure 4.15: GUI showing the entry of front end window and its thickness

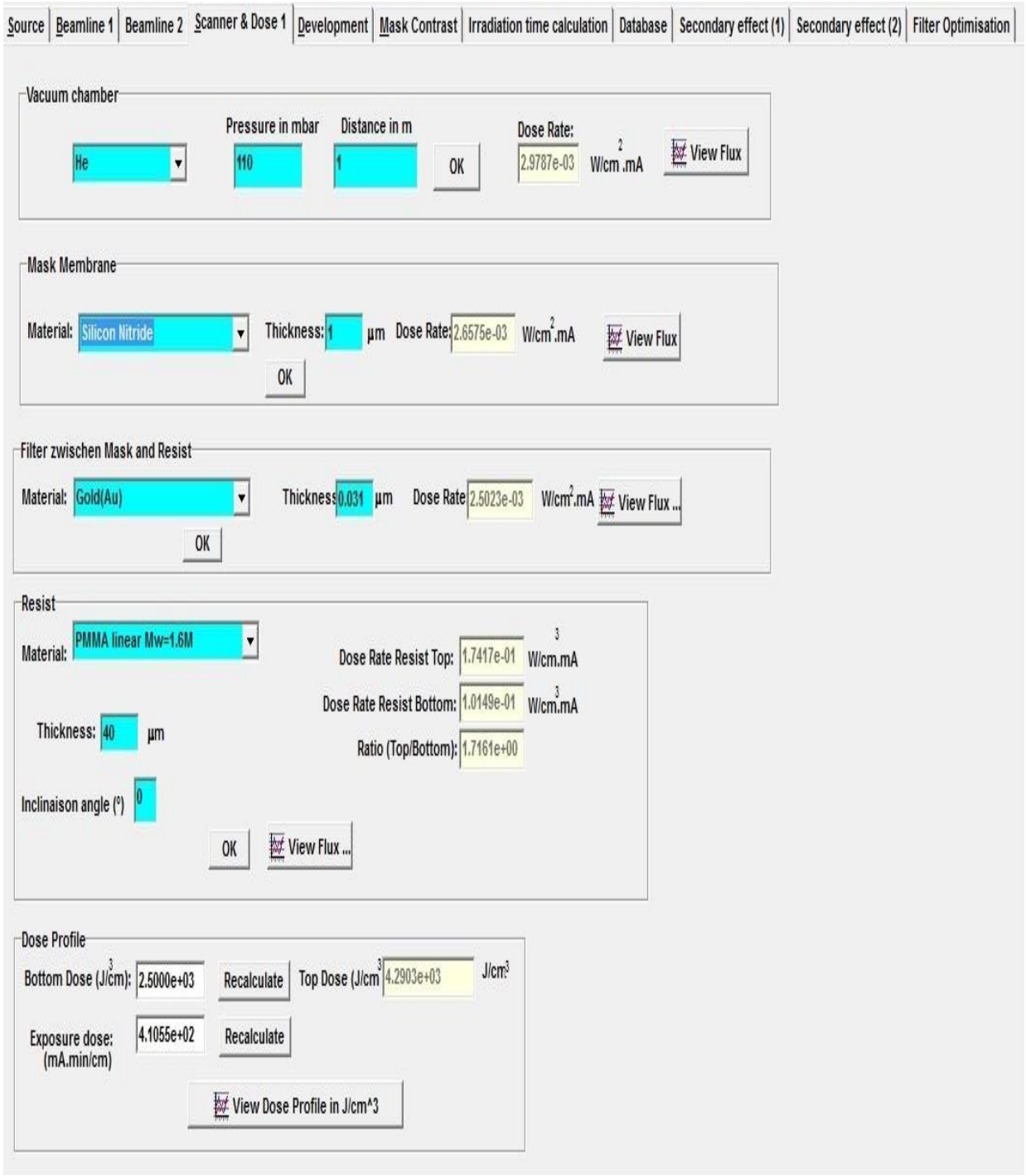

Figure 4.16: Information about Mask membrane, additional filter, Type of resist and its thickness and bottom dosage J/cm^3

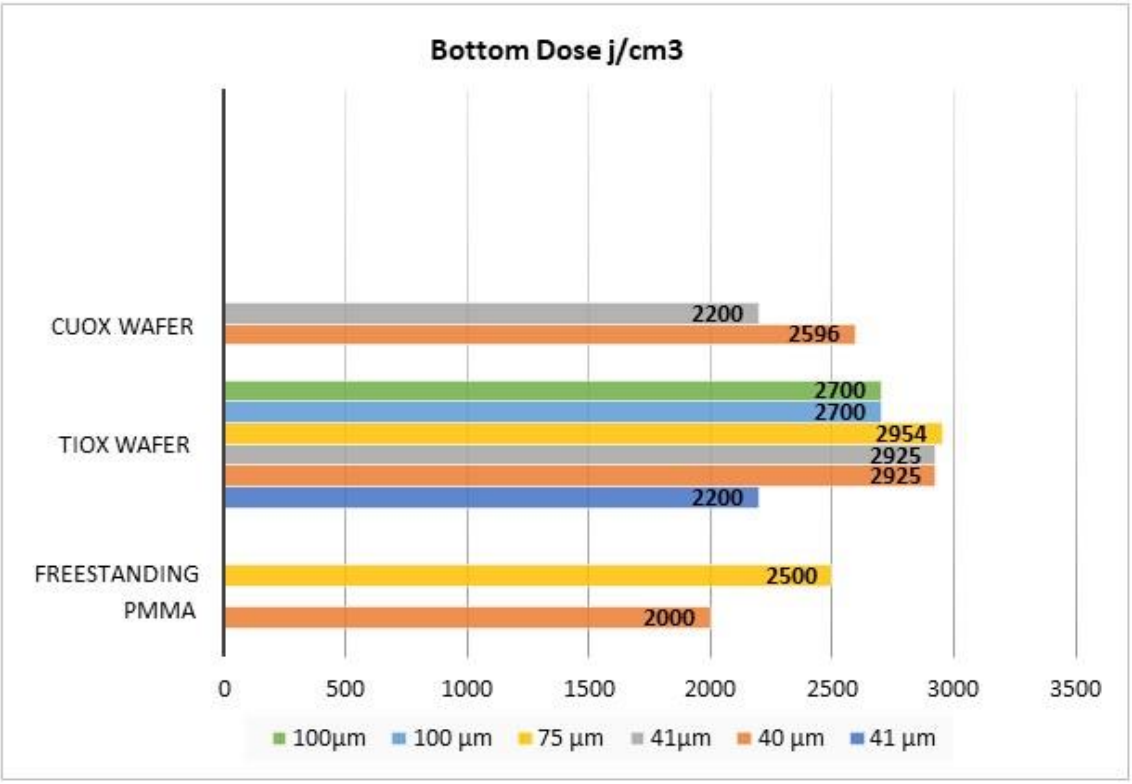

Figure 4.17: The record of X-Ray bottom dose given to PMMA resist

The last section of the widows need the bottom dose for calculating the exposure dose. The bottom dose it the minimum amount of radiation required for the breakdown of the long molecular chains in PMMA resist, which can be selectively removed after developing [24]. For this study the bottom dose ranged from 2000-30000 j/cm^3. Excess bottom dose could result in bubble formation in the resist. setting up the parameters in the window will result in exposure dose mA-min/cm. After exposure dose is calculated the dose it setup in the program that controls the XLRM1 beamline. The wafer is loaded at the end of the beamline as figure 4.18. The X-ray mask is loaded in the hatch through which the x-ray beam passes and hits the substrate. Figure 4.12, shows the setup for the X-ray exposure.

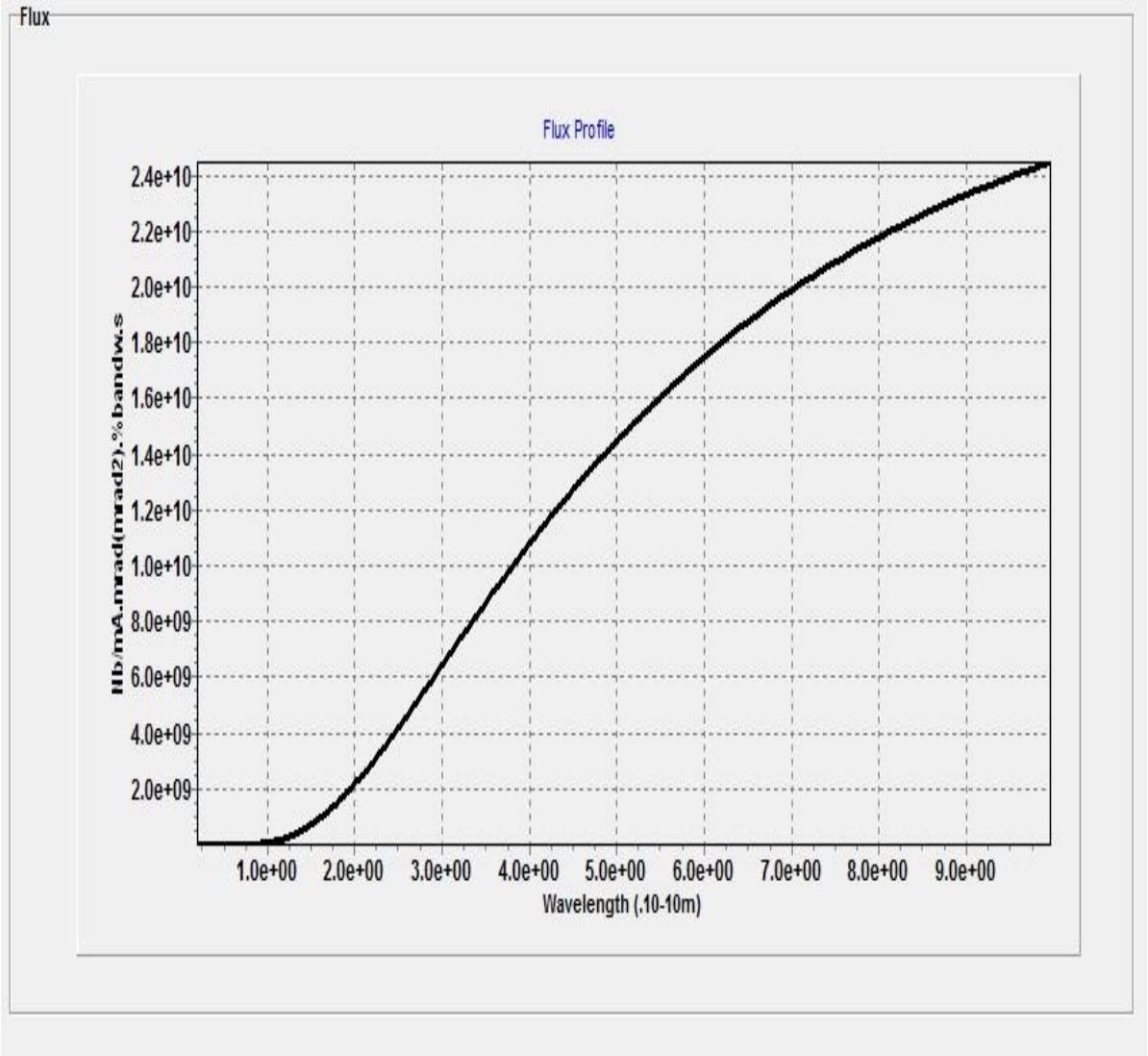

Figure 4.18: Bottom dose profile for the resist with respect to exposure depth

During exposure the PMMA resist can expand due to heat which can hard X-ray mask, shims are taped over the edges of the wafer to manage the safe distance in between mask and the wafer. It is important to choose the shim of right thickness otherwise it would affect the exposure results. Once the wafer is loaded properly the chamber is closed and the hatch is secured, and the exposure is started. The bottom dose given to the PMMA resist for freestanding PMMA, TiOx wafer and CuOx wafer is accounted in figure 4.29. The exposure

dose is calculated for these samples as per their bottom dose and PMMA thickness. Figure 4.30, is the bottom dose profile with respect to the exposure depth.

Table 4.6: Bottom dose and Exposure dose for the wafer exposed at XLRM1 beamline.

Wafer	Thickness	Bottom Dose	Exposure Dose	Shim
PMMA 1	40 μm	2200 (j/cm^3)	383 (mA.min/cm)	100 μm
PMMA 2	60 μm	2500 (j/cm^3)	538 (mA.min/cm)	100 μm
CuOx 1	40 μm	2200 (j/cm^3)	438 (mA.min/cm)	100 μm
CuOx 2	41 μm	2574 (j/cm^3)	438 (mA.min/cm)	100 μm
TiOx 1	40 μm	2574 (j/cm^3)	433 (mA.min/cm)	100 μm
TiOx 2	41 μm	2925 (j/cm^3)	492 (mA.min/cm)	100 μm
TiOx 3	90 μm	2700 (j/cm^3)	661 (mA.min/cm)	160 μm
TiOx 4	100 μm	2700 (j/cm^3)	745 (mA.min/cm)	160 μm
TiOx 5	100 μm	2700 (j/cm^3)	745 (mA.min/cm)	160 μm

4.4.3. Developing of irradiated PMMA resist and Analysis

Soon after exposure, the irradiated PMMA has to be develop in the developer. There are three types of developers available for irradiated PMMA resist. Methyl-iso-butyl-ketone (MIBK) is commercially available, it is a strong developer. However, it induced cracks in PMMA when used at the room temperature conditions. MIBK/IPA (1:3) is a standard developer for PMMA during X-ray lithography, it is an intermediate developer. Lastly, the GG developer, it is weak in between all three but it low stress developer perfectly suited for

deep X-ray developer. This study uses GG developer for irradiated PMMA resist. The chemical composition of GG developer is formulated by the Institute for Microstructure technology (IMT), Germany. It is prepared by 2-(2-Butoxyethoxy) Ethanol, Morpholine, and 2-Aminoethanol and DI water with the composition shown in table 4.7. The GG developer has high development rate and high selectivity at 35^0 C, and its suits the high bottom dose X-ray exposures but it is toxic, carcinogenic and mutagenic.

Table 4.7: Composition for GG developer and GG rinse.

1-liter GG developer.		
S. No.	Chemicals	Quantity
1	2-(2-Butoxyethoxy) Ethanol	600 L
2	Morpholine	200 L
3	2-Aminoethanol	150 L
4	DI water	50 L
1-liter GG Rinse.		
1	2-(2-Butoxyethoxy) Ethanol	800 L
2	DI water	200 L

This development process is an interrupted one because the developed PMMA settles down in the trenches and prevent the new developed surface from developing. GG rinse has a low developing rate, it cleans the settled down developed resist and it also helps in obtaining sharp edges. By increasing the developing time in rinse by 10 times will increase. the developing rate of irradiated PMMA by 5-6 times. [51] Later, the wafer is passed through the DI water to stop the developing process. The wafer is observed under microscope after the completion of each developing cycle.

Table 4.8: Post exposure PMMA development.

Exposure depth of PMMA	GG developer/GG rinse cycles
Development of Exposed freestanding PMMA resist.	
40 μm	20/40 and 5/60 mins and then 15 mins of DI water
60 μm	20/40 and 5/60 mins and then 15 mins of DI water
Development of Exposed CuOx wafer with PMMA resist.	
40 μm	5/20, 60 mins rinse, and 2 hours rinse followed by 5 mins of DI water
41 μm	5/420, 5/20, 5/20, 5/20, 5/20, 5/20 and 5/20 mins each cycle was followed by 5 mins DI water
Development of Exposed TiOx wafer with PMMA resist.	
40 μm	5/20 followed by 5 mins of DI water
41 μm	5/20, 5/ 60 each cycle was followed by 5 mins DI water
90 μm	20/40 followed by 5 mins DI water
100 μm	5/5, 10 min rinse 5/30, 5/10, 2/20, followed by 15 min DI water and 25% IPA and then drying
100 μm	5/5, 5/55, 35 min rinse, 20 min rinse, 20 min of rinse, followed by 15 min DI water and 25% IPA and then drying

4.4.4 Processing grating structures on Freestanding PMMA

Few freestanding PMMA are the PMMA disc in the hard plastic form. It is a 4-inch diameter disc with the thickness ranging from 2500-3000 μm. Here, different freestanding

PMMA discs are exposed for separate bottom dose of 2000 J/cm^3 and 2500 J/cm^3 for the exposure depth of 40 μm and 60 μm respectively. The table 4.6, enlist the exposure details for Freestanding PMMA. After the X-ray exposure the wafer was developed under GG developer. Table 4.8, presents the developing parameters for the exposed freestanding PMMA. Once the developing is complete, the PMMA disk is dipped into a solution 25 ml IPA and 75ml DI water for 3 minutes and dried by hanging under the hood.

4.4.5 Processing grating structures on CuOx and TiOx wafers

Initially, the CuOx and TiOx wafers with thinner PMMA resist (40 μm height) are exposed at XLRM1 beamline. The lesser aspect ratio of structures reduces the complexity of fabrication. exposure details are mentioned in table 4.6. Later, these wafers were developed using break developing method by passing through GG developer, GG rinse and DI water. Table 4.8, which enlist the developing cycles for all wafers, provides details for Later, these wafers are transferred in to the 25% IPA (50ml IPA and 200ml DI water) for 3 minutes and dried under the hood.

4.4.6 Etching the copper oxide from CuOx wafer

After developing, the CuOx wafer is passed through the CuOx etching solution. The etching solution will remove the CuOx from the wafer and expose the conductive surface of wafer. For copper etching solution is prepared by mixture 0.5M HCL and 0.5M KCL. The CuOx wafer is submerged into etching solution for 15-15 seconds cycles and then passed through the DI water. As mentioned in table 4.9, first wafer was etched for 9 cycles, while second wafer is etched for 3 cycles. In each cycle the wafer is passed through the solution for few seconds and then kept in DI water for some time to stop the etching process. CuOx etching is anisotropic in nature thus undercutting is very common.

Table 4.9: Etching cycles of oxide from the both the CuOx wafer.

Exposure depth of PMMA	CuOx etching solution /Di water
40 μm	30 sec/2 min, 8 cycles of 12 sec/2 min
41 μm	15 sec/2 min, 15 sec/ 2 min, 15 sec/ 2 min

4.4.7 Electroplating Nickel structures.

The chemical composition of nickel bath is presented in table 4.10, where Nickel sulfamate 75 g/l, boric acid 40 g/l and pitting 10 ml solution are mixed with DI water. The pH and operating temperature of nickel electroplating bath influences the quality of nickel plating. Therefore, the temperature of nickel electroplating bath maintained at 3.75 and 45 ^{0}C, respectively for optimum results. Post developing and copper etching the wafer is always kept wet. If wafer dries, then it is passed through plasma asher and dipped in 5% pitting solution, which reduces the surface tension between PMMA structures allowing the plating solution to enter in between narrow gaps. This wafer is loaded in the jig with single side opening. The gas kit to prevent the nickel plating in unwanted areas.

Table 4.10: Composition for Nickel electroplating bath.

S. No.	Chemicals	Quantity
1	Cooper Sulfate	70-80 g/l
2	Boric acid	35-40 g/l
3	Pitting solution	10 ml

Figure 4.19: The Nickel Plating Bath

The plating current and the time is calculated according to the desired thickness, the area receiving nickel plating and current density. This value of plating current and the duration is feed to the controller attached to nickel bath. Finally, the wafer is dipped into the nickel plating bath, shown in figure 4.19, and the plating is started.

4.4.8 Plasma Asher to remove the resist residue

Once the wafers are passed through to the solution of 25% IPA (50ml IPA and 200ml DI water) for 5 minutes and finally dried under the hood for 12 hours. Since there was some PMMA residue at the bottom of wafer, it was exposed to plasma in plasma asher at 200 watts with T_{max} = 50^0C. Few cycles of plasma asher induced cracks into the thin PMMA residue layer. Immediately after plasma asher, the wafer is transferred to the pitting solution. The pitting solution is used to reduce the surface tension between the gap, so that the plating solution can reach the bottom surface.

4.4.9 Flood Exposure

The wafer is again exposed to the X-ray at XLRM1 beamline without an X-ray mask or filter. The exposure dose is calculated for a very high bottom dose, such exposure is

referring as flood exposure. In food exposure, all the remaining PMMA on the wafer is exposed. This exposed PMMA is further stripped by passing the wafer through GG developer and acetone bath. If the wafer is copper then the CuOx layer underneath PMMA is exposed which is etched by CuOx etching solution and later dried for SEM analysis. For other wafers, they are dried after PMMA stripping and analyses under SEM. First, any dirt or oil is carefully cleaned from the wafer by using wipes and IPA. The polishing slurry have oil in their content, there is a chance that this oil will stay at the wafer surface. While X-ray exposure, the oil residue or dirt can heat up and cause temperature variance in PMMA. The table 4.11 mentions the details for Flood exposure parameters. The results obtained during fabrication process are discussed in next chapter.

Table 4.11: Record of Bottom dose and Exposure dose for the Flood exposure at XLRM1 beamline.

TiOx 3	90 μm	4000 (j/cm^3)	550 (mA.min/cm)
TiOx 4	100 μm	3000 (j/cm^3)	812 (mA.min/cm)
TiOx 5	100 μm	3000 (j/cm^3)	812 (mA.min/cm)

Chapter 5
Results and Discussion

The X-ray mask fabrication faces challenges like non-uniform resist coating, underdeveloped resist, washed off resist structures and protection of fragile Silicon nitride membranes. The photolithography processing issues are resolved with Design of Experiment (DOE) technique as section 4.3 discusses in previous chapter. Later the chapter follows the fabrication of HAR grating. Similar to X-ray mask, grating fabrication is also challenging, mainly due to debonding or bending of structures, electroplating nickel in between resist structure grooves and overplating. To overcome these challenges, techniques such as surface modification, plasma asher, polishing and many other.

5.1 X-ray Mask fabrication

The fabrication of X-ray mask is done on < 100 > silicon wafer, which both sides are coated with 1 μm stress controlled LPCVD silicon nitride. The X-ray mask fabrications is processed in two steps; 1). Patterning the Silicon nitride membranes at the backside of wafer and 2. Patterning the resist on the frontside of wafer, which serves as a mold into which gold is electroplated to make grating. However, the processing parameters for X-ray mask are established by DOE [section 4.3.2.4]. The result of X-ray mask fabrication is discussed below:

5.1.1 Patterning the Silicon nitride membranes at the backside of the wafer

The patterning of silicon nitride membrane starts with coating S-1808 resist followed by baking, exposure and developing. The processing parameters are mentioned in section 4.3.3, Figure 5.1, displays the patterned resist at the backside of the wafer. The developed resist exposes silicon nitride in the area of nine cells, which shows high contrast,

clean and sharp. While, the remaining resist covers rest of the wafer. Next, the exposed silicon nitride in cells is dry etched, to exposes silicon underneath it.

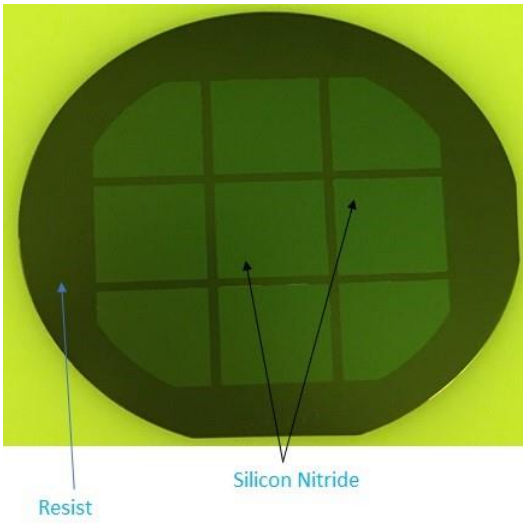

Figure 5.1: Patterning the S1808 resist at the backside of the wafer exposing silicon nitride windows in nine areas corresponding to nine areas to make grating on the frontside.

5.1.2 Establishing processing parameters by patterning on Test wafers.

Initially, the test run results were unsatisfactory, the photoresist was either underdeveloped or the structures were washed out. Figure 5.2, addresses some these issues related to resist processing. Image is figure 5.2 (a), shows the resist residue in between structure. This issue is due to lack of developing time. Similar issues can also be due to excess baking or exposure dose. Since the grating structure are patterned on negative photoresist NR 26, the insufficient exposure dose. One more reason is the high postbaking and softbaking temperature or baking time. This causes thermal cross-linking of polymer in the unexposed resist, which slows the developing rate in that area. The image in figure

5.2 (b), is presenting the washed off structures. It occurs due to overdeveloping that removes the resist from the wafer.

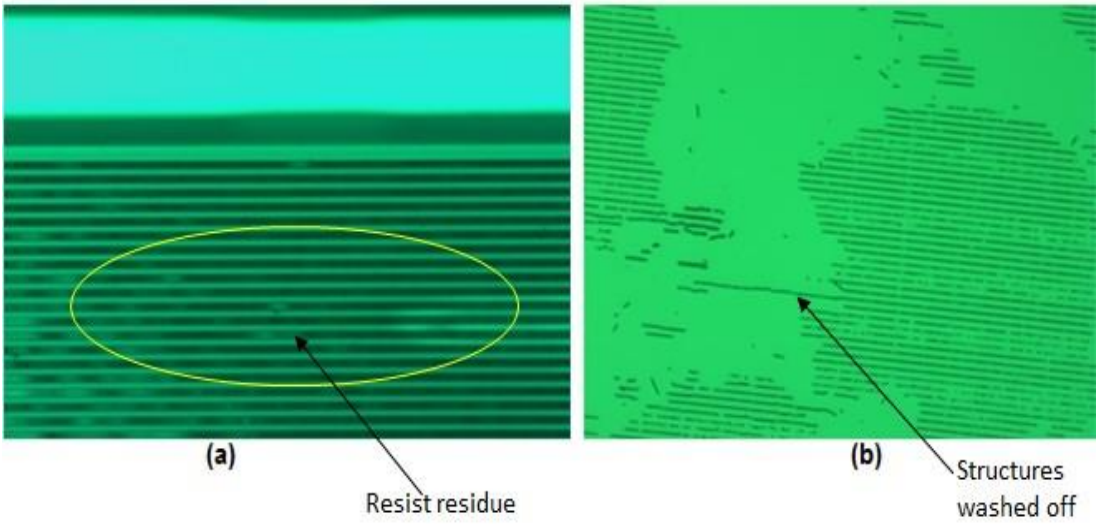

Figure 5.2: Initial Challenges faced during UV lithography:(a) the surface at the bottom of the structures in not clean. This resist residue at the bottom will affect the metal plating. (b) the structures are debonding from the wafer.

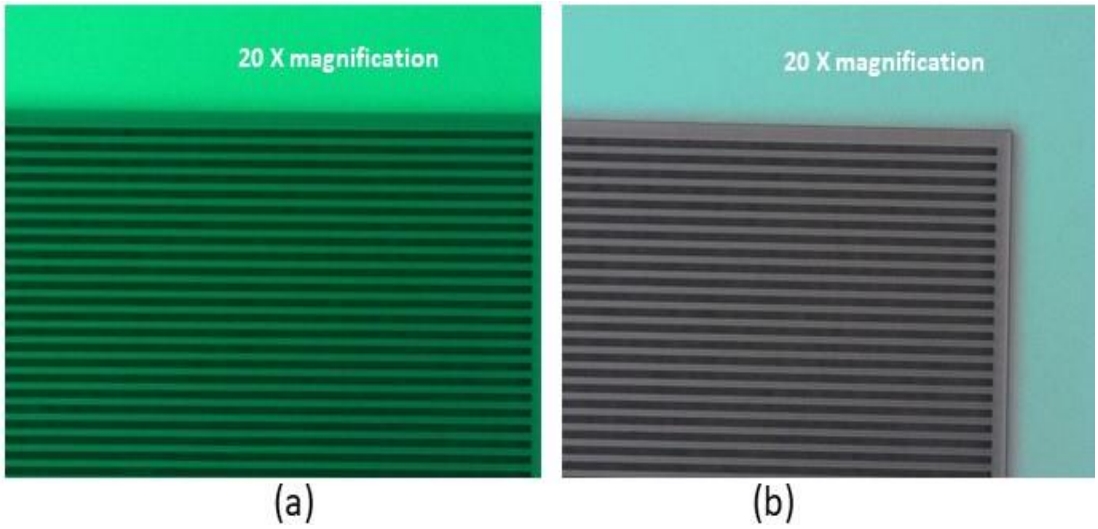

Figure 5.3: Figure (a)and (b): are the microscopic images obtained from test runs. The grating structures are of 8μm period with even spacing and 14 μm height. Structure profile is smooth and rectangular in both the images with clean bottom surface.

Optimizing the previous processing parameters, collateral grating structures with 8 μm period, 50% duty cycle and 14 μm thickness were achieved. The development parameters obtained from silicon wafer are carried to gold wafer. However, the adhesion properties of gold seed layer differ from that of silicon, the developing parameters are changed for the wafer with gold coating. Thus, the exposed photoresist requires extra developing time for the wafer with gold coating. Therefore, the wafer was kept for extra time in order to develop the photoresist structures completely. These test results are shown in figure 5.2, exhibiting the long grating structures. Both the images, 5.3 (a) and (b) highlights the edges and corners of the grating structures, which looks sharp and clean. Whereas, figure 5.4, is displaying the grating with support structure. The figures 5.4 (a) and (b), indicates the grating structures with straight and of sharp rectangular shapes. The surface at the bottom of structures also looks clean, however this will be further confirmed by was SEM analysis.

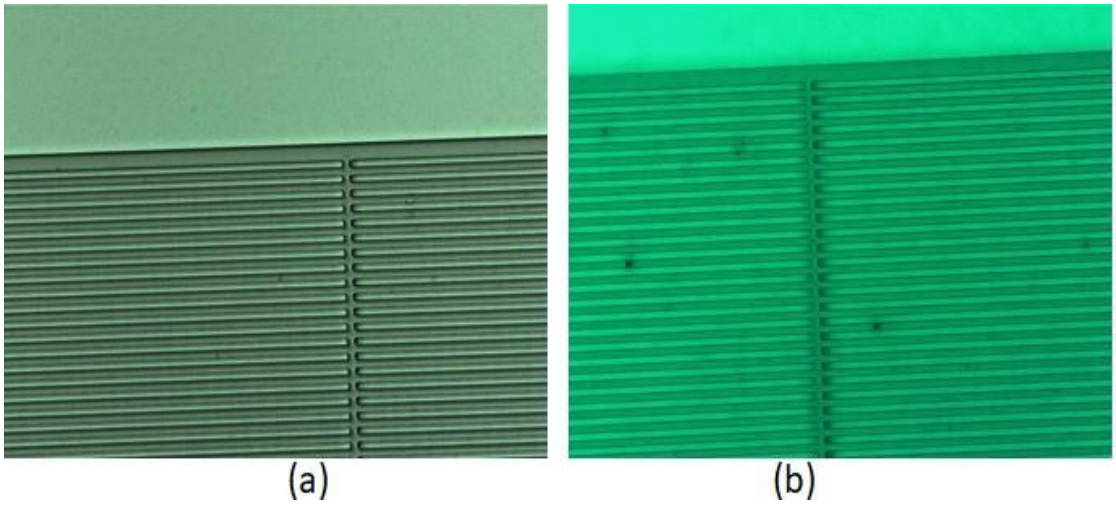

Figure 5.4: Support structures: (a) and (b) are the images taken near support area at 20X magnification. The resist profile looks smooth and even. The bottom surface is clean and the corners are also clean. These support structures are provided at every 2 mm distance.

SEM analysis of resist structure post developing*:* Post development, the wafers were analyzed under SEM for a closer look. Sidewalls of the structures, its bottom surface and the support structures are observed during SEM analysis. Figure 5.5, presents the images captured during SEM analyses. Figure 5.5 (a) and (b), exhibits the clean wafer surface without any resist residue.

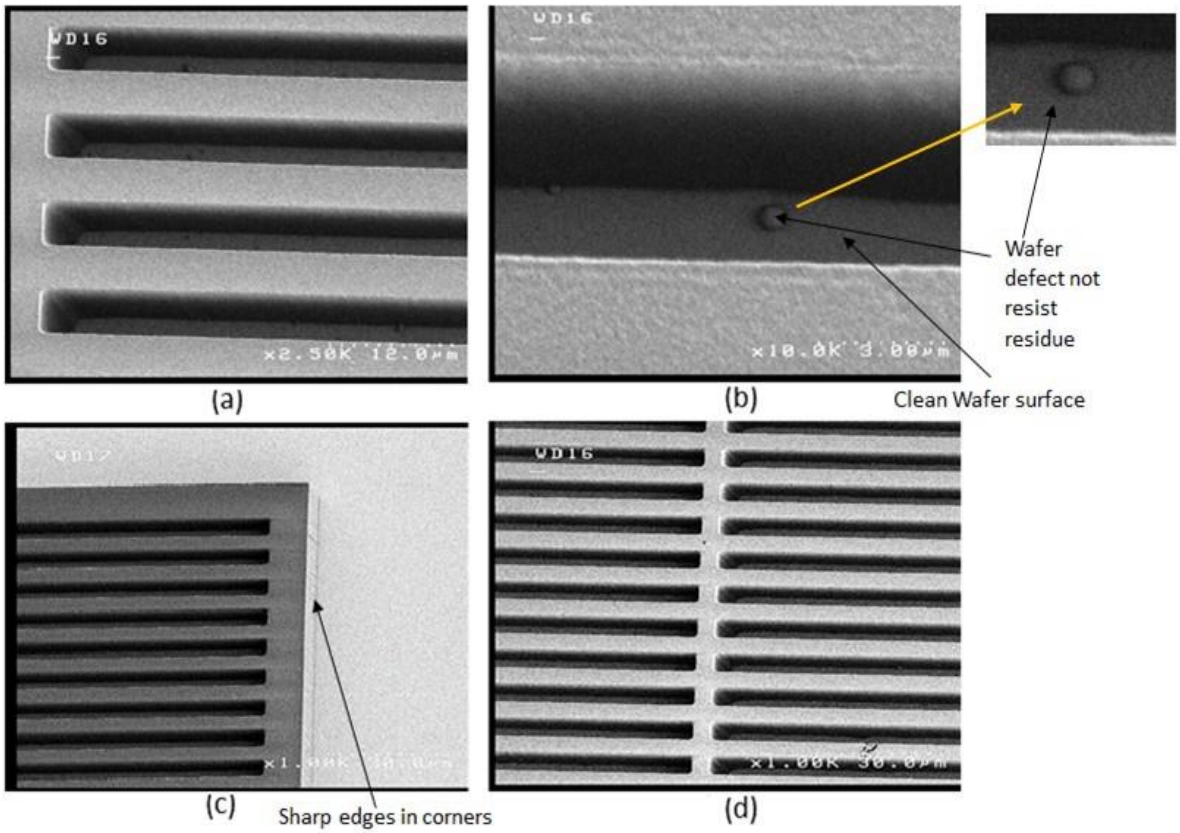

Figure 5.5: SEM analysis: (a) is the 4 μm area for long grating showing sidewall and bottom of structure. (b) is the magnified view of the structure to confirm that bottom surface is clean, inset indicates the bulge at the wafer surface is not resist (c) is the tilted view of gratings to check the sidewall and bottom surface. (d) is showing support structures in grating patterns, the corners and bottom of the gratings are clean.

Figure 5.5 (b) shows a bulge on the wafer surface which is a defect in wafer not resist residue as shown in the inset. The resist residue at the bottom of trenches will restrict

plating in that area, resulting in nonuniform grating structures. In addition, if the sidewall of the structures is not uniform then the profile of metal gratings will not be rectangular and even. The height of the resist structures is shown in figure 5.5 (c), which is 14 μm. Whereas, 5.5 (d) captures the support structure which is also clean and smooth. Figure 5.6, is measuring the gap between structure to be 4 μm, which is identical to photomask indicating minimal loss in dimension while pattern transferring.

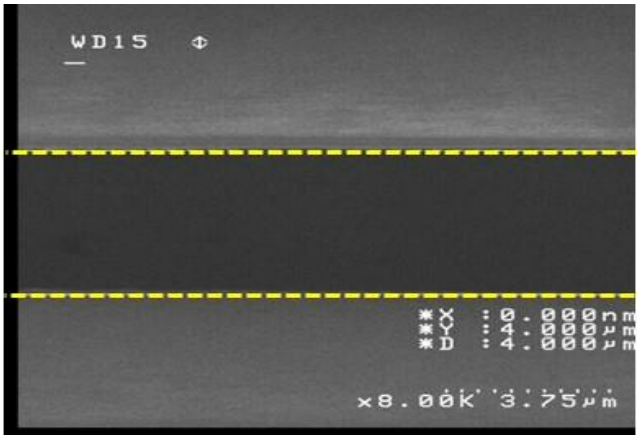

Figure 5.6: Measurement of resist structure: SEM measurement tool is reading the gap of 4μm between two structures.

5.1.2.1 Patterning the gold structures on the frontside of wafer for X-ray mask

The frontside of wafer is patterned according to the processing parameters presented in section 4.3.4 of previous chapter. Figure 5.7, is the analysis of the wafer post UV lithography. Images in 5.7 (a) and (b) indicates a clear wafer surface with a straight rectangular profile for resist structures. The width of trenches and grating is same which justifies the 50% duty cycle. Whereas, the figure 5.7 (c), presents the area near support structures. There is no under cutting on the edges and the wafer surface is also clean. However, the area near corner looks dark thus the wafer was also checked for striation.

The effects look same even after rotating the wafer so it in not striation effect. This bottom area near support structures is also analyzed under SEM to check for resist residue.

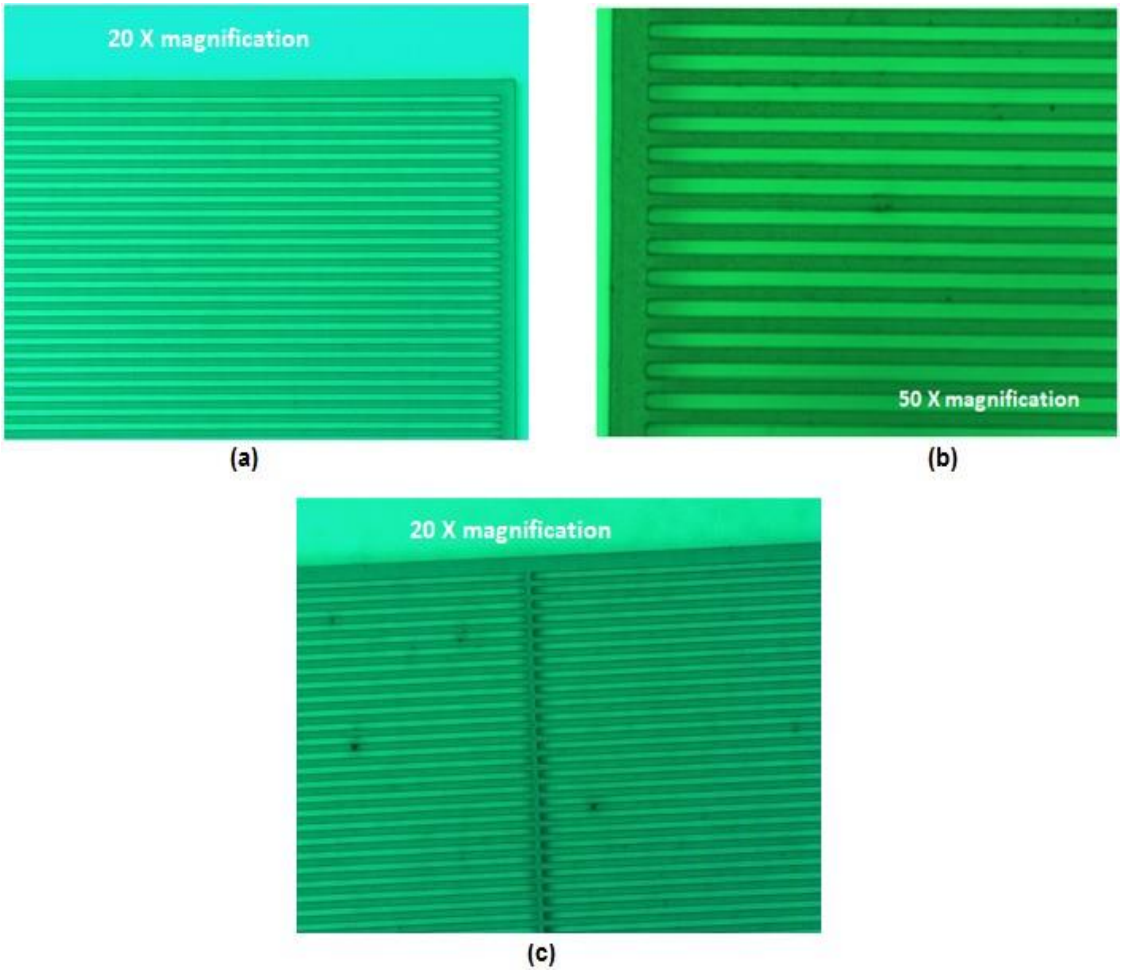

Figure 5.7: X-ray mask post developing:(a) and (b), are the images from 4μm region at 20 X magnification and 50 x magnification, respectively. It indicates that the profile of structures is smooth and well developed. The bottom surface also looks clean. (c), is presenting the support structures. The corners of the structures are smooth and clean.

The Electroplating conditions and procedure is illustrated in the section 4.3.4.2, of the previous chapter. Post electroplating, the remaining resist is stripped. The images in figure 5.8, shows the grating patterns on X-ray mask after gold electroplating and resist stripping.

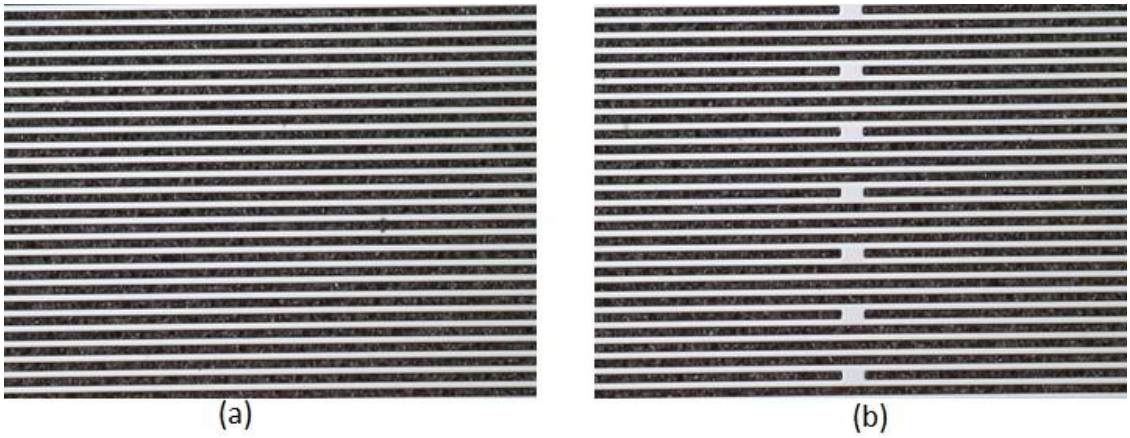

Figure 5.8: X-ray mask: (a) Optical microscope image of long grating structures at 20 X magnification. The period of the grating is 8 μm with 50 % duty cycle. (b) is the image from the support structures area.

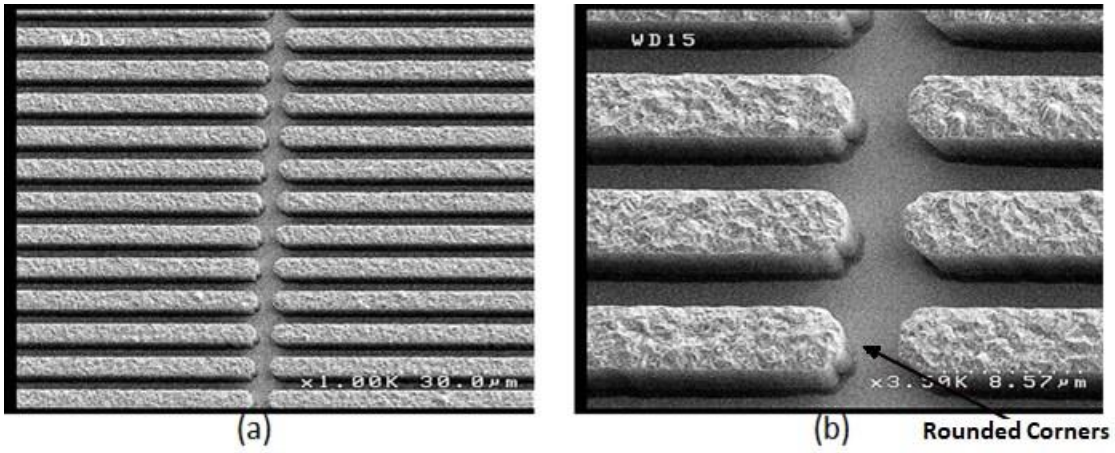

Figure 5.9: SEM analysis of metallic grating patter on X-ray mask: (a) and (b) are the images captured in support structure region. The top surface of the gratings highlights the roughness in gold, it will have no effect on X-ray exposure.

SEM analysis of frontside of the X-ray mask post gold electroplating*:* To examine the profile and dimension of grating structures, the X-ray mask is transferred to SEM. Figure 5.9, represent the SEM analysis of the X-ray mask. The image captured near support structures indicate that the grating structures are rectangular and sharp at the edges

with uniform height and thickness. However, as excepted the corners of structures are rounded. Ideally, corners of structures should be sharp edges but their rounded shape is very common in lithography. Further, figure 5.10 is a closer look at the bottom and sidewall of the structure. Both figure 5.10 (a) and (b), are the top and side view of the gratings, respectively, which indicate that the bottom is clear and there are no irregularities in sidewall of the grating. It also shows the height of the structures. Later, the dimension of the structures is measured using measuring tool features in SEM.

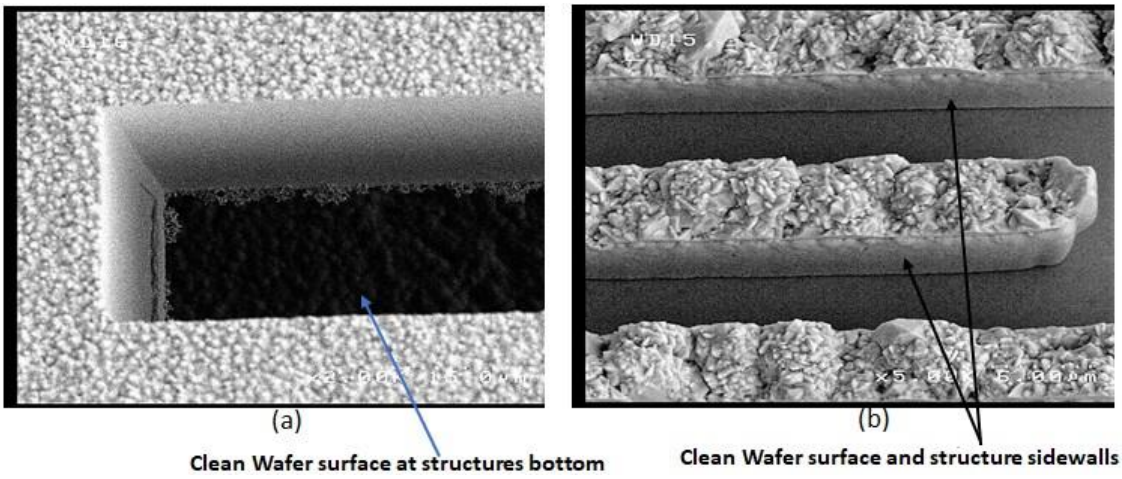

Figure 5.10: SEM analysis of metallic grating: (a) The top view highlights the top and sidewalls of the gratings. (b) tilted view of structure focusing on sidewalls and bottom. In both the images there is no resist residue at the bottom.

Figure 5.11, is showing the dimensions of metallic gratings. In first image of figure 5.11, the width of five periods is measured to be 40.9 μm whereas the second image is reading 16.2 μm for two periods. The average of these two readings suggest that the width of one period is closer to 8 μm. These SEM images provide a close visual representation of structures but they are not precise. Therefore, the dimensions of X-ray mask is very closer to the patterns on photomask.

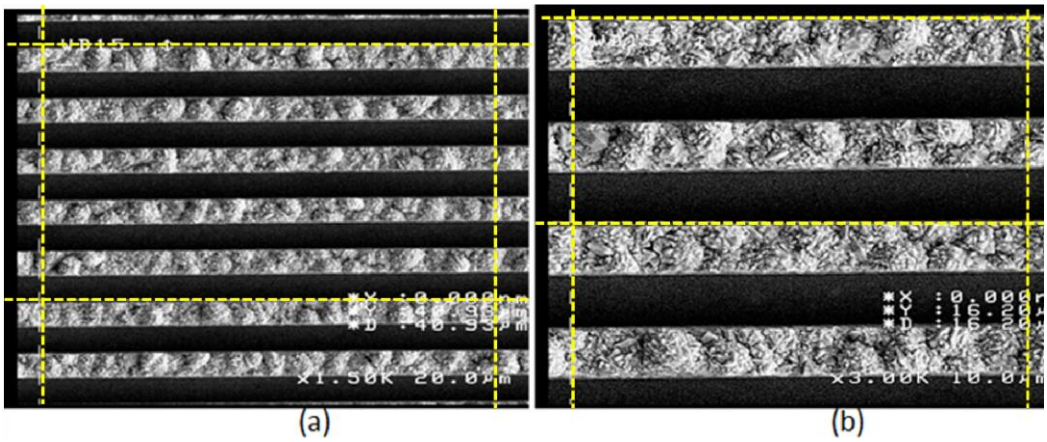

Figure 5.11: Measurement of metallic grating structure of X-ray mask: (a) measures the width of 5 period to be 40.9 μm, (b) the measured width for 2 periods and reads 16.2 μm.

5.1.2.2 Etching of silicon from the backside of wafer to create Silicon nitride membrane.

Once the frontside of the X-ray mask is patterned, the silicon from the backside of the wafer is etched. Figure 5.12, represents the backside of the X-ray mask. It has nine silicon nitride window membranes, which consist of grating pattern on the opposite side.

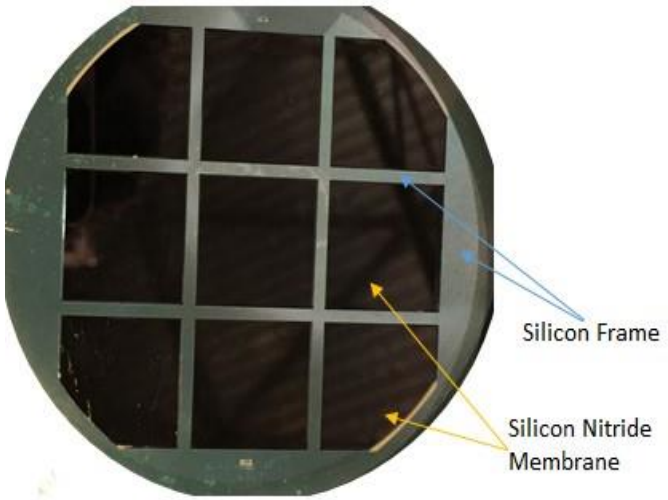

Figure 5.12: Silicon etching by KOH: back side of X-ray mask with 9 silicon nitride widows membrane with 1.5 μm thickness.

As membrane thickness is 1 μm and they are supported by the silicon frame. Later, the wafer is carefully dried under the hood. X-ray mask is very fragile so it is handled with great caution and kept in a protective box till further use.

5.2 Fabrication of Grating

The fabrication of Har gratings follows the procedure illustrated in section 4.1 in previous chapter. This section will discuss the challenges and outcomes of the grating fabrication.

5.2.1 Preparation of Substrate for X-ray exposure

The fabrication process starts with deposition of metallic layer that is oxidized later. This oxide layer acts as a seed layer and enhances the adhesion between substrate and the resist.

5.2.1.1 Electroplating Copper

The selected silicon wafer with gold and chromium coating is electroplated with copper, which is further planarized on flycuting and polishing machine. Figure 5.13, represents the copper electroplated wafer polished down to final thickness of 10 μm.

Figure 5.13: The modified substrate after copper electroplating and polishing.

5.2.1.2 Copper oxidation and Titanium oxidation

Further, the wafers, coated with copper or titanium are oxidized in the oxidization solution. This CuOx surface is a rough and porous black surface with an average surface roughness of 350nm. Figure 5.14, shows the images for the oxidation solution and copper oxide wafer. Similarly, wafer coated with titanium is oxidized in oxidization solution. Figure 5.15, represents the TiOx wafer, similar to CuOx the its surface is also rough.

Figure 5.14: (a)The Copper Oxidation Solution at a heater and the wafer before Oxidation. (b)The copper oxide wafer with a rough and black surface.

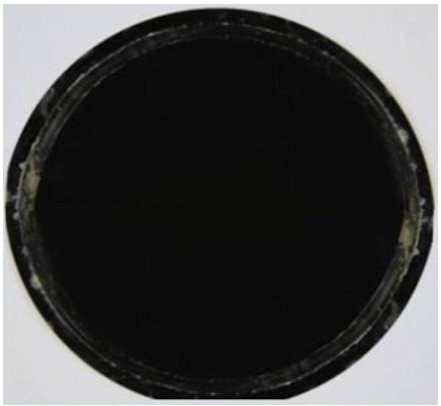

Figure 5.15: The titanium oxidized wafer

5.2.1.3 Bonding of PMMA resist on TiOx and CuOx wafer.

The PMMA resist is bonded over CuOx and TiOx wafers. Further, the wafers bonded with PMMA resist are prepared for exposure by flycutting the PMMA disc down to a desired thickness. Figure 5.16, displays the bonded and flycutted PMMA resist over the CuOx and TiOx wafer with each of 100μm thickness.

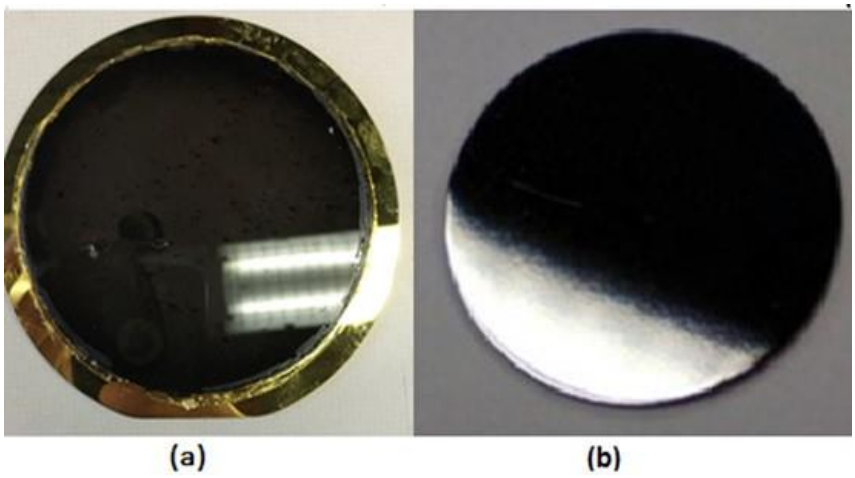

Figure 5.16: Flycuted PMMA wafer: The CuOx wafer bonded with PMMA is flycut to 100 μm (b) The TiOx wafer bonded flycuted down to 100 μm, both were flycut.

5.2.2 Processing the freestanding PMMA to verify the X-ray mask.

The quality of X-ray mask is verified before exposing any prepared substrate. The freestanding PMMA exposures and its development are processed according to the parameters from prior researches. Following is the discussion from the outcome:

Post exposure processing and analysis of PMMA disks with 40 µm exposure dept: Once the exposed PMMA is developed, the wafer is dried out transferred to SEM for analysis. Figure 5.17, collects the optical images from long grating are and support structure grating area, both are smooth and sharp rectangular edges. For further inspection, the wafer is

analyzed under SEM. Figure 5.18, emphasis on support structures and the corners of the grating, respectively. These images indicate that the edges and corners of the gratings are sharp and rectangular. This indicates that the X-ray mask is of good quality. Therefore, this X-ray mask with silicon nitrode is used for the exposures of TiOx and CuOx wafers in order to fabricate HAR gratings.

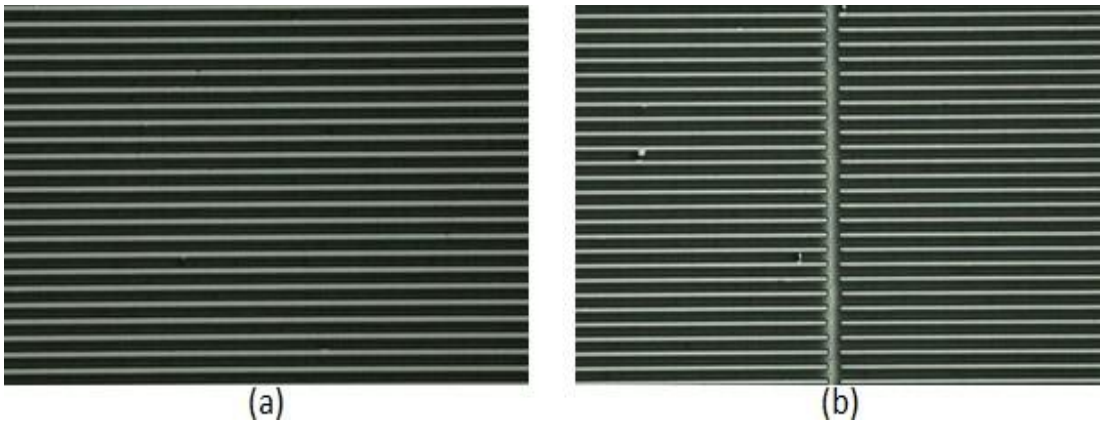

Figure 5.17: Freestanding PMMA exposure: (a) the long grating with 4 μm structures width. (b) highlight the support area, which is clean and smooth.

5.2.2.1 Exposure of CuOx wafer and grating development

Initially, the exposure was planned for thinner PMMA resist, as its processing is comparatively easier than 100 μm thickness. Therefore, the PMMA resist bonded over CuOx wafer is flycutted down to 40 μm. Further, these wafers are exposed to X-rays at XLRM1 beamline, the exposing parameters are shown in table 4.8. Immediately, after completion of exposure the sample is transferred to GG developer for developing.

Post exposure processing and observation: The PMMA was developed with break cycle. Table 4.8, mentions the developing cycles for both the wafers. The CuOx

is under water during optical microscope observation it is difficult to check the bottom of the trenches. Therefore, the bigger area and corners are checked for the PMMA development and based on this observation the status of PMMA development in between trenches is estimated. The first wafer was underdeveloped so the developing cycle for second CuOx wafer is increased, which increases its duration in GG developer. Table 4.8, highlights the developing cycle patterns for both CuOx wafers.

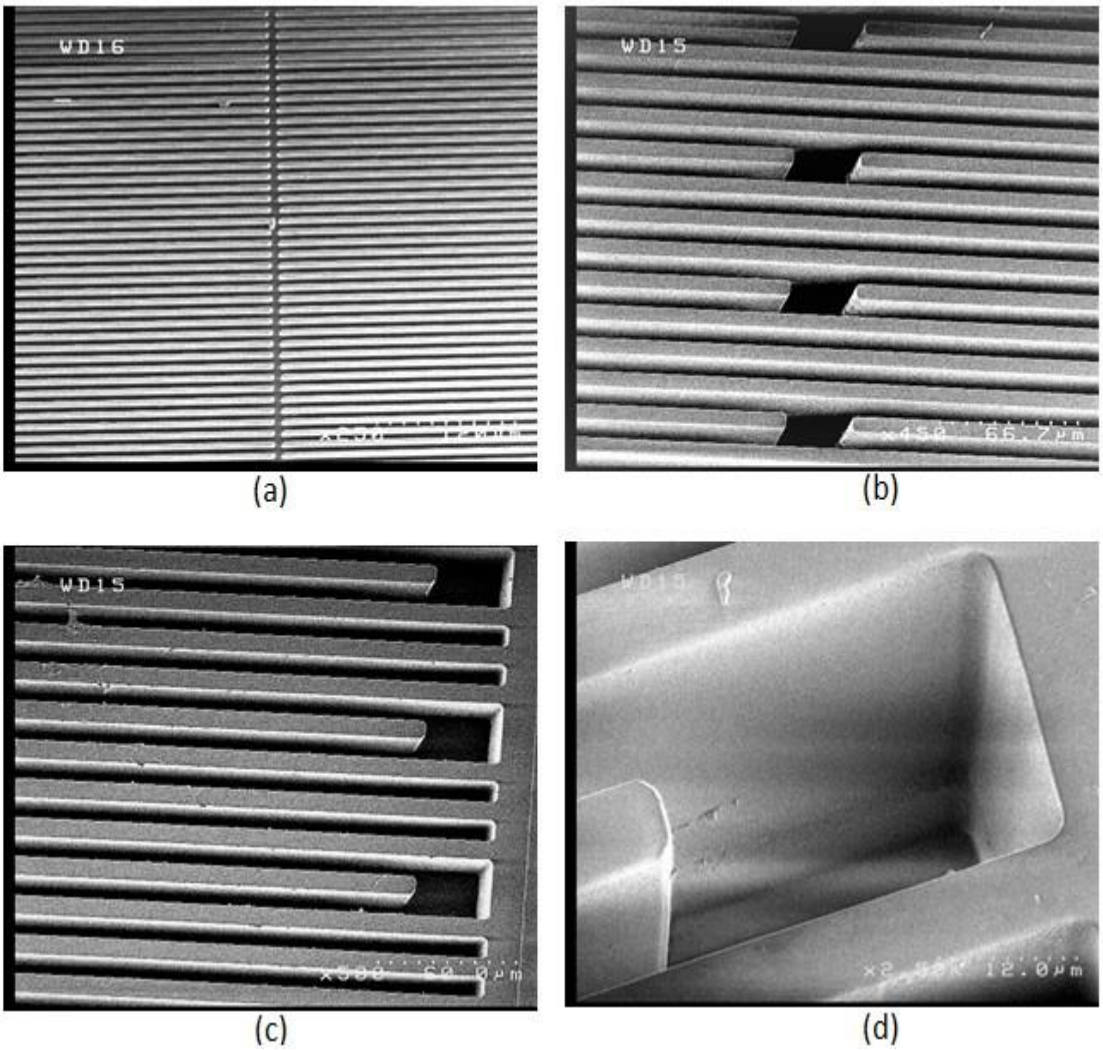

Figure 5.18: SEM analysis of freestanding PMMA: (a) and (b) are the images from 4 μm gratings with support structures. while c) and (d) are the images of the gratings near corner, these 4 μm gratings areas with a tilted view to check the sidewall of the structures, which are smooth and sharp.

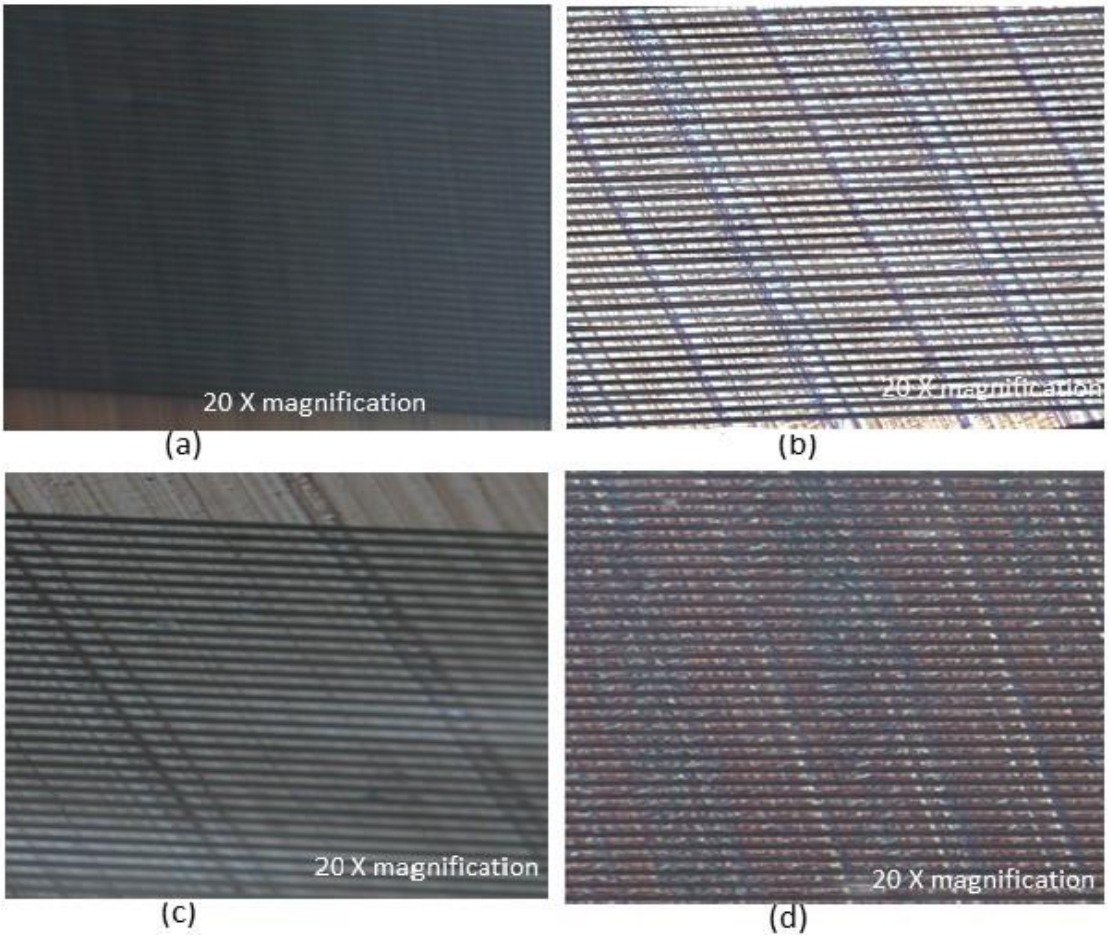

Figure 5.19: Analysis of PMMA development from second CuOx wafer:(a) and (b)are the images from the 4 μm area after second and third developing cycle. (c) and (d) are the similar results obtained from second CuOx wafer.

The wafer was observed under microscope after developing. Similar to the previous wafer the images are not clear under water. However, a closer look reveals that the structures are standing straight. Figure 5.19, is exhibiting the development of exposed PMMA resist. The images 5.19 (a) and (b) are taken from first CuOx wafer after second and last developing cycle. The grating structures looks straight and the duty cycle is also even. While, figure 5.19 (c) and (d) are the images from second CuOx wafer with last cycle. The developing results are similar to the first CuOx wafer. The grating structures

and trenches are much more evident in comparison to previous CuOx wafer. These images are captured from 4μm grating area.

Etching of CuOx from the wafer to expose the conductive surface underneath: The first CuOx wafer is etched for 9 cycles. By the end of last cycle, majority of the structures were bending or falling. Since the structures are of only 4 μm width, the undercutting beneath the structure bottom will results in bending or debonding of PMMA structures. Similar to first CuOx wafer, the second CuOx wafer is processed for copper oxide etching, only the developing cycle was reduced to three as shown in table 4.9. Still, the structure was falling even after reducing the etching cycles. Figure 5.20, are the images taken during CuOx etching of both the wafers. The broken structures and bending structures are shown in figure 5.20 (a) and (b), taken from first wafer analysis. While, the image 5.20 (c) and (d) are taken from second CuOx wafer, where first image focuses on the grating structures near corners, which are falling. Whereas, the last image is showing the copper layer underneath grating structures. Post etching the wafer was taken out for nickel electroplating.

Electroplating Nickel structures: Post PMMA development, and Copper oxide etching from copper wafer, the wafers were proceeded for nickel electroplating. The results for the nickel electroplating is discussed in this section below.

Electroplating of the first CuOx wafer**:** The wafer was plated for 10 μm with the current density of 14 mA/cm^2. The final results showed the overplating over the structures and underplating because the structures were lifted off. In some area PMMA was not developed all the way to the bottom, thus the wafer did not receive plating.

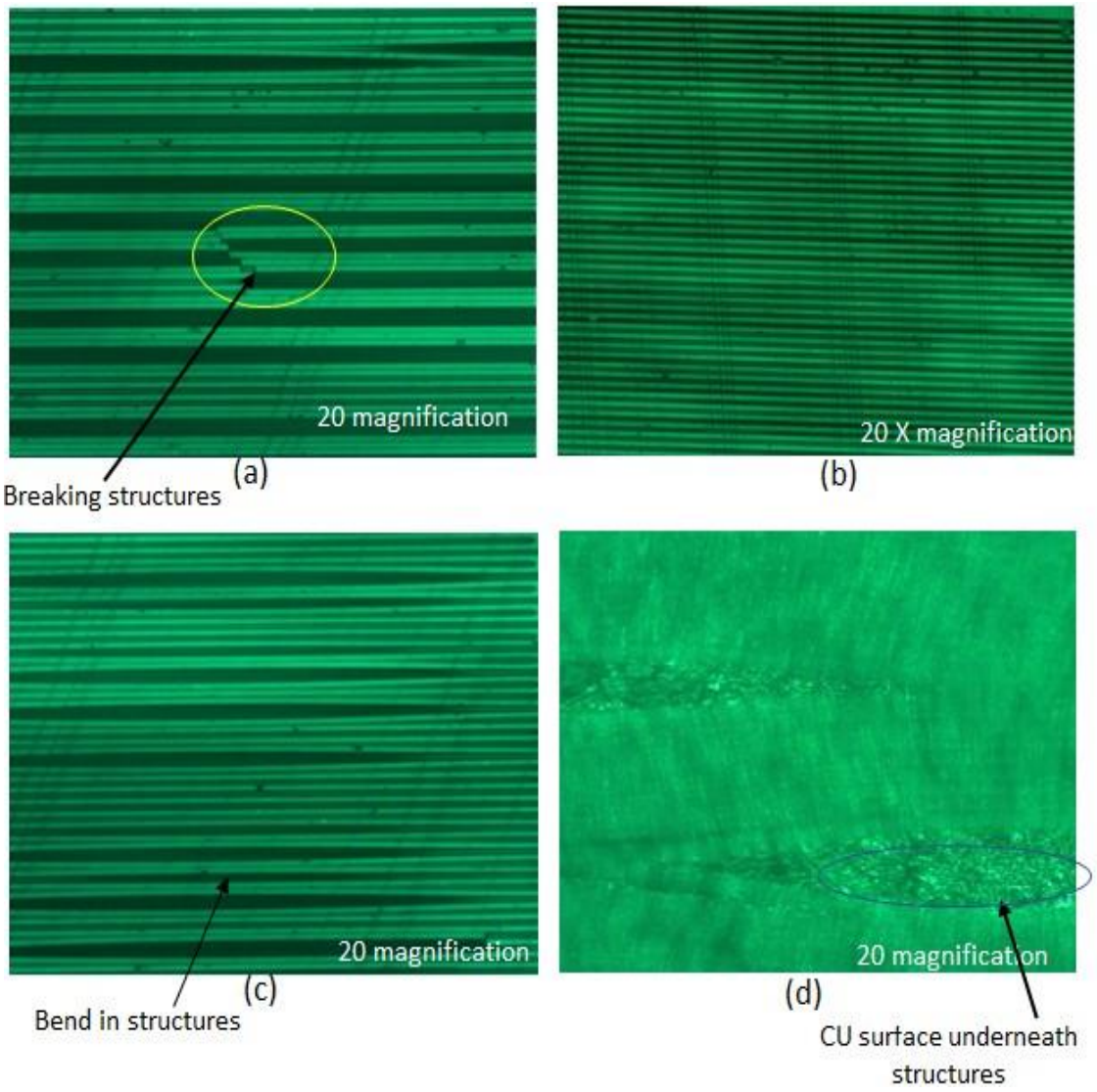

Figure 5.20: Etching the oxide layer from CuOx wafer: (a) and (b) 4μm gratings, the structures are falling and breaking due to overetching and undercutting. (c) area near edges, structures are standing with slightly widen trenches. (d) Focuses on the bottom of the wafer, where the copper layer can be seen in between the bending structures.

Electroplating of the second CuOx wafer*:* For second Cu wafer, post CuOx etching it is exposed to plasma asher. The hot plasma air reduces the contact angle between PMMA and plating solution and makes PMMA more hydrophilic, thus letting the solution enters in between [48] structures, which helps the plating solution to enter the trenches. This wafer is plated for 20 μm with the current density of 15 mA/cm^2. The nickel plating

was uneven, random and overplated at many places, any be because of debonding of resist structures. Figure 5.21, analysis the wafer after nickel plating. The image in figure 5.21 (c) is showing the area which did not received any plating. It may be due to improper etching the copper oxide is still present in this area, which makes the area non-conductive, thus restricting any plating. The PMMA residue due to underdevelopment may also make the area nonconducting resulting in no plating. Whereas, the overplating is seen in the image 5.21 (a) and (b), where the layer of nickel has covered the top of gratings. This effect is because the uneven plating has caused plating rate in a particular area to increase more in compare to other areas.

Samples with copper oxide layer provide good adhesion to the resist. The PMMA structures were standing good while PMMA development. However, during TiOx wafer processing, the PMMA structures were debonding even though the exposure dose and resist thickness are similar to CuOx wafer with lesser PMMA developing time. However, the etching of copper oxide is a major concern. Each time, the structures have fallen due to undercutting of PMMA strictures during the etching cycle.

Lastly, 5.21 (d) is showing the area where structures were already falling during CuOx etching and after plating their condition deteriorated further.

5.2.3. Post Exposure processing of TiOx wafer and analysis

The PMMA bonding of 40μm TiOx wafer was not good thus the PMMA resist structures debonded while developing. The debonding caused bending and falling of resist structures. Whereas, the second TiOx wafer, the 41μm resist thickness showed good results

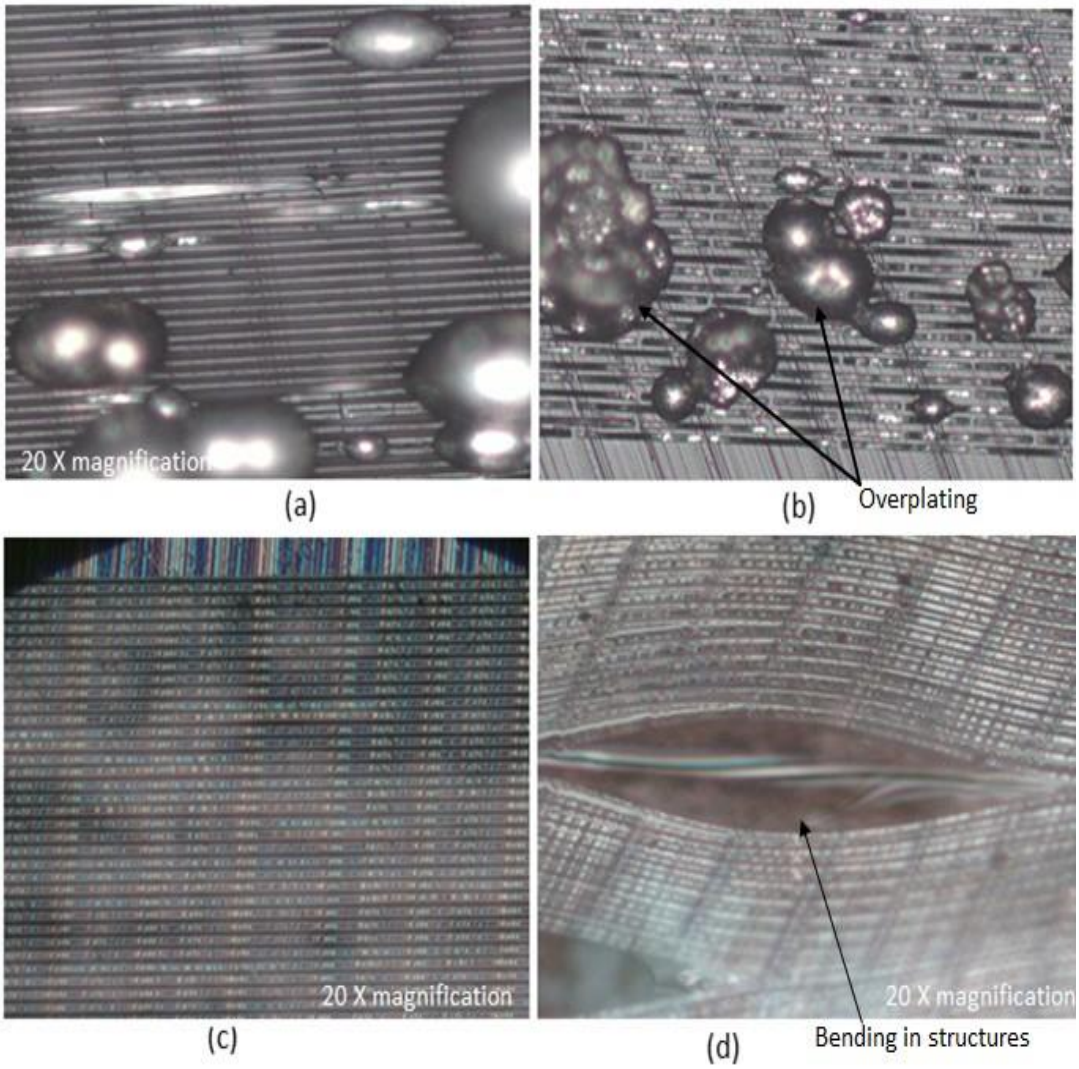

Figure 5.21: The nickel electroplating of first CuOx wafer: (a) The overplating is seen on the top of grating structure. (b) plating in this area is evident but it is uneven and overplated. (c) The plating in area where structures are falling post etching but no structure can be seen here. (d) this area did not received plating but structures are standing straight.

during development process. It was developed for two cycle and figure 5.22, shows the images captured during development of radiated PMMA. Where (a) is showing the bending structures in 40 μm TiOx wafer due to debonding of PMMA resist. The image 4.22 (b) is the 4 μm area gratings with support structures for 41 μm TiOx wafer. While image 4.22 (c) and (d) are 4 μm long gratings structures near corner and the center of the cell.

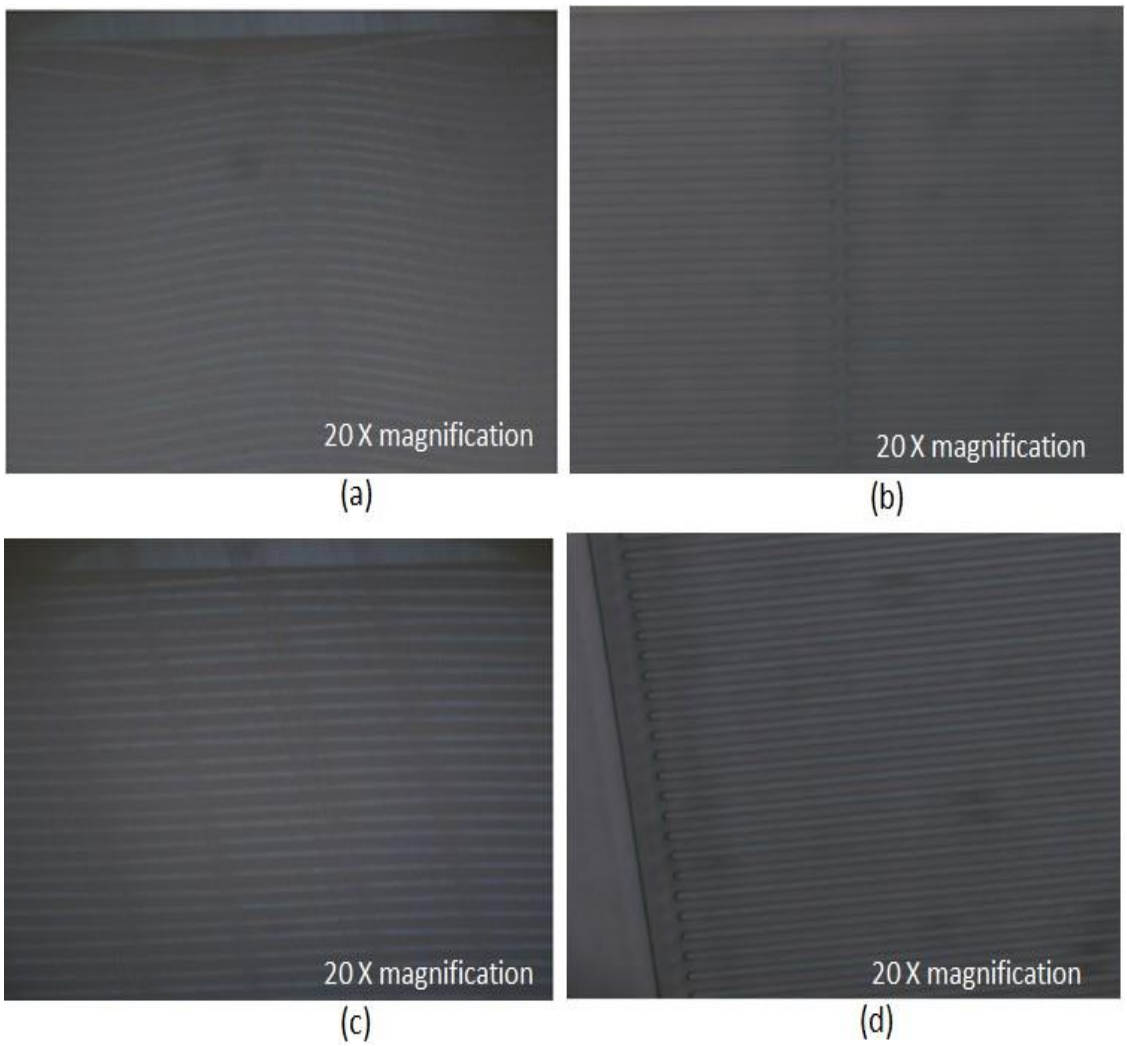

Figure 5.22: Developing the exposed PMMA resist for second TiOx wafer:(a) The falling structures in first TiOx wafer with 40 μm thick resist due to PMMA debonding. (b) The support structures grating after first developing cycle which looks straight. While, (c) and (d) are the images of long grating structures in 41 μm after the second developing cycle.

These structures look good with 50 % duty cycle; however, a closer look reveals the start of bending in structures. This is an indication that the developer has developed the exposed PMMA to the bottom and now started undercutting beneath the structures. Thus, the PMMA developing is stopped at this point and the wafer was proceeded to Nickel electroplating. After plating, the photoresist is stripped from the wafer and the plated Nickel structures are observed under SEM in order to learn the debonding mechanism.

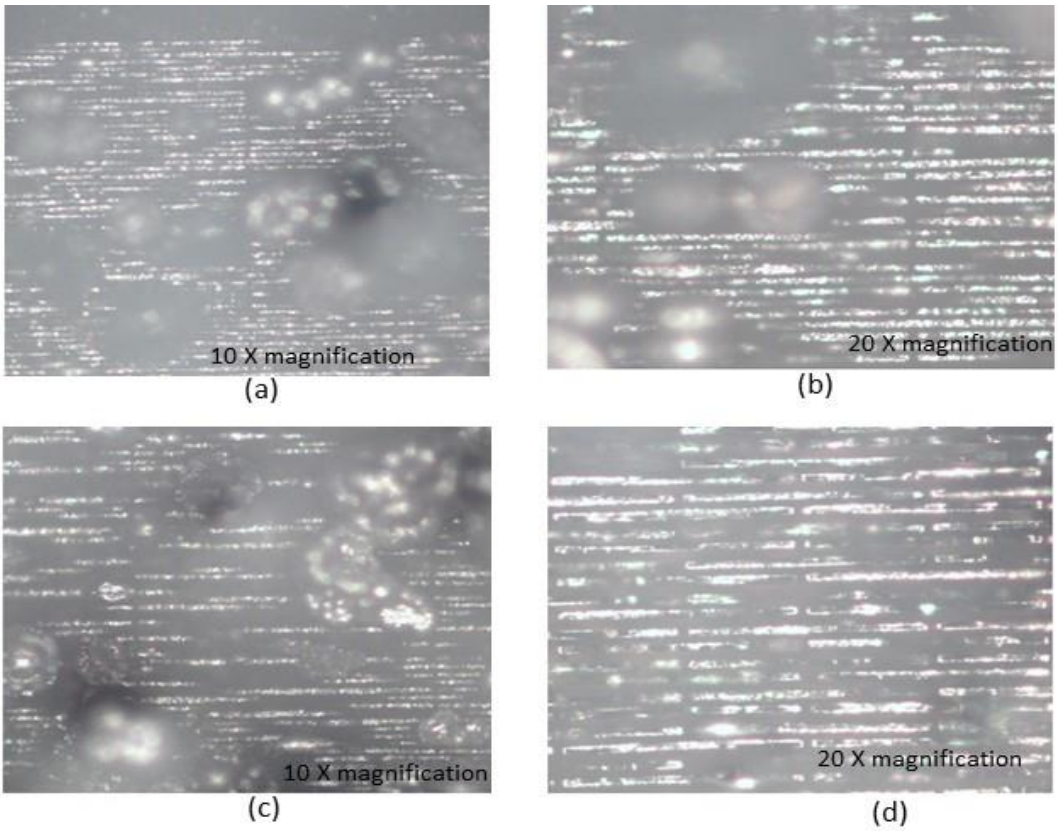

Figure 5.23: The Nickel electroplating of second TiOx wafer: (a) The 4 μ area with nickel grating structures but it has lot of overplating. (b) Same area 'a' with a focused view to closely check the structures. (c) and (d) are the other area with similar location have different magnification.

Electroplating of second TiOx wafer*:* The second wafer was electroplated for 20 μm thick nickel at the current density of 14 mA/cm^2. Observation revels that the electroplating is very uneven, some areas were overplated while the others did not receive any plating. Figure 5.23 (a) and (b) are the images taken post electroplating, the nickel structures can be seen in between PMMA structures, however the wafer has lot of overplating at the top of structure. The cause for overplating are similar to previous wafer Whereas, the images in 5.19 (c) and (d) are the pictures from other 4μm location, which

received plating. Here also the wafer got overplated and grating structures are underneath nickel layer.

The wafer was not flood exposed as there was lot of overplating and PMMA cannot be stripped. The processing of both TiOx wafers indicate that the development of exposed PMMA is uneven. There is PMMA residue left after development due to this the wafer surface is not uniformly conductive. To avoid overplating, it is essential to completely remove the PMMA from the bottom of the trenches.

Post exposure processing and analysis for TiOX wafer with increased PMMA thickness: To increase the aspect ratio for grating structures the thickness of the PMMA resist is increased. The X-ray exposure and PMMA development parameters were established by working on freestanding PMMA with 100 μm thickness. Later, TiOx wafer with PMMA resist was processed. First, the PMMA resist on TiOx wafer was flycut down to 90, 100 and 100 μm. Then, these wafers were exposed to X-rays and further developed in GG developer. The solution of GG developer is also changed for developing thick PMMA resist. Due to multiple use the exposed PMMA gets dissolved in GG solution which changes it composition and reduces the developing rate. Before developing the TiOx wafer, the developing rate of new GG developer is tested on other samples. The details of developing cycles are discussed in the table 4.8, in previous chapter.

The first TiOx wafer with 90 μm thick PMMA resist, post exposure was developed in GG developer and IPA solution as mentioned in table 4.8 in previous chapter. Unlike previous wafers this wafer was developed without breaking the developing cycle. The observation revels that the structures were bending and falling. Figure 5.24 (a) and (b) are showing the bent structures for long gratings and the gratings with support, respectively.

Further wafer was passed through IPA and dried, the image from dried area is shown in figure 5.24 (c), showing the damaged resist structure. The wafer was overdeveloped and due to undercutting the tension on structures caused bending. Thus, it is better to break the developing cycle and observe to avoid overdeveloping. The wafer was transferred to the electroplating stations and electroplated for 40 μm nickel thickness.

Flood exposure and resist striping*:* Post flood exposure and resist stripping results are arranged in figure 5.24, where (d) are the images from the overplated areas, few grating structures can be seen in between thick layer of nickel. Whereas, in image 5.20 (e) and(f) nickel grating structures are merged at the bottom, it happened because the structures were lifted during early stage of plating resulting in merger of nickel structures at the wafers surface.

Post exposure processing of TiOx wafer with 100 µm PMMA thickness*:* Further, two samples of TiOx wafer was prepared by bonding PMMA resist disc over it and then flycutting the resist down to 100 μm. These wafers are exposed at the XRLM1 beamline with the exposure parameters mentioned in table 4.6. *Developing the PMMA resist after exposure:* The development cycle for both the wafers is mentioned in the table 4.8. Figure 5.25, shows the images taken using optical microscope while observing the PMMA development for both the wafers. Figure 5.25 (a) and (b)shows the images captured from first TiOx wafer with 100 μm thick PMMA resist. These images highlight the long grating without and with support structures. The grating structures are standing straight with equal trenches width. Figure 5.25 (c) and (d), shares the similar information about second TiOx wafer, structure in this location are standing straight with smooth and sharp

edges. The images in figure 5.25 (e) and (f) are capture while focusing at the bottom after the last cycle of developing.

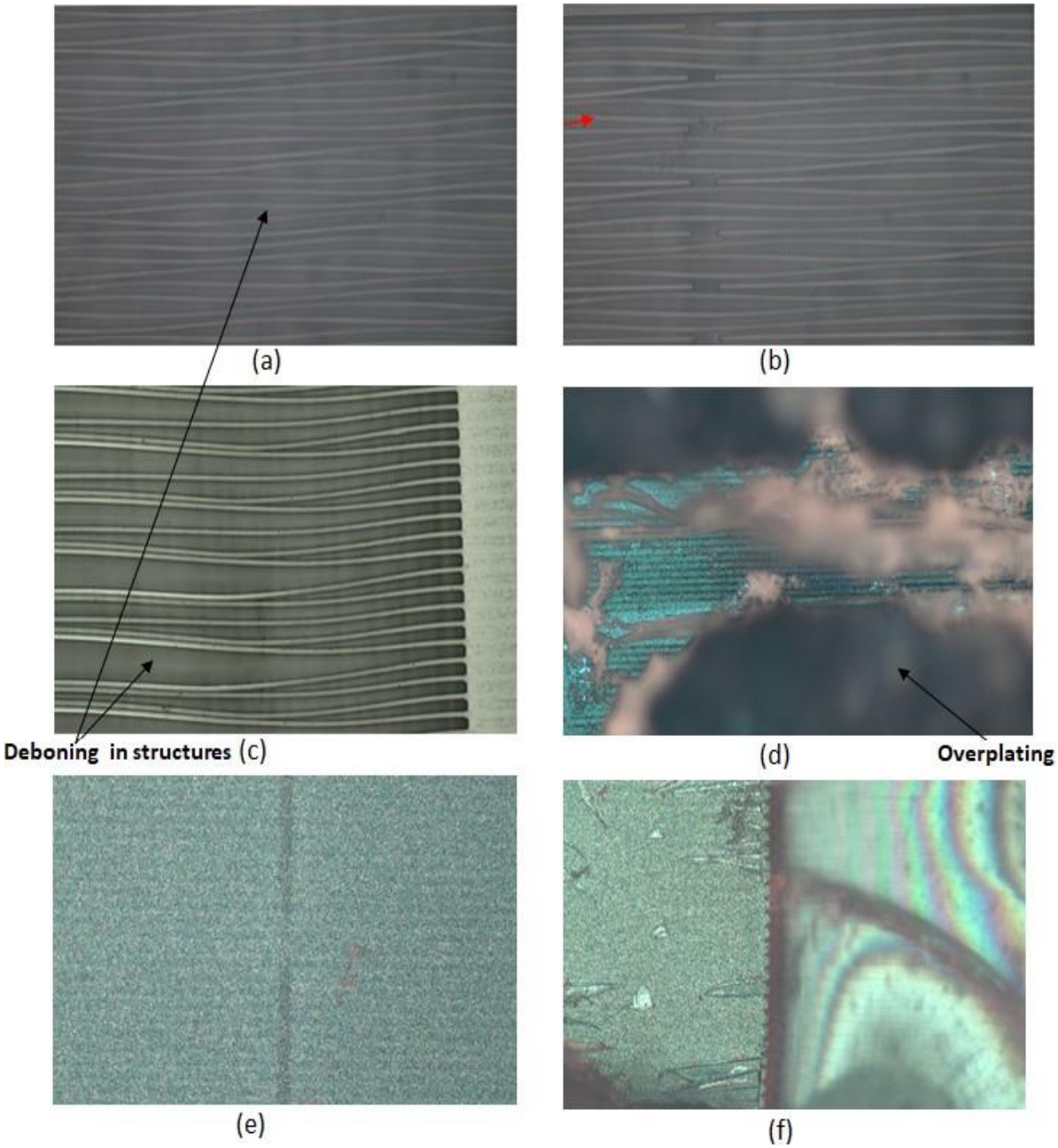

Figure 5.24: Microscopic Analysis of the 3rd TiOx wafer: The images (a) and (b) are from 8 μm period grating without and with support structure, respectively. The structures are falling for both areas. (c) is the images taken from the wafer after developing it in IPA solution and drying. (d) displays on the overplated area of the wafer. whereas, (e) and (f) are focusing on the wafer surface, where nickel structures are obtained post flood exposure.

Nickel electroplating for the TiOx wafer: Post developing, the TiOx wafer with 100 μm tall resist structures is processed for nickel electroplating. Initially, first wafer was plated by 60 μm thickness at 14 mA/cm^3 current density. As displayed in figure 5.26 (a), the wafer is densely overplated but it received nickel in between trenches. This indicates that some areas still have PMMA residue. Thus, to remove the overplating the wafer was polished on lapping and polishing machine. However, the wafer was over polished resulting in damaging many of the structures.

Similar to the first wafer, the second TiOx wafer, bonded with 100 μm thick PMMA resist is passed through plasma cycles at plasma asher. Since, previous wafer was left with PMMA residue even after plasma asher, four more plasma cycle were conducted on the second wafer to ensure that there is no PMMA residue at the bottom surface. Later, the wafer was plated for 100 μm thickness at the current density of 10 mA/cm^2 and 16 cm^2 area. The plating current was calculated as 160mA, while the plating voltage was monitored regularly to be 0.9 to 1.1 volts. The electroplated wafer was overplated but it was much less in comparison to previous TiOx wafer. Therefore, wafer is polished at the machine to remove the overplating from the wafer. In the last stage the wafer is polished by using cloth and 1μm water slurry to remove smearing on the top of structures. As a result, the gratings were uniform and smooth top surface. Figure 5.26 (c) and (d), presents the images taken under microscope at long grating structures after polishing. While figure 5.26 (e) and (f) are the images from grating with support structure area.

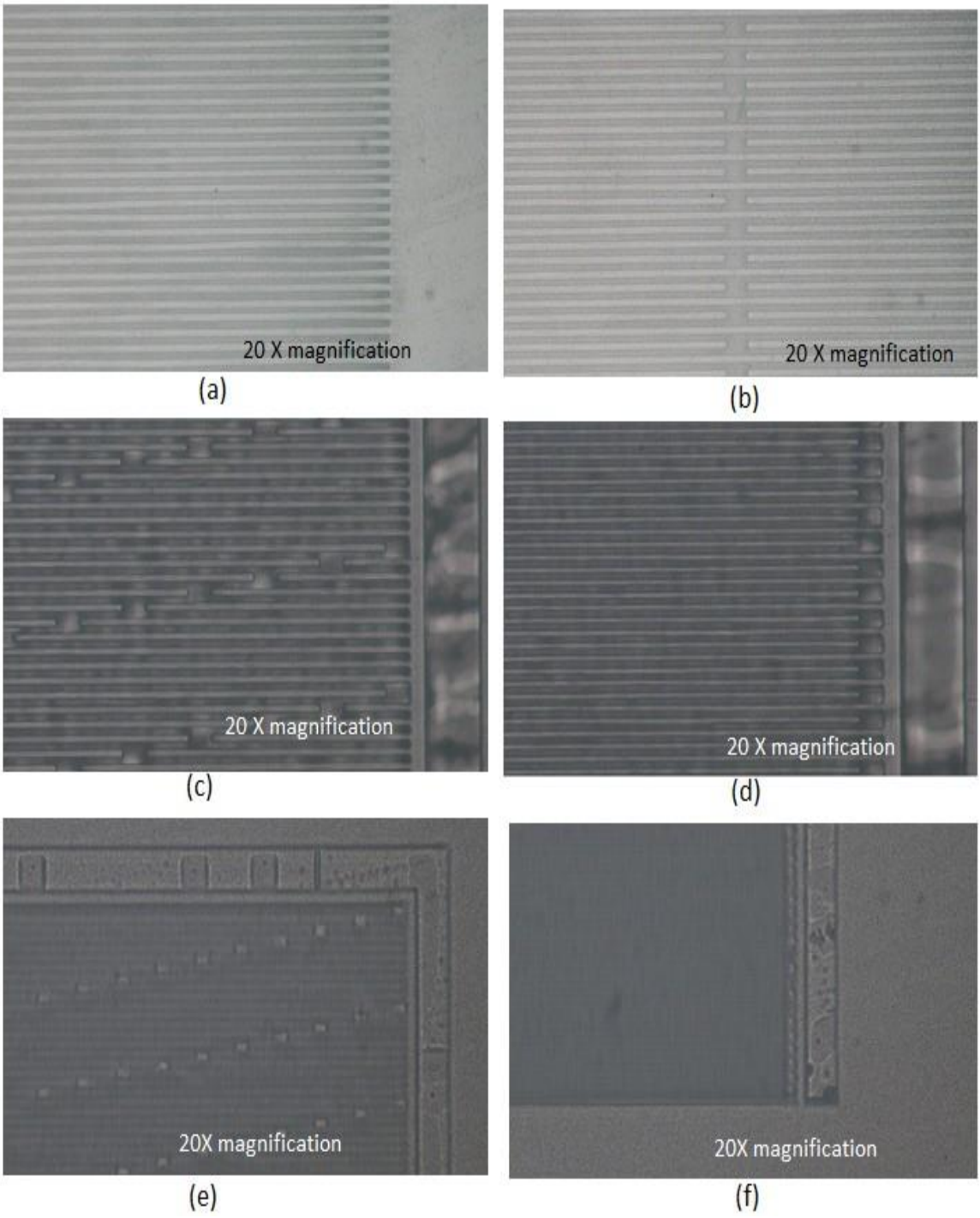

Figure 5.25: The PMMA developing of TiOx wafer:(a) and (b) displays the 4µm long grating and the gratings with support structures from the first TiOx wafer with 100 µm thick PMMA resist. Similarly, the image (c) and (d), shows the 4µm gratings from second TiOx wafer. Whereas, the image (e) and (f) are focusing on the bottom of structure to check the resist residue after IPA developing.

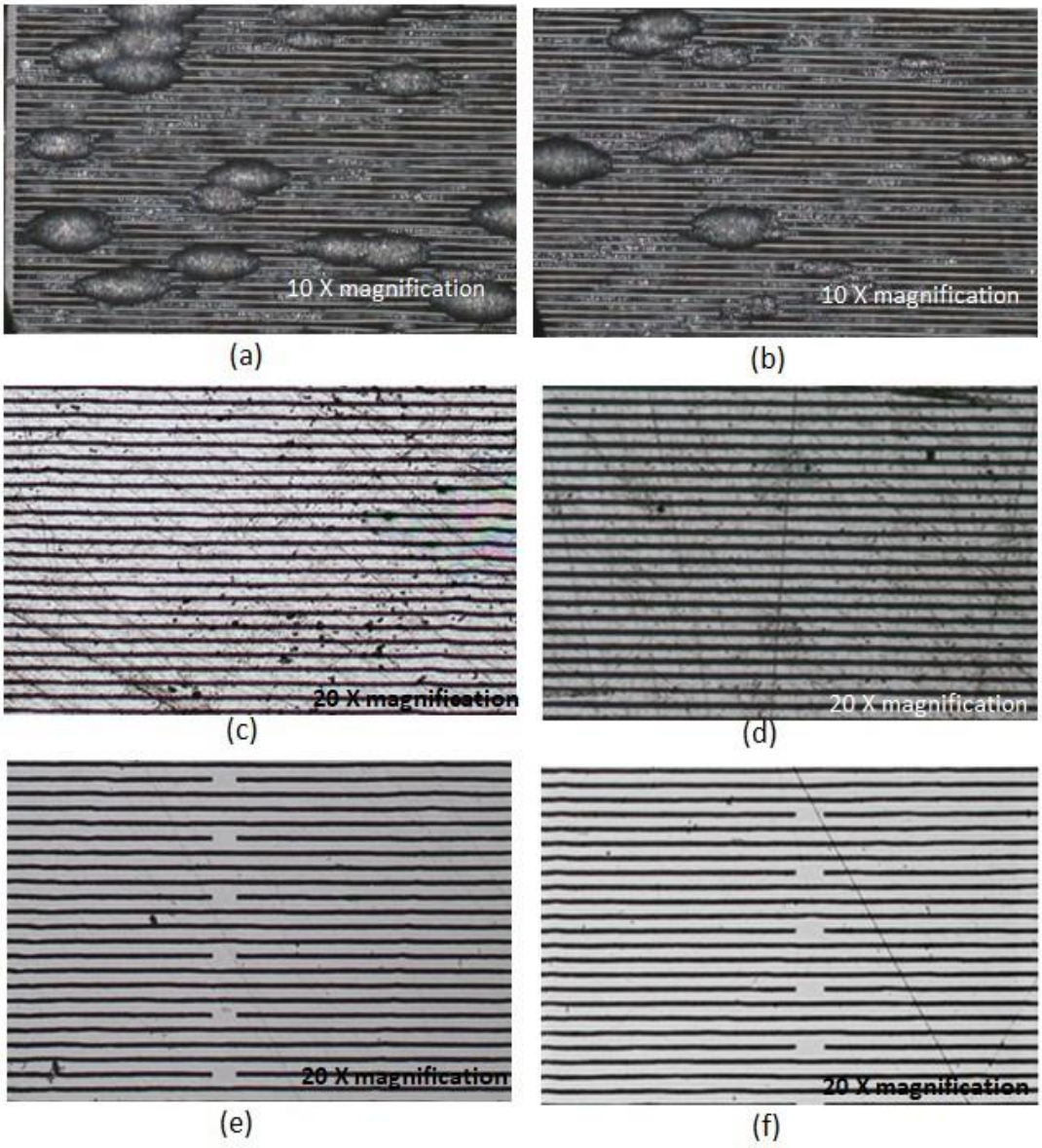

Figure 5.26: Electroplating the fourth TiOx wafer: (a)and (b) are images form 4 μm area, operplating is clearly visible on the wafer. (c) and (d) are showing similar results as previous two images. this area is densely overplated. (e) and (f) are the images from after polishing which resulted in damaging the structure.

Flood Exposure for both the TiOx wafers post electroplating*:* Once the overplated nickel is removed from the wafers by polishing. The PMMA resist between metallic structures is striped by flood exposure. Figure 5.27, shows the grating structure after flood exposure and resist stripping. The top profile of grating structure looks smooth.

The gratings near support structures are straight with sharp edges, the images in figure 5.27 (a) and (b) are grating with 8μm period and 50 % duty cycle from both the wafer. While, the figure 5.27 (c) and(d) are presenting the grating without support structure with 8μm period. The actual dimension of the grating is observed under SEM.

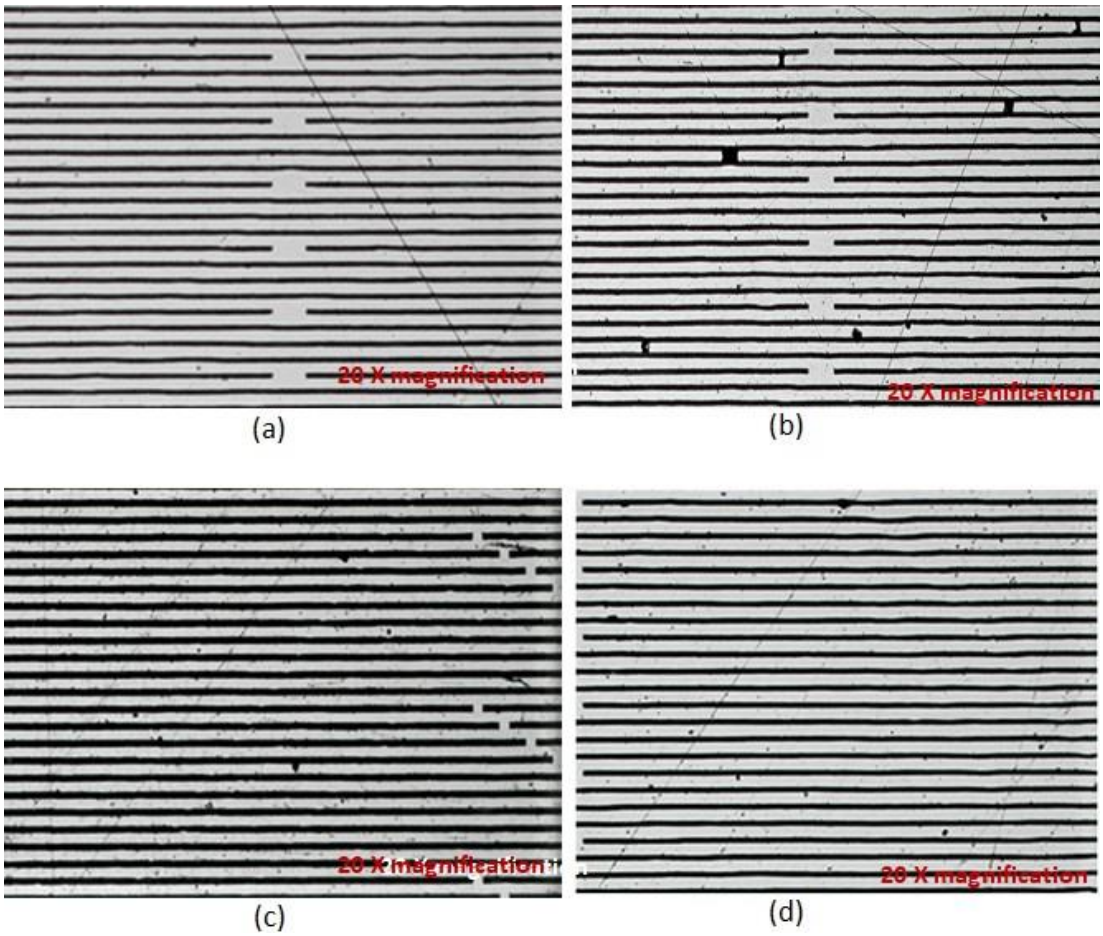

Figure 5.27: Flood exposure of TiOx wafer: (a) and (b) support structure gratings with 4 μm after flood exposure from first and second wafer, respectively. (c) and (d) are the images taken for 4 μm long gratings.

SEM analysis of first TiOx wafer with 100µm thick resist: Post flood exposure processing the wafer was analyzed under SEM. Figure 5.28, is representing the 8 μm period area. As previously mention, the wafer has resist residue at the wafer surface, which causes uneven plating. The images in figure 5.28 (a) and (b) exhibits the broken grating structures

due to non-uniform plating. Figure 5.29, presents a closer look to the broken structures. It is evident from the image that the area did not received plating. These defects are due to PMMA residue at the bottom surface of the wafer preventing any nickel plating.

SEM analysis of the second TiOx wafer with 100µm thick resist*:* Properly dried wafer is kept under SEM for analysis. Figure 5.30 exhibit images by the SEM analysis on wafer.

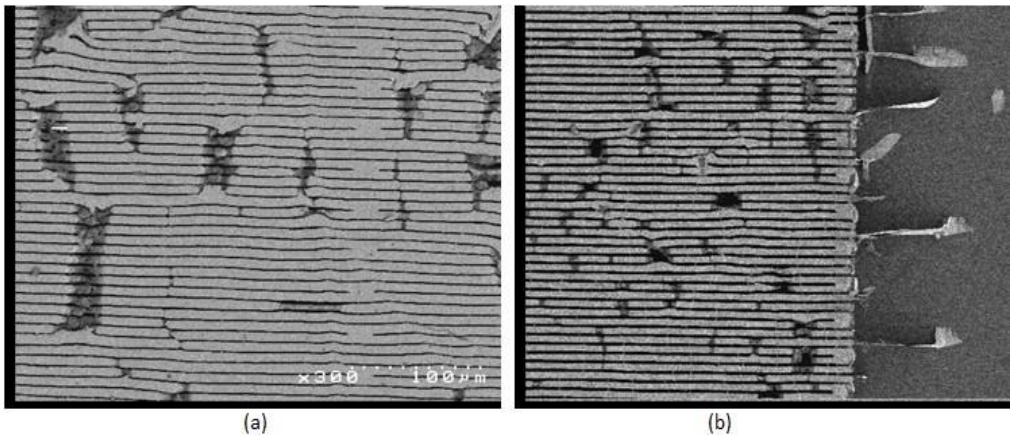

Figure 5.28: SEM analysis for damages structures: (a) The 8 μm period area, gratings are bending and broken (b) Top view of long gratings, the plating in the area uneven thus grating structures area broken.

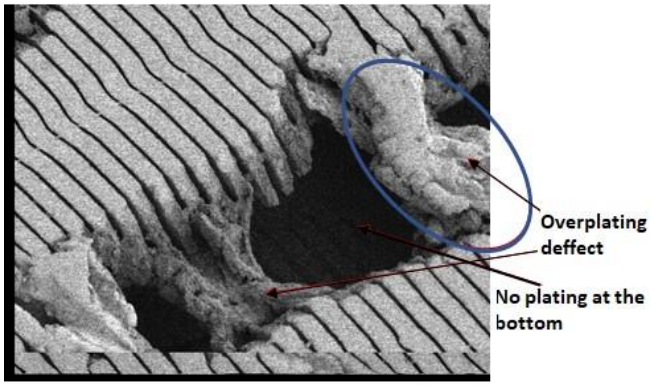

Figure 5.29: SEM image capturing overplating and also highlighting the bottom wafer surface where there is no evidence of nickel suggesting that it did not received plating solution, may be due to PMMA residue.

The SEM analysis of the TiOx wafer provides a closer look to the structures. The images are from same area with different magnification revealing that the nickel structures are straight and smooth. The top view of the grating structures is captured in figure 5.30, where gratings with support structures and the grating structures are displayed. The structures are straight with sharp edges. However, the corners are rounded similar to mask. Figure 5.31, captures the images from the areas of the 8μm period region, it captures a wider area to highlight the uniformity in grating structures. Figure 5.31 (a) is the 2-D view of the long grating with 90^0 rotation and 5.31 (b) displays the grating with support structures.

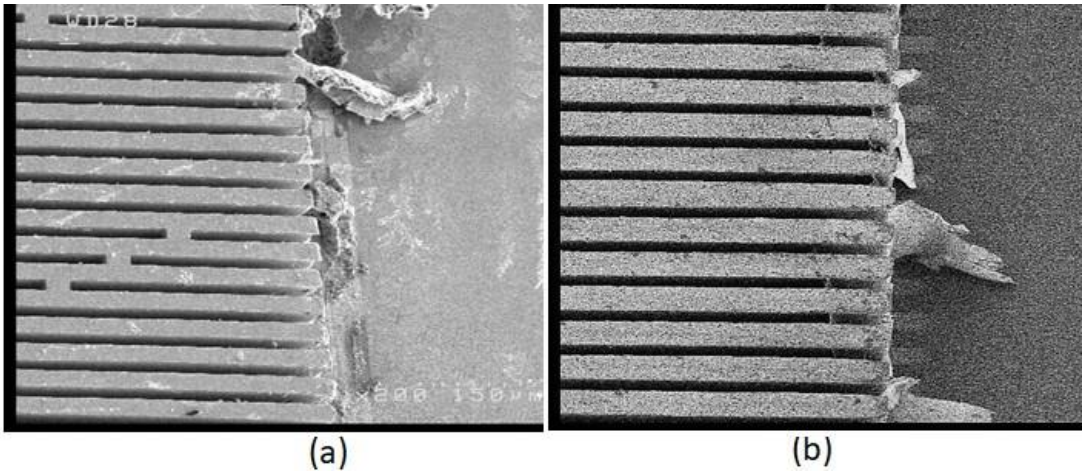

Figure 5.30: SEM analysis of the Ni gratings structures: (a) Highlights the gratings structures with staggered support structures in 8μm period. (b) Long grating structures at the cell corners.

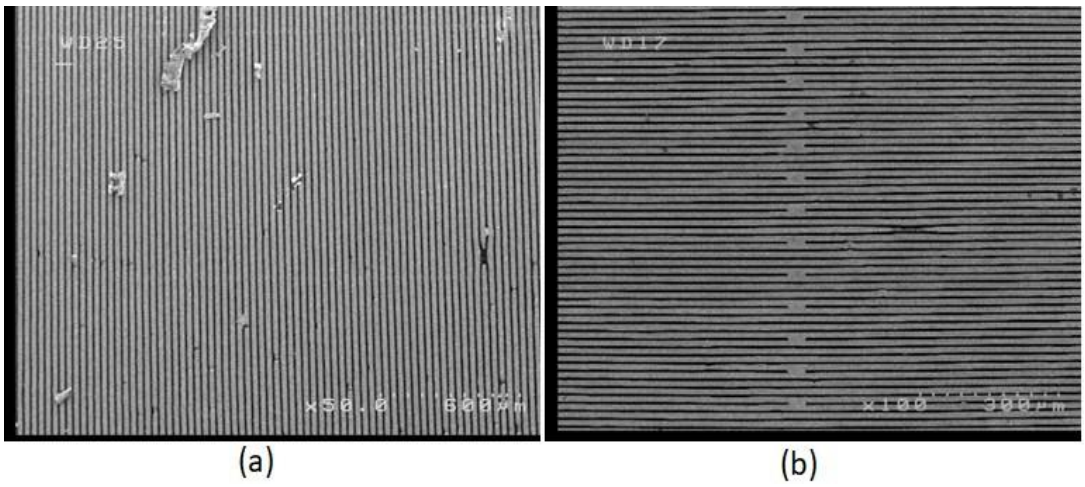

Figure 5.31: The top views of the grating structures under SEM: (a) is the 2-D view of the top surface 8 μm period long gratings at 50 X magnification to display uniformity, (b) The grating with support structures at 8μm period.

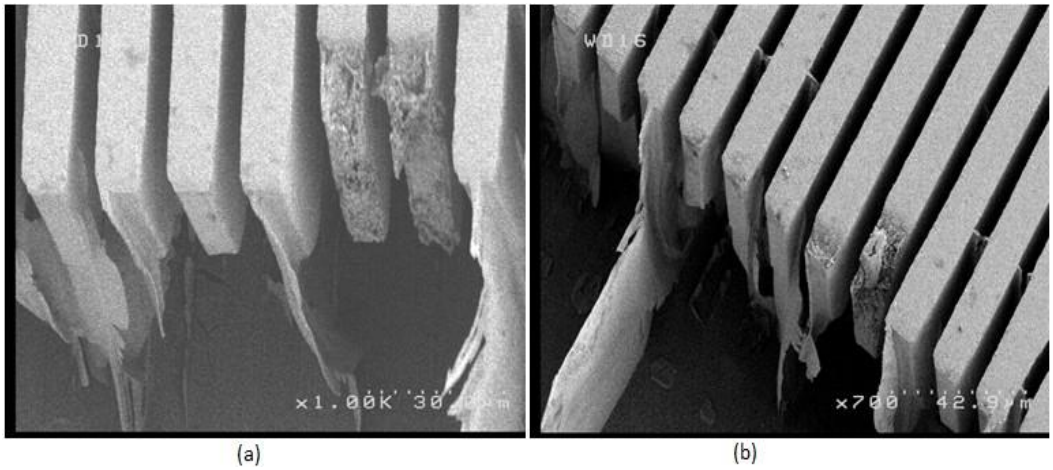

Figure 5.32: 3-D view of the grating under SEM: (a) The top view of the gratings with 8 μm period, (b) the tilted view on gratings at the cell corner with smooth rectangular profile.

The measurement of the grating structures: Figure 5.32 is presenting the rectangular corner gratings. The nickel structures are smooth and rectangular in profile. The image in figure 5.32 (a) showing the top of the Figure 5.32 (c), give a 3-D view of the walls of the highlighted grating. The grating structures are straight and gap is uniform but the width of structures look more than the gap. The dimension of gratings is analyzed by

measuring single grating and single gap, single period and multiple periods. Later, the average of these measurements provides an estimation for the width of grating, gap and period. Figure 5.33 (a), is showing the measured width of the grating to be 6.6 μm and the figure 5.33 (b), is the width of the period as 8.16 μm and the difference between two measurements is 1.4 μm. Whereas, figure 5.33 (c) and (d) are measuring 2 gratings and 2 gaps. The 2 gratings and a gap width is 15 μm and the width of including two gratings is 16.46 μm. Both measurements have a difference of one gap and the measurement reading differ by 1.4 μm, which is very close to previous measurement.

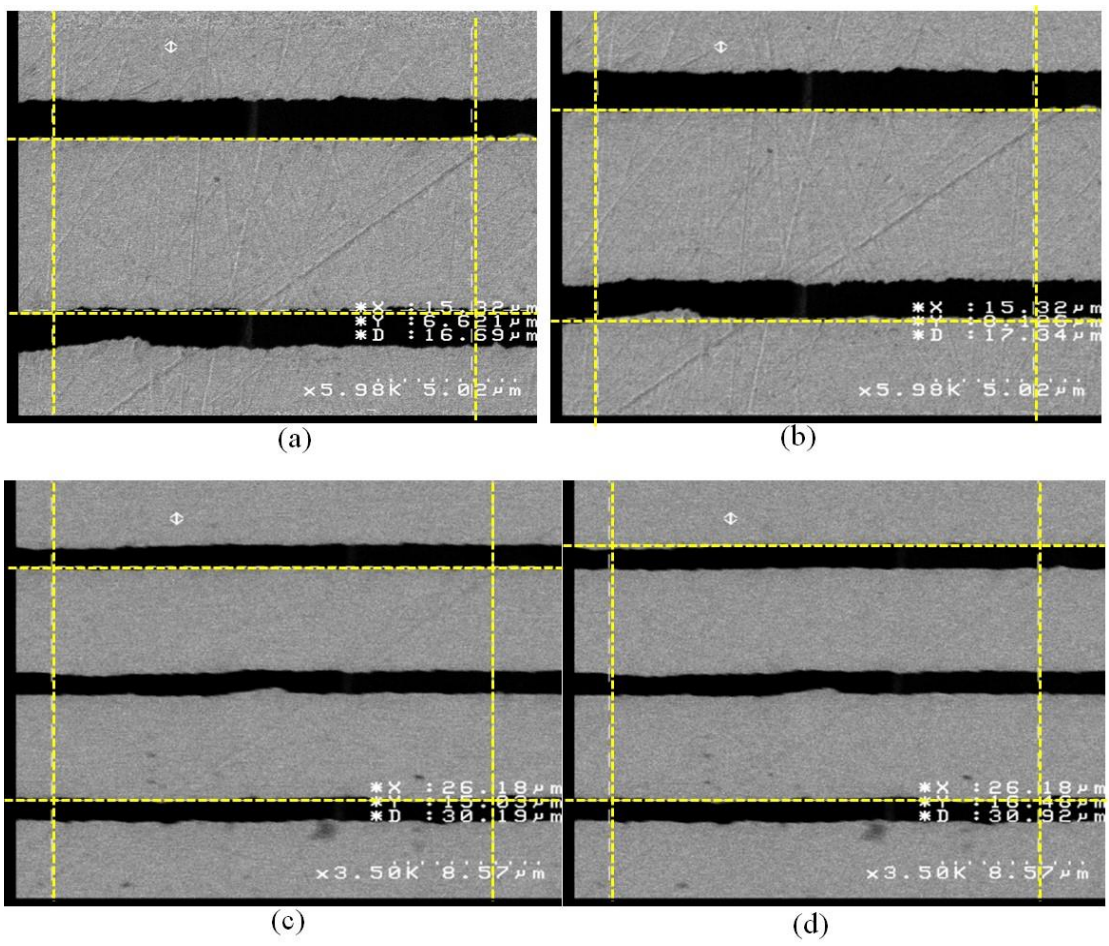

Figure 5.33: Measurement of the structures: (a) measurement of single gratin width, (b) Measurement for a single period. (c) is highlighting the measurement of two grating and a single gap and (d) is measurement for the two periods of grating structures.

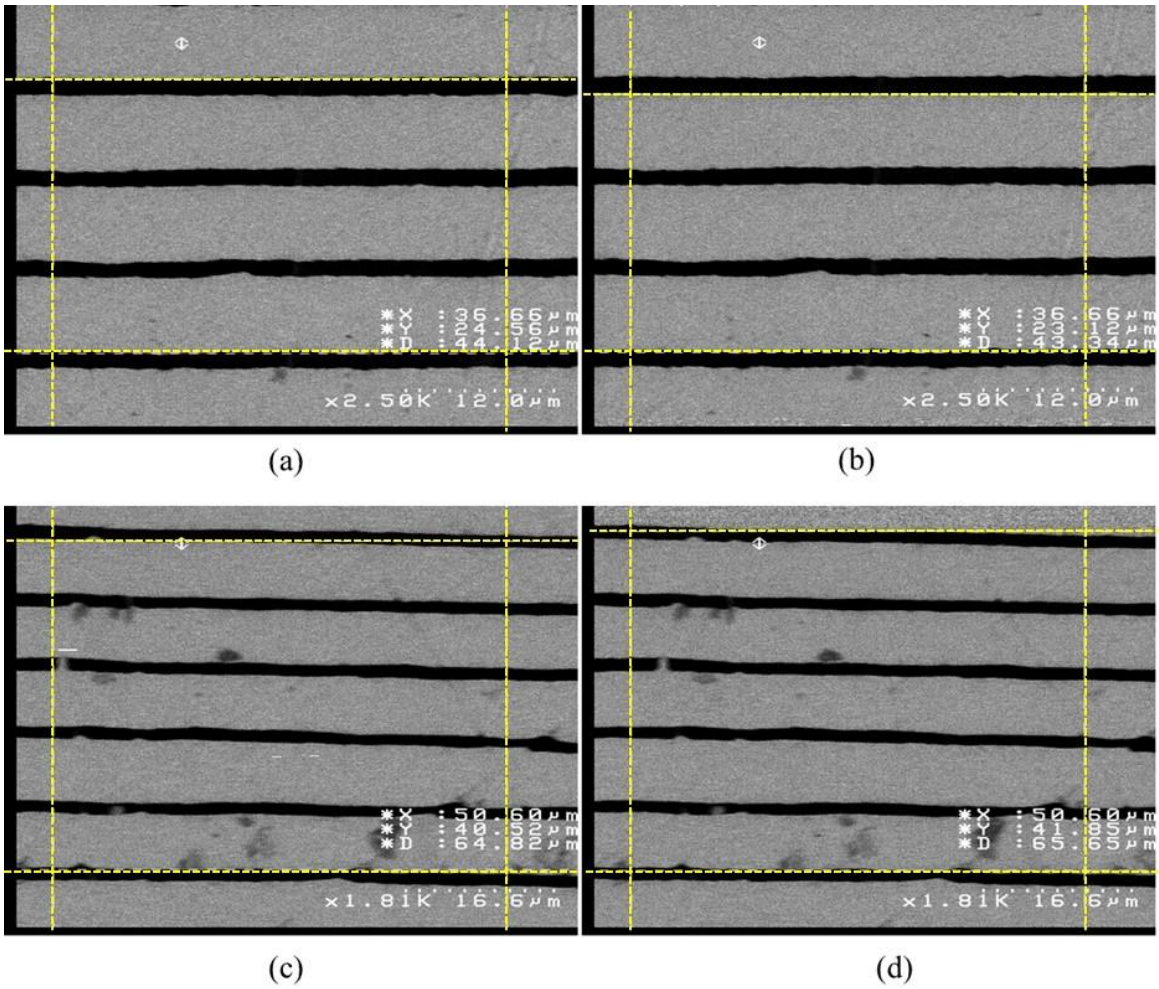

Figure 5.34: Measurement of the structures: (a) measurement of three periods for grating structures (b) is measuring the width of three grating and two gaps. (c) is highlighting the measurement of five gratings and a four gap and (d) is measurement for the five periods of grating structures.

More gratings were measured to check the uniformity in width and the period of grating, measurements are exhibited in figure 5.34. Here, figure 5.34 (a) captures the measurement of 3 gratings and three widths between them and measuring the length as 23.12 μm and the next image 5.34 (b) shows the 3 consecutive periods with 24.56 μm. Adding one more gap results in 1.4 μm difference in measurement. The following figure 5.34 (c) and (d), captures four grating and four gaps and four consecutive periods,

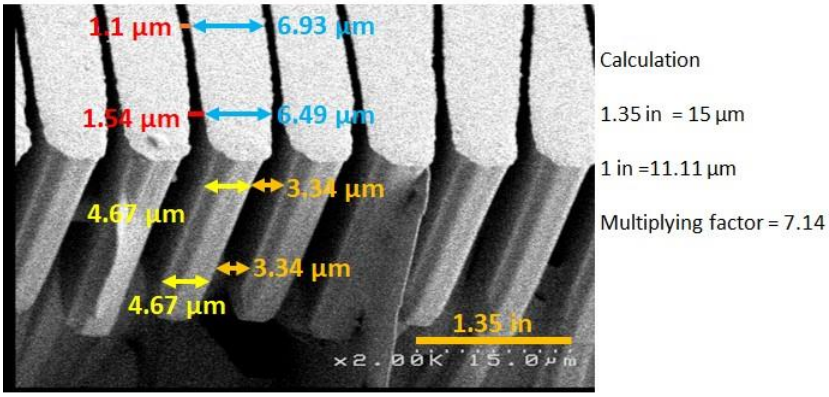

Figure 5.35: Measurement of grating dimension:

measuring 40.52 μm and 41.85 μm receptively, the difference of 1.3 μm between two is very close to previous measurement.

The dimensions of gratings are manually measured by considering the length of the reference bar at the bottom left of SEM image and calculating the multiplying factor. Further, this multiplying factor is used to calculate the width of the structures and the gap in between them. Figure 5.35, represents this analysis, where measurements are taken at the top and the bottom of the gratings to check for smearing effects. The grating width at the bottom is measured to be 4.67 μm, while the gap reads 3.34 μm, overall period of grating is 8 μm. Whereas, at the top of the grating width varies from 6.43 - 6.93 μm and the gap varying in between 1.1 - 1.54 μm. The dimension of the top is varying because of the smearing effect due to polishing.

The figure 5.35, suggest that the gap between grating structure is 3.34 μm, which suggest that PMMA wall were of 3.34 μm. Since the resist thickness was 100 μm, the aspect ratio of 30 was achieved. However, the duty cycle for PMMA structures was greater than 50 %. In order to achieve 50 % duty cycle, a bias has to be used as a compensation during next iteration.

Chapter 6
Conclusions and Future Work

In conclusion, of this thesis we have demonstrated that Cu substrate has better adhesion to the PMMA resist in comparison to titanium substrate. However, etching of copper oxide is a drawback for copper substrate as it causes debonding of PMMA structures. An optimized copper oxide etching will enable us to restrict debonding and reach higher aspect ratio. The complex structures of HAR gratings with 4.64 μm period and 100 μm height with aspect ratio of 21 were fabricated during the study. According to the X-ray absorption calculation this 100 μm thickness will provide approximately 95% X-ray absorption. In addition, PMMA structure with 30 aspect ratio and 100 μm height. However, the duty cycle was greater than 50%.

With current results, and replacing nickel with gold as grating material, the gratings can be used as analyzer gratings for Talbot interferometer. The grating will provide very high contrast and high sensitivity, which can be utilized for imaging. With increased sensitivity, Talbot interferometer can be used in imaging of various low absorbing material. Body tissues are one such example of low absorbing material, thus these gratings can be improving the Medical imaging applications such as imaging of soft tissues and internal organs.

References

[1] Momose A.), "Recent Advances in X-ray Phase Imaging." *Japanese Journal of Applied Physics,* 2005, 44(9A), 6355-6367. doi:10.1143/jjap.44.6355

[2] Weitkamp, T., Diaz, A., Stampanoni, M. (n.d). "X-ray phase imaging with a grating interferometer." *Optics Express,* 13(16), 6296-6304.

[3] Momose A., Kawamoto1 S., Koyama I., Hamaishi1 Y., Takai K., and Suzuki Y., "Demonstration of X-Ray Talbot Interferometry." *Japanese Journal of Applied Physics part 2 letter and express letter, 42(7B), L866-L868.*

[4] Kenntner, J., Altapova, V., Grund, T., Pantenburg, F. J., Meiser, J., Baumbach, T., & Mohr, J. "Fabrication and characterization of analyzer gratings with high aspect ratios for phase contrast imaging using a Talbot interferometer." *AIP Conference Proceedings,* 1437(1), 89-93. doi:10.1063/1.3703349

[5] E. W. Becker, W. Ehrfeld, P. Hagmann, A. Maner and D. Miinchmeyer, "Fabrication of microstructures with high aspect ratios and great structural heights by synchrotron radiation lithography, galvanoforming, and plastic molding (LIGA process)," *Micro-electronic Engineering*, Elsevier, 24 July 2002, www.sciencedirect.com/science/article/pii/0167931786900043.

[6] Wu, B., Kumar, A., & Pamarthy, S. (2010). "High aspect ratio silicon etch: A review." *Journal of Applied Physics,* 108(5), 051101. doi:10.1063/1.3474652

[7] Parsonage, E. E., Peppas, N. A., & Lee, P. I. "Properties of positive resists. II. Dissolution characteristics of irradiated poly (methyl methacrylate) and poly (methyl methacrylate-co-maleic anhydride)." *Journal of Vacuum Science* & *Technology: Part B-Microelectronics Processing* & *Phenomena,* 5(2), 538. doi:10.1116/1.583945

[8] Mohr, J., Grund, T., Kunka, D., Kenntner, J., Leuthold, J., Meiser, J., & ... Walter, M. (2012). "High aspect ratio gratings for X-ray phase contrast imaging. *AIP Conference Proceedings,* 1466(1), 41-50. doi:10.1063/1.4742267

[9] Vladimirsky, Y., et al, "PMMA as an X-Ray resist for micro-Machining application: Latent image formation and thickness losses," *Microelectronic Engineering*, vol. 30, no. 1-4, 1996, pp. 543546., doi:10.1016/0167-9317(95)00305-3.

[10] Kanigicherla, V. K. P., et al. "Enhanced adhesion of PMMA to copper with black oxide for electrodeposition of high aspect ratio nickel-Iron microstructures,"

Microsystem Technologies, vol. 4, no. 2, 1998, pp. 7781., doi:10.1007/s005420050100

[11] Sun, G., Zhao, X., & Kim, C., (2012). "Fabrication of Very-High-Aspect-Ratio Microstructures in Complex Patterns by Photoelectrochemical Etching." *Journal of MicroelectromechanicalSystems*,21(6),1504-1512. doi:10.1109/jmems.2012.2211574

[12] C. Gu, H. Xu, and T. Zhang, "Fabrication of high aspect ratio through-wafer copper interconnects by reverse pulse electroplating," *J. Micromech. Microeng.*, vol. 19, no. 6, pp. 065011-1065011-5, Jun. 2009.

[13] P. Dixit and J. Miao, "Aspect-ratio-dependent copper electrodeposition technique for very high aspect-ratio through-hole plating," *J. Electrochem. Soc.*, vol. 153, no. 6, pp. G552G559, Sep. 2006.

[14] Mohr, J., Requirements on resist layers in deep-Etch synchrotron radiation lithography. Journal of Vacuum Science & Technology, *Microelectronics and Nanometer Structures,* vol. 6, no. 6, 1988, p. 2264., doi:10.1116/1.584067.

[15] Blauw, M. A., Zijlstra, T., & Drift, E. V. (2001). "Balancing the etching and passivation in time-multiplexed deep dry etching of silicon." *Journal of Vacuum Science & Technology B: Microelectronics and Nanometer Structures,* 19(6), 2930. doi:10.1116/1.1415511

[16] Abdolvand, R., & Ayazi, F. (2008). "An advanced reactive ion etching process for very high aspect-ratio sub-micron wide trenches in silicon." *Sensors and Actuators A: Physical,* 144(1), 109-116. doi:10.1016/j.sna.2007.12.026

[17] A. Maner, S. Harsh, and W. Ehrfeld, "Mass production of microdevices with extreme aspect ratios by electroforming," *Plating and Surface Finishing*, vol. 75, no. 3, pp. 6065, 1988.

[18] Dierolf, M., Bunk, O., Gruenzweig, C., Pfeiffer, F., Bunk, O., Donath, T., & ... David, C. (n.d). "Design, fabrication, and characterization of diffraction gratings for neutron phase contrast imaging." *Review of Scientific Instruments*, 79(5),053703. doi:10.1063/1.2930866

[19] P. Hagmann, W. Ehrfeld, and H. Vollmer, "Fabrication of microstructures with extreme structural heights by reaction injection molding," *Makromolekulare ChemieMacromolecular Symposia*, vol. 24, 1989, pp. 241251.

[20] Hung, S. C., Shiu, S. C., Chao, J. J., & Lin, C. F. (2010). "Fabrication of Deep Si Trenches by Self-Assembled Wet Chemical Etching Process." *Journal of The Electrochemical Society,* 157(9), D496. doi:10.1149/1.3462976

[21] David, C., Nhammer, B., & Ziegler, E. (2001). "Wavelength tunable diffractive transmission lens for hard x rays*." Applied Physics Letters, 79(8), 1088-1090*. doi:10.1063/1.1379364

[22] Marques, C., et al. "Fabrication of high-Aspect-Ratio microstructures on planar and nonplanar surfaces using a modified LIGA process," *Journal of Microelectromechanical Systems*, vol. 6, no. 4, 1997, pp. 329336., doi:10.1109/84.650130.

[23] Tada, T., Murakoshi, D., Ishii, H., Hashimoto, A., Kaneko, Y., Ito, W., & Agano, T. (2012). "Fabrication of high aspect grating using bonded substrate for X-ray refraction imaging by Talbot-Lau interferometer." *AIP Conference Proceedings*, 1466(1 10.1063/1.4742289). doi:10.1063/1.4742289

[24] Schmalz, O., Hess, M., Kosfeld, R., "Structural changes in poly (methyl methacrylate) during deep-etch X-ray synchrotron radiation lithography .3. Mode of action of the developer." (n.d). *Angewandte Makromolekulare Chemie*, 23993-106.

[25] Jinka, O. (2012). "Combinatorial multi-level mold inserts using micro machining and X-ray lithography.". *[Baton Rouge, LA.: Louisiana State University,* 2012].

[26] Carlo, F. De, et al. "Characterization of exposure and processing of thick PMMA for deep x-Ray lithography using hard x-Rays," *Microsystem Technologies*, vol. 4, no. 2, 1998, pp. 8688., doi:10.1007/s005420050102.

[27] T.Gietzelt et al, "Manufacturing of microstructures with high aspect ratio by micromachining, *Microsystem Technologies,* (2008) 14: 1525-1529

[28] Willson, C. G., Dammel, R. R., & Reiser, A. (1997). "Photoresist materials: A historical perspective." *Metrology, Inspection, and Process Control for Microlithography XI.* doi:10.1117/12.275921

[29] Matsumoto, Masatake, et al. "Fabrication of diffraction grating for X-Ray Talbot interferometer," *Microsystem Technologies*, vol. 13, no. 5-6, Oct. 2006, pp. 543546., doi:10.1007/s00542-006-0226-8.

[30] Malek, C. K., & Saile, V. (2004). "Applications of LIGA technology to precision manufacturing of high-aspect-ratio micro-components and -systems: A review." *Microelectronics Journal,* 35(2), 131-143. doi:10.1016/j.mejo.2003.10.003

[31] James J. Kelly and S.H. Goods, X-ray Lithography Techniques, LIGA-Based Microsystem Manufacturing: The Electrochemistry of Through-Mold Deposition and Material Properties, pg 79-93

[32] Daiji, N., Tsujii, H., Takahashi, N., & Hattori, T. (2009). "Fabrication of X-Ray Gratings Using X-Ray Lithography Technique for X-Ray Talbot Interferometer." *Journal of The Electrochemical Society,* 156(5), 299. doi:10.1149/1.3082377

[33] Takahashi, N., Tujii, H., Yamashita, K., Noda, D., Hattori, T., & Katori, M. (n.d). "Fabrication of X-rays mask with carbon membrane for diffraction gratings." *Microsystem Technologies-Micro-And Nanosystems-Information Storage And Processing Systems,* 16(8-9), 1303-1307.

[34] Madou, M. J. (2009). *Fundamentals of microfabrication and nanotechnology. Manufacturing techniques for microfabrication and nanotechnology.*

[35] Daiji, N., Tokuoka, A., & Hattori, T. (2012). "Fabrication of high aspect ratio X-ray grating using silicon dry etching method." *AIP Conference Proceedings,* 1466(1), 187-192. doi:10.1063/1.4742290

[36] Daiji, N., Makoto, T., Kazuma, S., Wataru, Y., Atsushi, M., & Tadashi, H. (2008). "Fabrication of large area diffraction grating using LIGA process." *Microsystem Technologies,* 14(9-11), 1311-1315.

[37] Cerrina F, *"Handbook on Lithography,"* SPIE edition, 1996

[38] Smith, H. I., Bernacki, S. E., Spears, D. L. "X-Ray Lithography: A Complementary Technique to Electron Beam Lithography." *Journal of Vacuum Science and Technology,* 10, 913th ser. doi:https://doi.org/10.1116/1.1318514

[39] Backer, E. W., Ehrfeld, W., Mnchmeyer, D., Betz, H., Heuberger, A., Pongratz, S., . . . Siemens, R. V. (1982). "Production of separation-nozzle systems for uranium enrichment by a combination of X-ray lithography and galvanoplastics." *Naturwissenschaften,* 69(11), 520-523. doi:10.1007/bf00463495

[40] Ehrfeld, W., & Lehr, H. (1995). "Deep X-ray lithography for the production of three-dimensional microstructures from metals, polymers and ceramics." *Radiation*

Physics and Chemistry, 45(Applications of synchrotron X-radiation), 349-365. doi:10.1016/0969-806X(93)E0007-R

[41] H. F. Talbot, 1836 *Facts relating to optical science* No. IV, Phil.

[42] Simon, R. (2013). "X-ray grating interferometry for imaging and metrology." *ETH ZURICH.* doi:https://doi.org/10.3929/ethz-a-009753051

[43] Maner, A., & Ehrfeld, W. (1989). "Electroforming Techniques in The Liga Process for The Production of Microdevices." *Materials and Manufacturing Processes,* 4(4), 527-537. doi:10.1080/10426918908956313

[44] Baur, R. M. (2013). *Development and application of a grating interferometer at the Cornell high energy synchrotron source.* Cornell University.

[45] Bech, M. (2009). *X-ray imaging with a grating interferometer* University of Copenhagen.

[46] Griffiths, K. S. "Fundamental limitations of LIGA x-ray lithography: sidewall offset, slope and minimum feature size." *Journal of Micromechanics and Microengineering,* 14(7), 999-1011.

[47] Griffiths, S. K., Hruby, J. M., and Ting, A. (1999). "The influence of feature sidewall tolerance on minimum absorber thickness for LIGA x-ray masks." *Journal of Micromechanics and Microengineering,* doi:10.2172/751005

[48] Hoysz, L., Rymuszka, D., Chibowski, E., & Terpiowski, K. (2015). "Changes in surface properties of polymethylmethacrylate (PMMA) treated with air plasma." *Annales UMCS, Chemistry,* 70(1), 65-78. doi:10.1515/umcschem-2015-0006

[49] Rooks, M. J., Kratschmer, E., Viswanathan, R., Katine, J., Fontana, R. E., and MacDonald, S. A. (2002). "Low stress development of poly(methylmethacrylate) for high aspect ratio structures." *Journal of Vacuum Science & Technology: Part BMicroelectronics & Nanometer Structures,* 20(6), 2937. doi:10.1116/1.1524971

[50] Mazher I, M., Muhd Nazrul Hisham Zainal, A., Abbas, K., & Ian, G. (2017). "Fabrication of microfluidic devices: improvement of surface quality of CO2 laser machined poly(methylmethacrylate) polymer." *Journal of Micromechanics & Microengineering,* 27(1), 1. doi:10.1088/0960-1317/27/1/015021

[51] Malek, C. K., & Yajamanyam, S. (2000). "Evaluation of alternative development process for high-aspect-ratio poly(methylmethacrylate) microstructures in deep x-ray lithography." *Journal Of Vacuum Science & Technology: Part B-Microelectronics & Nanometer Structures,* 18(6), 3354. doi:10.1116/1.1321759

[52] Yajamanyam, S. (1999). *Factors affecting the development of PMMA in deep x-ray lithography.* 1999.

[53] Yashiro, W., Wan, K., Wan, K., Takeda, Y., Yashiro, W., and Momose, A. (n.d). "Fabrication of multiple slit using stacked-sliced method for hard X-ray Talbot-Lau interferometer." *Japanese Journal of Applied Physics,* 47(9), 7412-7414.

[54] David, C., Bruder, J., Rohbeck, T., Grnzweig, C., Kottler, C., Diaz, A., and Pfeiffer, F. (2007). "Fabrication of diffraction gratings for hard X-ray phase contrast imaging." *Microelectronic Engineering,* 841172-1177. doi:10.1016/j.mee.2007.01.151

[55] Guckel, H., Christenson, T., R., and Skorbis, K., "Formation of microstructures using a preformed photoresist sheet." *US patent* No. 5,378,583 (1993)

[56] A.E Kholi et al, "Alternative resist adhesion and electroplating layers for LIGA process", *Microsystem technologies,* 6 (2000) 161-164

[57] Weitkamp, T., Rutishauser, S., Bednarzik, M., David, C., Zanette, I., Weitkamp, T., and Mohr, J. (n.d). "Fabrication of two-dimensional hard X-ray diffraction gratings." *Microelectronic Engineering,* 10112-16.

Vita

Vikaram Singh was born in 1987, Lucknow, Uttar Pradesh, India. In 2010, he completed his bachelor's in electrical engineering from Ideal Institute of Technology (Affiliated to Uttar Pradesh Technological University) Ghaziabad, Uttar Pradesh, India. Further, in 2104, he completed his master's in power system from Veermata Jijabai Technological Institute (Affiliated to Mumbai University), Mumba, Maharashtra, India. Worked as a research scientist in Intelligent communication Lab. in Mumbai, India, from August 2012 to July 2015. Later, he joined Louisiana State University in fall 2015 to pursue his Master of Science in Electrical Engineering.